DIELECTRIC FORMULATION OF THE THREE- AND TWO-DIMENSIONAL
QUANTUM MANY-ELECTRON SYSTEMS

A THESIS SUBMITTED TO
THE GRADUATE SCHOOL OF NATURAL AND APPLIED SCIENCES
OF
THE MIDDLE EAST TECHNICAL UNIVERSITY

BY

CEYHUN BULUTAY.

IN PARTIAL FULFILLMENT OF THE REQUIREMENTS FOR THE DEGREE OF

DOCTOR OF PHILOSOPHY

IN

THE DEPARTMENT OF ELECTRICAL AND ELECTRONICS ENGINEERING

MAY 1997

Approval of the Graduate School of Natural and Applied Sciences.

Prof. Dr. Tayfur Öztürk
Director

I certify that this thesis satisfies all the requirements as a thesis for the degree of Doctor of Philosophy.

Prof. Dr. Fatih Canatan
Head of Department

This is to certify that we have read this thesis and that in our opinion it is fully adequate, in scope and quality, as a thesis for the degree of Doctor of Philosophy.

Prof. Dr. Mehmet Tomak
Co-Supervisor

Prof. Dr. Nilgün Günalp
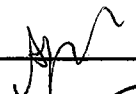Supervisor

Examining Committee Members

Prof. Dr. Mehmet Tomak

Prof. Dr. Nilgün Günalp

Assoc. Prof. Dr. Ahmet Gökalp

Assoc. Prof. Dr. Bilal Tanatar

Assist. Prof. Dr. Cengiz Beşikçi

ABSTRACT

DIELECTRIC FORMULATION OF THE THREE- AND TWO-DIMENSIONAL QUANTUM MANY-ELECTRON SYSTEMS

Bulutay, Ceyhun

Ph.D., Department of Electrical and Electronics Engineering

Supervisor: Prof. Dr. Nilgün Günalp

Co-Supervisor: Prof. Dr. Mehmet Tomak

May 1997, 155 pages.

Low-dimensional and small-scale electronic systems is the common field of interest of the electrical engineers and the physicists, collaboration of which gave rise to this work. First, a solid-state electron biprism is proposed based on the phase-coherent electron beams. Motivated by the phase-breaking effect of the electron-electron interaction, many-body effects in the three- (3D) and two-dimensional (2D) electronic systems are targeted in the core of the work. The dielectric formulation of the many-body problem is preferred and the longitudinal dielectric function of the electron liquid (EL) is obtained using the self-consistent local-field correction scheme, known as STLS. The performance of this formalism is compared in both 3D and 2D by the quantum Monte Carlo data and the pseudopotential approach introduced by Pines and co-workers. STLS is observed to be a highly satisfactory technique, with some reservations on the long-wavelength behaviour. The dielectric properties of the quasi-two-dimensional (Q2D) EL formed in semiconductor heterojunctions is accurately characterized taking into account carrier penetration to barrier-acting material, and the image charges due to background dielectric discontinuity. Analytical forms are presented for the local-field correction and the dielectric function of the 2D and Q2D ELs for a wide range of electronic densities and the relevant parameters. Finally, Mott transitions in 3D and 2D EL are investigated using the STLS screening, giving

due importance to exchange effects. With the aim of a high accuracy, a formulation leading to an integral equation is obtained. The exchange effects are observed to be very influential in spin-polarized ELs. Mott transition does not exist in single-valley 2D ELs with spin-polarized and normal-state cases. All of the formulation and the results are obtained under the zero-temperature framework.

Keywords: Many-body, screening, electron-electron interaction, electron liquid, electron gas, low-dimensional systems, mesoscopic devices, dielectric function, local-field correction, correlation energy, heterojunctions, Mott transition, exchange effects.

ÖZ

ÜÇ VE İKİ BOYUTLU KUANTUM ÇOK-ELEKTRONLU ELEKTRONİK SİSTEMLERİN DİELEKTRİK FORMULASYONU

Bulutay, Ceyhun

Doktora, Elektrik ve Elektronik Mühendisliği Bölümü

Tez Yöneticisi: Prof. Dr. Nilgün Günalp

Ortak Tez Yöneticisi: Prof. Dr. Mehmet Tomak

Mayıs 1997, 155 sayfa.

Bu çalısma, elektrik mühendisleri ve fizikçilerin ortak ilgi alanını oluşturan düşük-boyutlu ve küçük-ölçekli elektronik sistemler konusundaki ortak incelemelerinin sonucudur. İlk olarak, faz-uyumlu elektron hüzmelerine dayalı bir katı-hal elektron çift-prizması önerilmiştir. Çalışmanın ana bölümünde, elektron-elektron etkileşmesinin faz kırma etkisinden güdümle, üç ve iki boyutlu elektronik sistemlerde çok-cisimcik etkileri hedeflenmiştir. Çok-cisimcik probleminin dielektrik çözümlemesi seçilerek, elektron sıvısının uzunlamasına dielektrik fonksiyonu, STLS olarak bilinen öz-tutarlı yerel-alan düzeltmesi düzeninde elde edilmiştir. Bu yaklaşımın sonuçları, kuantum Monte Carlo ve Pines ve grubunun ileri sürdüğü görünür-potansiyel yaklaşımıyla karşılaştırılmıştır. Uzun dalgaboyu davranışı dışında STLS'in son derece tatmin edici olduğu gözlenmiştir. Yarıiletken heteroekleminde oluşan iki boyutumsu elektron sıvısının dielektrik özellikleri, taşıyıcıların engel gibi davranan bölgeyi delmeleri ve geriplan dielektrik süreksizliğinden doğan imaj yükler de dikkate alınarak, hassas olarak işlenmiştir. Tam iki boyutlu ve iki boyutumsu elektron sıvılarının yerel-alan düzeltme ve dielektrik fonksiyonlarına, yaygın elektron yoğunlukları ve diğer parametreleri için analitik ifadeler önerilmiştir. Son olarak, STLS perdelemesi içinde, üç ve iki boyutlu elektron sıvılarında, değiş-tokuş etkilerine özel önem vererek Mott geçişi incelenmiştir. Yüksek hassasiyet amacıyla, entegral denklemiyle sonuçlanan

bir yöntem kullanılmıştır. Spin-kutuplu elektron sıvılarında değiş-tokuş etkisinin çok etkin olduğu gözlenmiştir. Normal-hal ve spin-kutuplu tek vadili iki boyutlu elektron sıvılarında Mott geçişi yoktur. Bütün işlemler ve sonuçlar sıfır sıcaklık çerçevesinde elde edilmiştir.

Anahtar Kelimeler: Çok-cisimcik, perdeleme, elektron-elektron etkileşimi, elektron sıvısı, elektron gazı, düşük-boyutlu sistemler, mezoskopik aygıtlar, dielektrik fonksiyonu, yerel-alan düzeltmesi, korelasyon enerjisi, heteroeklemler, Mott geçişi, değiş-tokuş etkileri.

... BABAM ORHAN BULUTAY'IN ANISINA

ANNEM GÜLSEVİN BULUTAY'A
ve
ABİM KAZIM BULUTAY'A

ACKNOWLEDGMENTS

PREFACE

Electrical engineers and in particular, the device engineers, have been involved in an endeavor for the journey towards the microscopic world, started about fifty years ago from the macroscopic one. In these years, this tour is approaching towards the half-way, the mesoscopic world, with the rules of its own. Condensed matter physicists have arrived at this point earlier and developed a fair understanding of the underlying phenomena. As a matter of fact, the current electronics enterprise owes its birth to basic research, conducted by the physicists Bardeen and Brattain on the *surface states* in semiconductors that unexpectedly gave rise to the first transistor, the point-contact transistor.

This work is an interdisciplinary study in collaboration with the physicists, having the goal of understanding and characterizing many-electron systems with three- and two-dimensional structures. There is concrete evidence that quantum mechanical and statistical effects have substantial part in the mesoscopic phenomena. In the first chapter, we introduce a novel mesoscopic device, an electron biprism, based on phase-coherent electron beams. We, then question the role of many-body effects and build strong motivation for investigating these many-body effects in basic electronic systems. In Chapter 2, we first discriminate the longitudinal and transverse dielectric functions and present the general dielectric formulation of a many-body system. Chapter 3 contains the explicit expressions to be used for the three- and two-dimensional electron liquids, as well as a detailed derivation of the STLS technique, that we choose to employ in this work. The results utilizing these expressions are presented in Chapter 4, where we establish a sound assessment of our approach. We give special importance to the quasi-two-dimensional electron liquids and spare Chapter 5 to its comprehensive discussion. Chapter 6 on the Mott transition gives us

the opportunity to display the full strength of our formulation, which we also think that has a contribution to this long-standing subject. Finally, we summarize our main findings and list possible improvements and future directions in Chapter 7. The appendix includes the variational energy expression for a heterojunction.

Most of the results that we present are original, which were already published or sent for publication to scientific journals. We make every effort to cite the scientific work that we made use of. For the critical and subtle discussions we prefer to give expert opinions and occasionally make quotations rather than rephrasing the original ideas.

TABLE OF CONTENTS

CHAPTER 1

INTRODUCTION

Electronics is becoming continuously richer and exciting. The evolution of the electronics was initiated by the metal-semiconductor Schottky contact more than fifty years ago [1] and followed by the bipolar junction transistors, field-effect transistors, semiconductor lasers, superlattices, heterojunctions, quantum wells, wires and dots. The materials used changed considerably as well, from group IV semiconductors to III-V and II-VI binary compounds, then the ternary alloys and oxide compounds for high-temperature superconductors, and also from inorganic semiconductors to organic ones [2]. What has been tried should not make us think that we are running out of the possibilities in the periodic table. "Already for a quaternary crystal, with four elements per unit cell, there are over a hundred million possible crystalline materials, only a tiny fraction of which has been made" [3]. Electronics is no longer under the realm of electrical engineering or physics, but an interdisciplinary field with close ties to chemistry, material science, and probably in the future biology, no need to

1

mention mathematics and the computing science which serve to all present-day high-tech fields. Given this highly multi-cultural scientific environment, professional life becomes quite challenging for the candidates to pursue a career in this field.

From its first days solid-state electronics had continuously been attracted by ever smaller sizes. This is in fact described by Moore's law, named after the scientist of the Fairchild Semiconductor, Dr. Gordon Moore, who developed the first planar transistor. Dr. Moore stated his law in 1965 in the Electronics Magazine, with the statement that every year the number of components on an integrated circuit doubles. In the past thirty years, this statement ruled the electronics industry and it became a widely-accepted law. However, two effects come into play when very small geometrical dimensions are reached: the quantum mechanical effects and the sample-specific fluctuations [4]. These two, actually underlie a new physics that has been named as the *mesoscopic physics*, a word borrowed from statistical mechanics [5, 6]. In this new *mesoscopic* world, an injected electron is seen to preserve its phase memory within the active device (about few microns) at low temperatures (such as 1K). Thus, the electrons demonstrate a coherent electron wave picture just as in conventional optical and microwave devices. This similarity of the phase-coherent electron waves and the classical electromagnetic waves arose a big excitement in the technical community towards the beginning of 1990's. The table reproduced below due to Datta and McLennan [7], lists the analogous quantities of electron waves and classical electromagnetic waves.

This remarkable similarity also attracted us to this mesoscopic arena[1]. In the next section we present an original solid-state device that we proposed as a potential

---

[1] In particular, a paper [8] presented in the IEEE microwave symposium in 1991, where the author was also participating, has been extremely influential.

Table 1.1: Datta and McLennan's chart[7] of analogies between coherent electron waves and electromagnetic (EM) waves.

Electron Waves	EM Waves
$\Psi(\vec{r}, t) = \psi(\vec{r})\, e^{-iEt/\hbar}$	$\vec{\mathrm{E}}(\vec{r}, t) = \vec{E}(\vec{r})\, e^{-i\omega t}$
Energy E	Frequency ω
Confined channels	Waveguides
Subbands	Transverse modes
Ψ	$\vec{\mathrm{E}}$
$\nabla\Psi$	$\vec{\mathrm{H}}$
Charge density	Energy density
Current density	Poynting's vector
$\nabla^2\psi = -\frac{2m^*}{\hbar^2}(E - V)$	$\nabla^2\vec{E} = -\omega^2\,\mu\,\epsilon\,E$

mesoscopic device.

1.1 Solid-State Electron Biprism

1.1.1 Motivation

About four decades ago Möllenstedt and Düker have utilized the wave nature of electron beams by inventing a vacuum electron biprism [10]. This device has become an essential component in electron microscopy and recently used for research in electron holography [11, 12]. Here we explore a solid-state counterpart to the vacuum electron biprism by employing the split-gate heterostructure geometry [13] having an impurity within the channel. The similarity between the two is remarkable as can be seen in Figs. 1.1 and 1.2. Up to now, impurities were identified as undesirable, degrading device performance [14, 15], however, an intentionally implanted one can be of advantage in the above mentioned configuration provided that the biprism effect also exists in this structure. In the literature, both the split-gate geometry [13] and the case of an impurity within the channel [14, 15, 16, 17, 18, 19, 20] have been extensively

3

studied. But, the main focus has been on the conductance of the constriction with the primary observation being the distortion in the quantized conductance plateaus due to the impurity potential. We anticipate an impurity assisted interference that can radically alter the functionality of the split-gate geometry. But there are certain questions that can be raised on the realization of such a device and on the possibility of implanting an impurity of the desired form within the channel. As for the former, recent results obtained by Okada and co-workers [21] have demonstrated for the first time double peaks in the angular distribution of electrons in a quantum point contact indicating the rigidity of multimode operation of these heterostructures. As a remedy for the latter, the scanning tunneling microscopy (STM) has been used to manipulate even the strongly bound silicon atoms or clusters at room temperature [22]. By this means, surface atoms can be removed and deposited on the STM tip. The tip can then be positioned over a predetermined surface site and it can implant the foreign atoms much like a winch [22], or alternatively, the STM tip can approach closely to a targeted atom and then drag it to a new location [23]. Moreover, experimental reports show that exacting operations can be performed over length scales as small as 0.9 nm with the generated marks being stable over extended time periods [24]. These experimental achievments provide a support for the theoretical investigation of a solid-state electron interferometer based on the fundamental principle of Möllenstedt biprism.

4
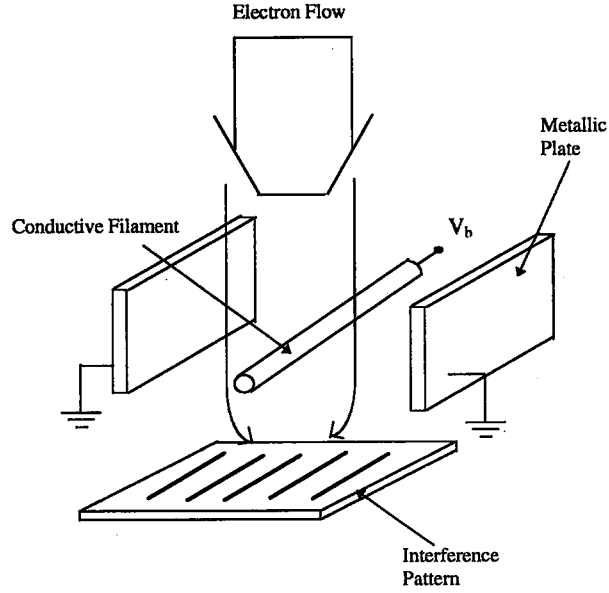
Figure 1.1: Möllenstedt biprism - a vacuum electron device. The biprism consists of two parallel grounded plates with a fine filament between them, the latter having a potential V_b relative to the former.
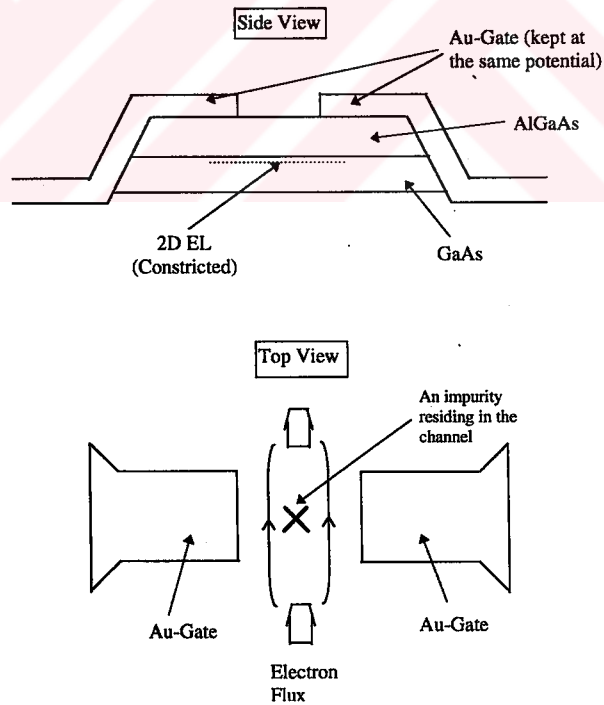
Figure 1.2: Side and top views of split-gate configuration. Top view in the case of an impurity resembles Möllenstedt biprism in Fig. 1.1.

1.1.2 Description

The split-gate geometry is commonly realized using a GaAs/AlGaAs heterostructure (Fig. 1.2) resulting in a high electron mobility (see for e.g., Ref. [2]). The triangular-like barrier confinement along the third dimension (the $y-$axis in Fig. 1.3) in these structures reduces the effective physical dimension to two. The reason is that due to the doping level usually only the lowest subband (mode) of this triangular barrier is populated. The physical geometry of the problem suggests the space to be divided into 4 regions (labeled with (a) to (d)) as indicated in Fig. 1.3. An incident electron beam in region (a) is represented by a unit-amplitude right-going plane wave, $\Psi^i(x,z) = e^{ik_{0x}x}\,e^{ik_{0z}z}$ having an energy E_0, with $2m^*E_0/\hbar^2 = k_{0x}^2 + k_{0z}^2 \equiv k_F^2$. The scattered wave function in each region is considered in its most general form with unknown expansion coefficients. Particularly, in regions (b) and (c), the forms of the scattered waves are discrete spectrum waveguide modes, and in regions (a) and (d) they are continuous spectrum modes, just as in the classical microwave and RF phenomena. The formulation proceeds by matching the wave functions and their derivatives across the region boundaries [26]. These equations are then built into coupled matrix equations[2] with a source term representing the incident wave in region (a). The solution of this matrix equation yields the expansion coefficients of interest in all regions. As our emphasis here is not on the technical details of this analysis, we refer to our paper [9] about the elaborate mathematical formulation.

---

[2] A valuable resource in this field is the Ph. D. thesis of E. Tekman[25].

6
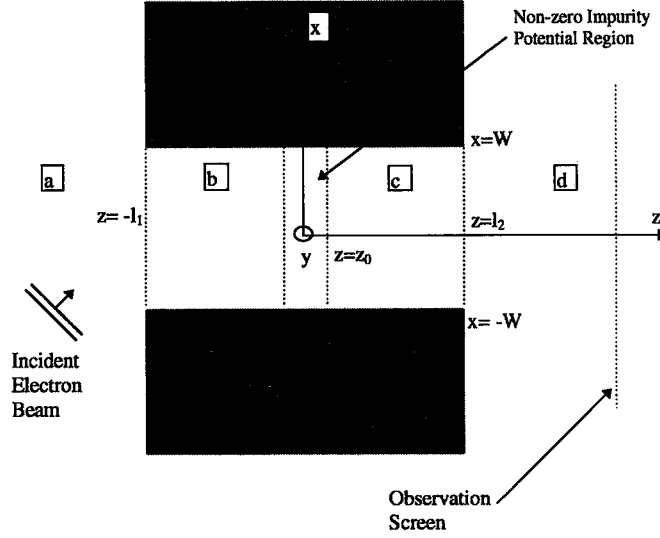
Figure 1.3: Top view of the split-gate geometry containing the necessary spatial dimensions and the labels referred in the mathematical formulation.

1.1.3 Operation

As opposed to the conductance point of view [14, 15, 16, 17, 18, 19, 20], the problem of an impurity in a split-gate geometry is now revisited to manifest its parallelism with the Möllenstedt biprism. The information about the excitation, impurity profile, and the geometrical dimensions used in our theoretical investigation are provided in Table 1.2. They are chosen so as to closely resemble a practical problem. In GaAs a Fermi wave number of $k_F = 0.13 \text{nm}^{-1}$ corresponds to an energy of $E_0 \simeq 10 \text{meV}$.

Before presenting the results, in order to get a base for comparison we need to know the behavior of the system in the case of *no-impurity* within the channel. The result is given in Fig. 1.4 by the dashed line, showing the probability amplitude (Ψ_d) variation in region (d) calculated at $z = 15W$ (W being the half-width of the channel). The waveform corresponds to the well-known diffraction pattern having a very big main lobe compared to the neighboring side lobes. Now, if we turn on the

7

Table 1.2: Data related to geometry of the split-gate, excitation and impurity profile (Infinite-wall confinement is considered in regions (b) and (c)).

Geometry:	$W = 110$ nm
	$l_1 = 0.75W$
	$l_2 = 0.75W$
Excitation:	$k_F = 0.13$ nm^{-1}
	$k_{0z} = k_F$ (i.e., $k_{0x} = 0$)
Impurity Profile:	$U_{imp}(x,z) = U_0 \exp\left(-\alpha x^2\right)\delta(z)$
	$U_0 = -10^4 E_0$ where $E_0 = k_F^2 \hbar^2 / (2m^*)$
	$\alpha = 1/(0.3W)^2$
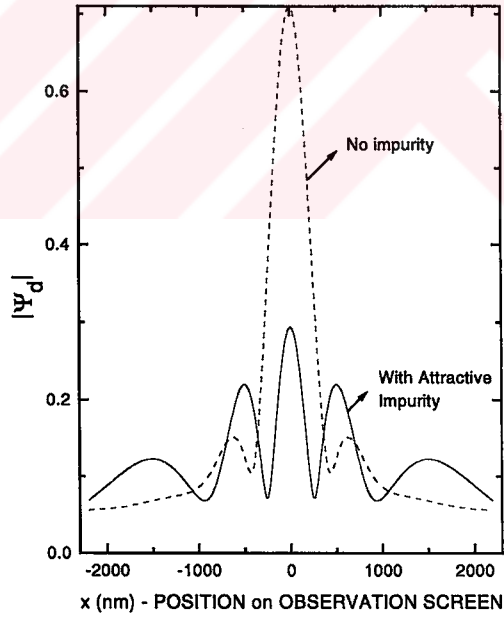
Figure 1.4: Magnitude of probability amplitude variation calculated at $z = 15W$. The dashed line corresponds to an impurity-free channel and the solid line illustrates an attractive impurity at the origin. Refer to Table 1.2 for the dimensions and excitation.

8
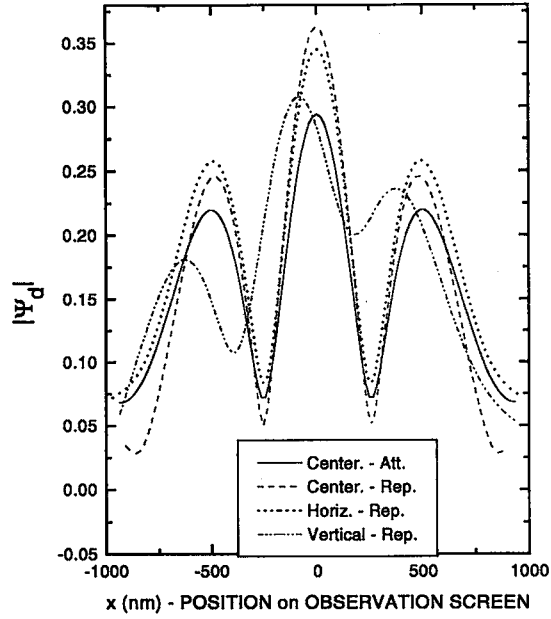
Figure 1.5: Effects of the position of the Gaussian impurity on the interference pattern computed at $z = 15W$. An attractive impurity at the origin is compared with repulsive impurities at the origin and with horizontal and vertical displacements given. The horizontally shifted repulsive impurity is located at z=-0.45W, x=0 and the vertically shifted repulsive impurity is positioned at x=0.2W, z=0. Amplitudes and variances of all Gaussian impurities are the same as in Table 1.2.

impurity potential then the associated probability amplitude variation is shown with the solid line in the same figure. Clearly the neighboring fringes are grossly enhanced as compared to the impurity-free channel case. The reflected electron flux is, however, appreciably increased due to the high impurity potential as can be observed in Fig. 1.4 from the lower value of $|\Psi|$ in region (d). To assess the sensitivity of the interference pattern to the location and the lateral functional profile of the impurity, several cases are considered. In Fig. 1.5 the centered, horizontally shifted and vertically shifted (all being repulsive) Gaussian impurity profile responses are compared to that of the centered attractive Gaussian impurity (all of them of the same magnitude). It is seen that the pattern is more vulnerable to the vertical shift of the impurity location. Finally, Fig. 1.6 illustrates the effect of the gate width on the interference pattern.

9

As the channel is constricted the number of propagating modes (subbands) decreases and the effective impurity width increases resulting in a diminished wave function transmitted to region (d).
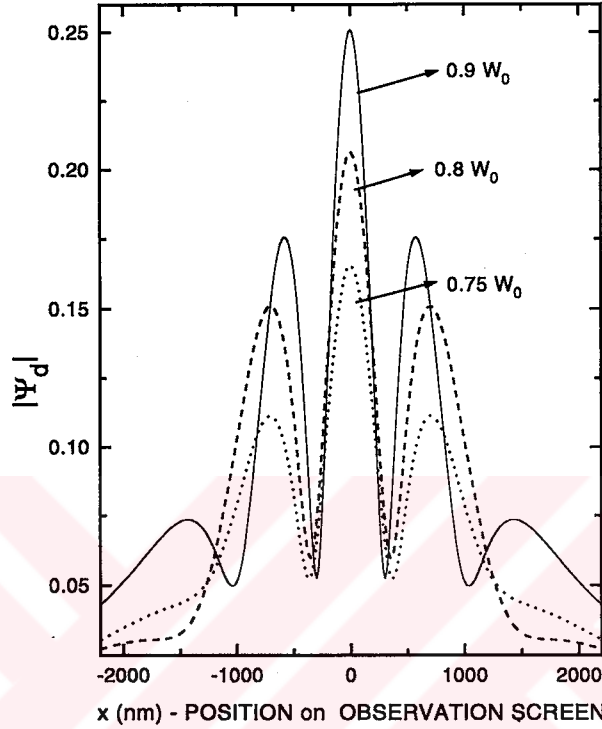
Figure 1.6: Effect of gate width on the interference pattern as the channel is symmetrically constricted. W_0 is the original dimension given in Table 1.2. There are 8 modes that can propagate in the constriction for $W = 0.9W_0$. For $W = 0.8W_0$ 7 modes are propagating and for $W = 0.75W_0$ the first 6 modes can only propagate. The parameters in Table 1.2 are used with the impurity potential being repulsive rather than attractive.

1.2 The Fate of the Mesoscopic Devices ?

The proposed solid-state electron biprism has one superiority over similar devices such as the quantum interference transistors proposed by Datta [27] and Sols *et al.* [28]. These latter device prototypes favor only a single-mode operation, that is to say, the basic device operation is based on a single-subband being populated. This

requirement severely restricts the current driving ability. In case more subbands are allowed to be populated, then the 100% conductance modulation property of these quantum interference is highly degraded. In contrast, we demonstrate the theoretical performance of the solid-state electron biprism under nine subbands being populated in Fig. 1.4.

Unfortunately, there are other concerns about the future of the mesoscopic devices. Thornton [29] has critically examined the mesoscopic devices and concluded that quantum interference type devices suffer from severe practical limitations. The basic drawback of these devices is the fragility of the phase coherence of the electron waves. First of all, at high temperatures due to inelastic phonon scattering the phase memory of the electron beam gets randomized. Ikoma *et al.* [30] have observed the rapid drop of the phase coherence time in the GaAs/AlGaAs system above 5K. As a result, the phonon scattering needs to be suppressed for room temperature operations. The analogy between phase-coherent electron beams and classical electromagnetic waves breaks down when the many-body effects are considered. The analogy chart in Table 1.1 is based on the single-electron Schrödinger equation, however, in any electronic device, a high density of electrons exists making up the electric current. In many-body aspects electrons and photons are quite different: the former obeys Fermi-Dirac statistics and are called fermions, whereas the latter are governed by Bose-Einstein statistics and are called bosons. Furthermore, the Coulomb repulsion between the electrons produce non-trivial effects as we illustrate in the following chapters. Two experiments done by the IBM group in USA [31] and the Jülich group [32] in Germany have cast more doubts on the fate of the mesoscopic devices. These two groups reached the same conclusion about the ballistic electron beams:

electron-electron interaction in ballistic electron beams is a serious basic limitation for future devices based on the transport of the electrons in the mesoscopic transport regime. In other words, the interaction between any two electrons in an electron beam is claimed to be an important source for the phase memory loss. Thorton's criticisms and these experimental facts have urged us to divert our attention from phase-coherent mesoscopic devices to many-electron effects in such devices. It is now becoming a well-agreed fact that many-body effects will rule the next generation electronic devices and materials (refer to, for instance, to Refs. [33, 34]).

1.3 Many-Particle Electronics

After 1950's extensive research efforts on classical and quantum many-particle systems have produced a fruitful body of knowledge that had also technological implications. However, undergraduate quantum mechanics education in the physics and electrical engineering curriculum is still dominated by the single-particle quantum mechanics which dates back to 1920's. Admittedly, many-body quantum mechanics is quite an advanced subject, as a matter of fact, Supriyo Datta in his graduate textbook entitled, *Quantum Phenomena* [35] has the following interesting comment: "A complete quantum mechanical formalism exists, ... However, these concepts are difficult and only the very best scientists have a clear comprehension of the complex multiparticle dynamics. Lesser mortals are usually content with trying to unravel the consequences of the one-electron Schrödinger equation."

Beginners of the many-body theory are astonished by the overwhelming varieties of methods in reaching the same end result, each resorting to extremely different mathematical tools. Actually, the pioneers of this field who laid the foundations in

1950's also felt the same way as the beginners of today. A good example is the so-called random phase approximation (a many-body technique) that has been rediscovered during a ten-year period between 1950 to 1960, about half a dozen times, each time aiming to tackle the problem in a completely different way [36].

The essential ingredient in standard many-body approaches is the *perturbation theory*. Namely, the two-particle interaction is treated as a small perturbation over a soluble non-interacting part. The dynamical nature of the quantum particles necessitates the perturbative approach to be also time-dependent. The challenge is that, for most many-body systems, such as the electrons in a metal or a doped semiconductor, the perturbation is not small. Even worse, the perturbation series is not a decreasing one in amplitude, but has most of the terms diverging. Surprisingly, a working theory was reached when scientists insisted to apply the time-dependent perturbation theory to such pathological cases. Their recipe was to sum a certain class of most-divergent terms, ending up having a finite result, due to apparent cancellations among the terms. The justification of their approach was the qualitative agreement with the experiments.

There are quite a number of different many-body approaches with differing levels of theoretical difficulty (for a variety of books on this subject, see [37, 38, 39, 40, 41, 42, 43]. The dielectric formulation of the many-body problem [36] has a modest complexity and moreover, is unquestionably the most appealing approach for the electrical engineers, due to its conceptual familiarity, where the formulation is based on a frequency- and wave number-dependent dielectric function of the system. This function contains a wealth of information about the system, and essential equilibrium and transport parameters are then accessible by straightforward means.

13

As the quantum many-body system we choose the electron liquid in three, two and quasi-two dimensions. This choice is rather obvious, these systems form the generic models of the bulk and low-dimensional electronic systems, bringing into foreground the electronic phenomena at the expense of suppressing the crystal structure which is material-dependent.

CHAPTER 2

MANY-ELECTRON PHYSICS

USING THE DIELECTRIC FORMULATION

2.1 Introduction

The present chapter forms the backbone of this work on the dielectric characterization of electronic materials. The electronic properties (such as transport) of electronic devices are characterized by the longitudinal dielectric function whereas the optoelectronic properties are determined by the transverse dielectric function. However, the distinction between these two dielectric functions is seldom made in the literature. We establish this division by introducing the longitudinal and transverse dielectric functions starting from Maxwell's equations with a homogeneous medium in mind. Within this context we bring up the gauge choice discussion for the electromagnetic potentials. In the remaining part of this thesis, the term "dielectric function" refers to the *longitudinal* one, which plays an utmost role in many physical quantities like carrier lifetime, mobility, ground-state energy, isothermal compressibility etc. The

15

density response function is introduced based on the linear response formalism. Following this, we show the connection of the dielectric function with the diagrammatic quantity, the polarization insertion. Then, the widely used random phase approximation is obtained. The relations between the dynamic and static structure factors and the dielectric function are given. Finally, we close by presenting the role of dynamic local-field correction. The treatment in this chapter is general within the linear response framework and is not specific to three- and two-dimensions. As a matter of fact, the formalism can easily be extended from electrons to nonrelativistic nucleons[1] and also from fermions to bosons as well.

2.2 The Dielectric Function Concept

To know any electronic response of a specific medium, we need to apply an excitation. For this purpose we assume an applied external charge density, $\varrho_{ext}(\vec{r}, t)$ and its associated motion giving rise to the current density $\vec{j}_{ext}(\vec{r}, t)$. In particular, we choose the excitation to be of a travelling-wave type with spatial variation characterized by wave number q and temporal variation by the angular frequency ω, so that,

$$\varrho_{ext}(\vec{r}, t) = \rho_{ext}(\vec{q}, \omega)\, e^{i\vec{q}\cdot\vec{r}} e^{-i\omega t}, \tag{2.1}$$

$$\vec{j}_{ext}(\vec{r}, t) = \vec{J}_{ext}(\vec{q}, \omega)\, e^{i\vec{q}\cdot\vec{r}} e^{-i\omega t}. \tag{2.2}$$

Note that, any arbitrary function of $(\vec{r}, t)$ can be synthesized using the particular forms in Eqs. (2.1),(2.2) by means of the Fourier transform. In developing the formulation we have a homogeneous medium, in our minds. We must also mention that, we have independent control on the variables $\vec{q}$ and ω separately, that is to say, they are not related. Especially, those with antenna and electromagnetic theory background

---

[1] See our further remarks in the final conclusion chapter.

16

are inclined to think that $\omega/q = c$ which only governs the dispersion relation for free space electromagnetic wave propagation [44]. So, we probe the electric response of the medium under an excitation with an arbitrary $(\vec{q}, \omega)$ pair.

The charge and current densities are not independent but constrained by the continuity equation as

$$\nabla_{\vec{r}} \cdot \vec{j}_{ext}(\vec{r}, t) = -\frac{\partial \varrho_{ext}(\vec{r}, t)}{\partial t}, \qquad (2.3)$$

which becomes in $(\vec{q}, \omega)$ space

$$i\vec{q} \cdot \vec{J}_{ext}(\vec{q}, \omega) = i\omega \rho_{ext}(\vec{q}, \omega). \qquad (2.4)$$

As a response to these excitations an electromagnetic field will be generated in the medium governed by Maxwell's equations which are listed below[2] in 3D Fourier domain

$$i\vec{q} \times \vec{B}(\vec{q}, \omega) = -\frac{i\omega}{c} \vec{D}(\vec{q}, \omega) + \frac{4\pi}{c} \vec{J}_{ext}(\vec{q}, \omega), \qquad (2.5)$$

$$i\vec{q} \times \vec{E}(\vec{q}, \omega) = \frac{i\omega}{c} \vec{B}(\vec{q}, \omega), \qquad (2.6)$$

$$i\vec{q} \cdot \vec{D}(\vec{q}, \omega) = 4\pi \rho_{ext}(\vec{q}, \omega), \qquad (2.7)$$

$$i\vec{q} \cdot \vec{B}(\vec{q}, \omega) = 0. \qquad (2.8)$$

The dielectric function (DF) of a medium which is the primary quantity of interest is in general a tensor that relates the total electric field $\vec{E}$ to the displacement field $\vec{D}$ in that medium. If this relation is taken to be a linear one[3], it becomes

$$\vec{D}(\vec{q}, \omega) = \overline{\overline{\epsilon}}\,(\vec{q}, \omega)\,\vec{E}(\vec{q}, \omega). \qquad (2.9)$$

---

[2] cgs unit system is used throughout the text as this is more common and convenient in the small-scale device literature.

[3] This restricts our treatment to low electric field values. For example, in three-dimensional quantum Monte Carlo simulations, it has been observed that electric fields upto 2.0×10^8 V/cm, insure the linearity of the response [45].

It needs to be mentioned that, the dielectric constant was initially introduced to describe the reduction of the external field by the medium [44]. The classical texts on macroscopic electromagnetics (such as Ref. [46]) consider the dielectric constant concept to be applicable to dielectrics, that is to say, a medium having only bound charges that can to some extend polarize under an excitation. Here, we apply the dielectric constant concept (which now becomes a function of $\vec{q}$ and ω) to a medium made up of unbound electrons, called the electron liquid. For such a medium the wave number q dependence is inevitable, which needs to be briefly explained. To begin with, the DF depends on ω, which is also the case for dielectrics; for rapidly time-varying excitations, the constituent charges of the medium due to their finite masses follow the excitation by some delay. Furthermore, for the case of unbound carriers the response, or equivalently the DF has a spatial dispersion. In other words, the response at a specific point in space is governed by the magnitudes of the excitation at preceding moments of time not only at that particular space point but also in a certain neighborhood of that point. This is due to *motion* of the carriers which retain traces of the excitation at previous times, while being at other space locations [44]. To have an order of magnitude feeling, an appropriate length-scale for characterizing the size of the so-called nonlocality radius can be the Fermi wavelength, λ_F. In a medium with $n_{3D} = 10^{18}$ free electrons per cm^3, Fermi wave number is $k_F = \left(3\pi^2 n_{3D}\right)^{1/3} \simeq 3.1 \times 10^6$ cm^{-1}, and $\lambda_F = 2\pi/k_F \simeq 20$ nm. So, crudely speaking, an external perturbation in such a medium with a wavelength larger than say 100 nm will not be able to resolve the nonlocality present in the response, hence, such an excitation can enjoy a spatially nondispersive response, $\bar{\bar{\epsilon}}\ (q = 0, \omega)$.

2.3 Longitudinal versus Transverse Dielectric Functions

Recall that we have chosen the excitation to be of a travelling-wave type along the direction $\vec{q}$, so, we split the tensorial DF into longitudinal and transverse parts with respect to the propagation direction of the excitation, $\vec{q}$. Then [47],

$$\bar{\bar{\epsilon}}\,(\vec{q},\omega) = \epsilon_{\parallel}(\vec{q},\omega)\,\frac{\vec{q}\otimes\vec{q}}{q^2} + \epsilon_{\perp}(\vec{q},\omega)\left(\bar{\bar{1}} - \frac{\vec{q}\otimes\vec{q}}{q^2}\right). \qquad (2.10)$$

This equation only means that $\epsilon_{\parallel}(\vec{q},\omega)$ relates the component of the total $\vec{E}$ field along the $\vec{q}$ (i.e., wave propagation) direction to the same component of the displacement field, in other words, a longitudinal relation. Our work concerns only the longitudinal part of the tensorial DF. As a side note, the reason why macroscopic electromagnetic theory is ignorant to the discrimination between the longitudinal and transverse DFs is due to the fact that, in the long wavelength limit these two DFs become equal [47] as:

$$\lim_{\vec{q}\to 0}\epsilon_{\perp}(\vec{q},\omega) = \lim_{\vec{q}\to 0}\epsilon_{\parallel}(\vec{q},\omega) = \epsilon(\omega). \qquad (2.11)$$

To see the physical significance of the longitudinal DF, we first supplement the Maxwell's equations with the scalar and vector potentials $(V, \vec{A})$ as

$$\vec{B}(\vec{q},\omega) = i\vec{q}\times\vec{A}(\vec{q},\omega), \qquad (2.12)$$

$$\vec{E}(\vec{q},\omega) = \frac{i\omega}{c}\,\vec{A}(\vec{q},\omega) - i\vec{q}V(\vec{q},\omega). \qquad (2.13)$$

Of particular importance is the choice of the gauge and in this work we use the Coulomb gauge[4] also known as the transverse or radiation gauges. The name "radiation gauge" stems from the fact that transverse radiation fields are given by the vector potential $\vec{A}$ alone, the instantaneous Coulomb potential contributing only to

---

[4] This is the most common choice in nonrelativistic many-body treatments.

near fields. This gauge is particularly useful in quantum electrodynamics as a quantum mechanical description of photon necessitates the quantization of only the vector potential [48], whereas the instantaneous Coulomb field does not represent independent dynamical degrees of freedom but is fully determined by the charges [49]. In the Coulomb gauge we have

$$i\vec{q} \cdot \vec{A}(\vec{q}, \omega) = 0. \tag{2.14}$$

That is, the vector potential is transverse (with respect to wave propagation direction, $\vec{q}$). Then Gauss's law turns into

$$
\begin{aligned}
4\pi\rho_{ext}(\vec{q}, \omega) &= i\vec{q} \cdot \vec{D}(\vec{q}, \omega), \\
&= i\vec{q} \cdot \overline{\overline{\epsilon}}\,(\vec{q}, \omega)\,\vec{E}(\vec{q}, \omega).
\end{aligned}
\tag{2.15}
$$

Due to the dot product with $\vec{q}$ only the longitudinal component of $\overline{\overline{\epsilon}}$ is selected, giving

$$4\pi\rho_{ext}(\vec{q}, \omega) = i\epsilon_\|(\vec{q}, \omega)\,\vec{q} \cdot \vec{E}(\vec{q}, \omega), \tag{2.16}$$

and using Eq. (2.13) we obtain for the scalar potential

$$V(\vec{q}, \omega) = \frac{4\pi\rho_{ext}(\vec{q}, \omega)}{\epsilon_\|(\vec{q}, \omega)\,q^2}. \tag{2.17}$$

Hence, this equation reminds us that Poisson's equation is also valid for the AC (time-varying) case, provided that we work in the Coulomb gauge. It is important to note that the (screened) scalar potential depends only on the longitudinal DF. Thus the interaction of two electrons via a screened Coulomb potential energy is

$$U_{scr}(\vec{q}, \omega) = e^2 \frac{4\pi}{\epsilon_\|(\vec{q}, \omega)\,q^2}. \tag{2.18}$$

In this expression if we identify the electronic charge e as the coupling constant, then the remaining term corresponds to the dressed propagator of a longitudinal photon

as

$$D_{\parallel}(\vec{q},\omega) = \frac{4\pi}{\epsilon_{\parallel}(\vec{q},\omega)\, q^2}, \tag{2.19}$$

so that diagrammatically we represent the Coulomb electron-electron interaction as

the exchange of a longitudinal photon.
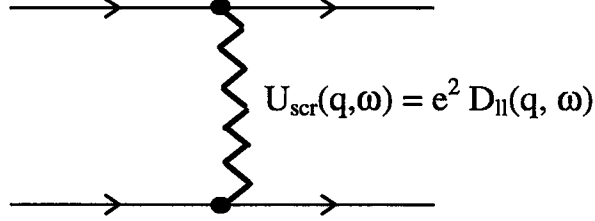
Figure 2.1: Diagram showing the dressed longitudinal photon exchange by the zig zag lines. The solid line indicates the electron propagator.

For completeness, we also list the dressed transverse photon propagator [47]

$$\bar{\bar{D}}_{\perp}(\vec{q},\omega) = \frac{4\pi c}{\omega^2\, \epsilon_{\perp}(\vec{q},\omega) - q^2\, c^2} \left(\bar{\bar{1}} - \frac{\vec{q} \otimes \vec{q}}{q^2} \right). \tag{2.20}$$

The poles of the longitudinal and transverse photon propagators determine respectively the longitudinal and transverse eigenmodes of the dielectric medium, which are given by

$$\epsilon_{\parallel}(\vec{q},\omega) = 0, \tag{2.21}$$

$$\omega^2\, \epsilon_{\perp}(\vec{q},\omega) = q^2\, c^2. \tag{2.22}$$

These two equations yield the longitudinal and transverse modes that the medium is willing to support, just like an LC resonance circuit that is willing to oscillate at the frequency $\omega_0 = \frac{1}{\sqrt{LC}}$. The main additional requirement of quantum mechanics is that these oscillations should be in discrete packets (quanta) of energy. The quantum of a

21

longitudinal/transverse oscillation of the EL is given the name longitudinal/transverse plasmon. In our work the former plays a decisive role.

In the literature, instead of the word "longitudinal photon", just Coulomb interaction is used, and *photon* is reserved to describe the transverse propagator. At this point we can quote Mahan [42]: "One should keep in mind that the interaction between two charges occurs via both scalar and vector potentials. How we divide the interaction between scalar and vector potentials is somewhat arbitrary and is determined by the gauge condition. After making this choice, we assigned the word *photon* to the vector potential part. This division between photon and Coulomb is arbitrary, and both parts should really be viewed as arising from photons."

A frequently used gauge in quantum field theory is the Lorentz gauge having manifestly covariant form. In the Lorentz gauge all four auxiliary potentials $(V, \vec{A})$ are quantized leading to two transverse photons (as in the Coulomb gauge), one longitudinal photon and one scalar (time-like) photon. The last two are virtual quanta which cannot be probed as free particles. It can be shown that the overall effect of the longitudinal and scalar photons of the Lorentz gauge is equivalent to the instantaneous Coulomb interaction of the Coulomb gauge [49][5]. Another noteworthy point is that, in the Coulomb gauge, the scalar potential $V(\vec{r}, t)$ mediates the excitation $\rho_{ext}(\vec{r}, t)$ without any time delay, that is to say, the Coulomb interaction is instantaneous. This does not contradict with relativity, again quoting Mahan [42] here:

> The net[6] interaction may not have a component which is instantaneous. In fact, for a frequency-dependent charge density, at distances large compared to c/ω, one finds that the photon part of the interaction produces a term $-e^2/r$ which exactly cancels the instantaneous Coulomb interaction. The remaining parts of the photon contribution are the net retarded

---

[5] I would like to express my gratitude to Prof. A. Gökalp for an illuminating discussion on this subject.

[6] Coulomb plus photon is meant.

interaction. In solids we are usually concerned with interaction over short distances. Then the retardation is unimportant for most problems. In the study of the homogeneous electron gas, the photon part is small and may be neglected. In real solids, the photon part causes some crystal field effects, which is an unexciting many-body effect. The main effect of retardation is the polariton effects at long wavelength. In general, we have chosen the Coulomb gauge because the instantaneous Coulomb interaction is usually a large term which forms a central part of the analysis, while the photon parts are usually secondary. Like most generalizations, this one has its exceptions.

Based on Mahan's comments above, especially regarding the homogeneous electron gas (liquid), we do not include the electron-electron interaction mediated by the vector potential $\vec{A}$ (photons) while working in the Coulomb gauge. We shall again be ignorant to photon part in the quasi-two-dimensional EL which is not a homogeneous system[7].

2.4 The Computation of the Dielectric Function

Having discussed the basic character of the DF in the previous section, there remains its computation. This is not an easy task for the EL which is a quantum many-body system; the first successful attempts came not until 1950's, even though the foundations of the solid-state quantum mechanics were laid before 1930's. We defer the detailed discussion of the EL model till the next chapter.

As in the previous section we consider some arbitrary charge density $\varrho_{ext}(\vec{r}, t)$ and the associated current density $\vec{j}_{ext}(\vec{r}, t)$. We saw also in the previous section that the longitudinal DF characterizes how charge densities interact, whereas the current density interactions are described by the tensorial transverse DF. As a matter of fact, they are related to density-density and current-current correlation functions,

---

[7] Those who are interested in the use of transverse DF in quasi-two-dimensional systems can refer to Dahl and Sham's work [50].

respectively [47]. The EL in response to the external charge density, ϱ_{ext} will screen this perturbation but subject to two important constraints i) Pauli exclusion principle, and ii) Coulomb repulsion among the constituent electrons of the EL. A successful longitudinal DF should take into account these two effects as much as possible. Due to $\varrho_{ext}(\vec{r}, t)$, the EL no longer preserves its homogeneity and an induced charge density $\varrho_{ind}(\vec{r}, t)$ is produced in response. Hence, the total screened charge density becomes

$$\varrho_{scr}(\vec{r}, t) = \varrho_{ext}(\vec{r}, t) + \varrho_{ind}(\vec{r}, t), \qquad (2.23)$$

which is in reciprocal space

$$\rho_{scr}(\vec{q}, \omega) = \rho_{ext}(\vec{q}, \omega) + \rho_{ind}(\vec{q}, \omega). \qquad (2.24)$$

We denote the corresponding number densities by $n_{scr}(\vec{q}, \omega)$, $n_{ext}(\vec{q}, \omega)$ and $n_{ind}(\vec{q}, \omega)$ with the definition $\rho(\vec{q}, \omega) = e\, n(\vec{q}, \omega)$ where e denotes the positron charge. These, in turn, generate the potential energies[8]

$$U_{ext}(\vec{q}, \omega) = U^0(\vec{q})\, n_{ext}(\vec{q}, \omega), \qquad (2.25)$$

$$U_{ind}(\vec{q}, \omega) = U^0(\vec{q})\, n_{ind}(\vec{q}, \omega), \qquad (2.26)$$

$$U_{scr}(\vec{q}, \omega) = U^0(\vec{q})\, n_{scr}(\vec{q}, \omega),$$

$$= U_{ext}(\vec{q}, \omega) + U_{ind}(\vec{q}, \omega), \qquad (2.27)$$

where $U^0(\vec{q})$ denotes the instantaneous bare $1/R$ Coulomb interaction which is

$$U^0(\vec{q}) = \begin{cases} \frac{4\pi e^2}{q^2} & \text{in 3D} \\ \\ \frac{2\pi e^2}{q} & \text{in 2D} \end{cases} \qquad (2.28)$$

---

[8] In the literature the word potential is used instead of potential energy and denoted by V instead of U. We try to avoid this, as it becomes confusing when the actual scalar potential is also used in the same text.

The relation between the potential energies is through the longitudinal DF as

$$U_{scr}(\vec{q}, \omega) = \frac{U_{ext}(\vec{q}, \omega)}{\epsilon(\vec{q}, \omega)}, \tag{2.29}$$

implying

$$n_{scr}(\vec{q}, \omega) = \frac{n_{ext}(\vec{q}, \omega)}{\epsilon(\vec{q}, \omega)}. \tag{2.30}$$

Note that in these equations and in the rest of this work we denote the longitudinal DF simply as

$$\epsilon_{\parallel}(\vec{q}, \omega) \rightarrow \epsilon(\vec{q}, \omega),$$

for notational brevity an also the word "longitudinal" will be dropped, as we address only density-density interactions.

2.4.1   Density Response Function

The following relation is enforced between the external density and the induced density:

$$n_{ind}(\vec{q}, \omega) = \chi(\vec{q}, \omega)\, U^0(\vec{q})\, n_{ext}(\vec{q}, \omega) = \chi(\vec{q}, \omega)\, U_{ext}(\vec{q}, \omega), \tag{2.31}$$

being a linear relation, this restricts our formulation to the linear response framework; that is to say, response to each frequency component of the excitation is assumed to be independent, or in electrical engineering terminology, intermodulation products are ignored under a two-tone excitation. χ here, is referred as the density response function or just as the susceptibility. So, we arrive at the following equation that relates the density response function to the DF

$$\frac{1}{\epsilon(\vec{q}, \omega)} = 1 + U^0(\vec{q})\, \chi(\vec{q}, \omega). \tag{2.32}$$

25

An alternative expression is reached if we introduce the screened density response function by

$$n_{ind}(\vec{q}, \omega) = \chi_{scr}(\vec{q}, \omega) \, U^0(\vec{q}) \, n_{scr}(\vec{q}, \omega), \qquad (2.33)$$

as

$$\epsilon(\vec{q}, \omega) = 1 - U^0(\vec{q}) \, \chi_{scr}(\vec{q}, \omega). \qquad (2.34)$$

2.4.2 Polarization Insertion

These equations help to follow the literature more easily, however, still there remains the question: *How to compute* $\epsilon(\vec{q}, \omega)$? So, we introduce yet one more expression for the DF, but this time using Feynman's diagrammatic techniques we can reach to concrete computation. Simply, the screened (dressed) two-body interaction potential $U(\vec{q}, \omega)$ using Dyson's equation [51] becomes

$$U(\vec{q}, \omega) = U^0(\vec{q}) + U^0(\vec{q}) \, \pi^*(\vec{q}, \omega) \, U(\vec{q}, \omega). \qquad (2.35)$$

$\pi^*(\vec{q}, \omega)$ is the so-called proper polarization insertion. Eq. (2.35) is represented diagrammatically as
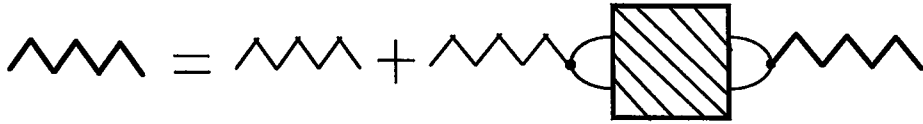
Figure 2.2: Diagrammatic representation of the Dyson's equation for the dressed insertion, shown by the heavy zig-zag lines and the bare interaction is indicated by the normal zig-zag lines. The sectioned box stands for the proper polarization insertion.

So we get

$$U(\vec{q}, \omega) = \frac{U^0(\vec{q})}{\epsilon(\vec{q}, \omega)} = \frac{U^0(\vec{q})}{1 - U^0(\vec{q}) \, \pi^*(\vec{q}, \omega)}, \qquad (2.36)$$

26

which gives

$$\epsilon(\vec{q},\omega) = 1 - U^0(\vec{q})\,\pi^*(\vec{q},\omega). \tag{2.37}$$

When diagrammatic quantities come into play, a word of caution is generally made regarding causality. The Wick's theorem [51] which underlies Feynman's diagrammatic rules, is applicable to time-ordered operators. However, the real physical quantities (actually the response functions) need to be retarded functions due to the causality principle. For this reason, the diagrammatic quantities, after being computed in time-ordered form should be converted to retarded form using the analytic relation between the two [51]. In our work, all response functions such as the DF refers to retarded functions, but for notational simplicity an extra label is not put.

The equation above reveals that the screened density response function, $\chi_{scr}(\vec{q},\omega)$ corresponds to the proper polarization insertion in the diagrammatic dictionary. Similarly, the density response function $\chi(\vec{q},\omega)$ corresponds to the polarization insertion

$$\chi(\vec{q},\omega) = \frac{\chi_{scr}(\vec{q},\omega)}{\epsilon(\vec{q},\omega)} = \pi(\vec{q},\omega). \tag{2.38}$$

2.4.3 Random Phase Approximation

Now we are in a position to propose the first approximation for the DF by replacing the $\pi^*(\vec{q},\omega)$ with $\pi^0(\vec{q},\omega)$, where the latter refers to the simple ring diagram without any interaction lines present, noninteracting EL polarization insertion

As π^0 replaces the proper polarization insertion, it corresponds to the summation of all ring diagrams for the polarization insertion $\pi(\vec{q},\omega)$. This approximation is the celebrated random phase approximation (RPA) and $\pi^0(\vec{q},\omega)$ is generally called the Lindhard function [52][9]. Equivalently, RPA corresponds to approximating the

---

[9] Actually Lindhard is a generic name but we shall also use the word Stern function for the 2D EL.

$G^0_{\sigma,\nu}(k)$

q

q

$G^0_{\sigma,\nu}(k+q)$
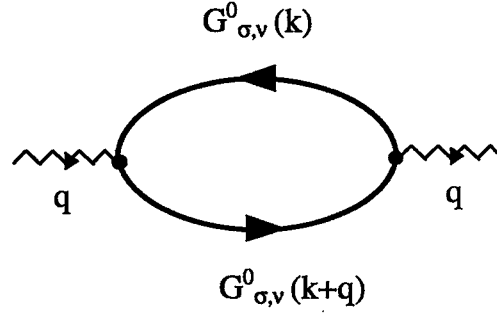
Figure 2.3: Simple ring diagram, with the spin and valley labels of the electrons indicated.

screened density response function by the Lindhard function (also to be denoted in this text by $\chi^0(\vec{q},\omega)$). Summarizing the relations for the RPA,

$$\chi^{RPA}_{scr}(\vec{q},\omega) = \chi^0(\vec{q},\omega), \qquad (2.39)$$

$$\epsilon^{RPA}(\vec{q},\omega) = 1 - U^0(\vec{q})\,\chi^0(\vec{q},\omega), \qquad (2.40)$$

$$\chi^{RPA}(\vec{q},\omega) = \frac{\chi^0(\vec{q},\omega)}{1 - U^0(\vec{q})\,\chi^0(\vec{q},\omega)}. \qquad (2.41)$$

The physical outcome of these approximations is that the electrons of the EL are regarded as noninteracting particles but within a field of the external potential as well as the self-consistent average field of the induced charges. So, the many-body effects are to some extend contained in this mean field. However, RPA is well-known to be successful for the long wavelength phenomena. One of the aims of this work is to have a better feeling about the validity range of the widely used RPA.

2.5   Relation to Dynamic and Static Structure Factors

In the following chapter it is shown that the DF is complex for an arbitrary value of $(\vec{q},\omega)$. Through Eq. (2.32) one can see that the density response function will also be

28

complex. In other words, they are of the form

$$\epsilon(\vec{q},\omega) \;=\; \epsilon_{Re}(\vec{q},\omega) + i\,\epsilon_{Im}(\vec{q},\omega),$$

$$\chi(\vec{q},\omega) \;=\; \chi_{Re}(\vec{q},\omega) + i\,\chi_{Im}(\vec{q},\omega).$$

The real parts of these functions represent the actual polarization of the medium (screening), which is a reversible event, whereas the imaginary parts account for the energy transfer *from* the external source *to* the medium[10], an irreversible process. The energy transfer to the medium is possible when the medium has an eigenstate at that particular $(\vec{q},\omega)$ excitation. Actually these eigenoscillations are rather called *the elementary excitations* of the medium, which are for the density excitations [36]: i) single electron-hole pair excitations, ii) multiple electron-hole pair excitations iii) collective plasma wave excitations. Quantum mechanics also tells us that these excitation energies should be multiples of certain quanta. However, one should not think that the second item, multiple pair excitations are just the multiple single-pair quanta; multiple pair excitations account for the nonlinear processes within the medium and as a matter of fact they are very hard to include in the theory and usually left out altogether as in our case. The point we want to make about the real and imaginary parts of $\epsilon(\vec{q},\omega)$ and $\chi(\vec{q},\omega)$ is that the screening act is inevitably accompanied by the energy absorbtion from the external source in the form of elementary excitations. We would like to quote Pines and Nozières [36] here "... (plasma oscillation) is complementary to the existence of screening. When the electrons move to screen a charge disturbance in the plasma, they will, in general, tend to overshoot the mark somewhat. They are consequently pulled back toward that region, overshoot again, etc.,

---

[10] Note that the energy transfer is one-way as we work at $T = 0^{\circ}K$, and the medium is in its lowest (ground) state.

in such a way that an oscillation is set up about the state of charge neutrality."

The function which characterizes the density excitation spectrum of the medium at hand is the dynamic structure (form) factor, denoted by $S(\vec{q}, \omega)$. Based on the discussion in the previous paragraph, it will not be a surprise to see that the dynamic form factor is related to the imaginary (i.e., dissipative) parts of ϵ and χ as

$$S(\vec{q}, \omega) = -\frac{\hbar}{n \pi} \text{Im}\{\chi(\vec{q}, \omega)\} = -\frac{\hbar}{n \pi U^0(\vec{q})} \text{Im}\{\frac{1}{\epsilon(\vec{q}, \omega)}\}, \qquad (2.42)$$

where n is the particle density of the medium. The dynamic form factor, $S(\vec{q}, \omega)$ is also the Fourier transform of $S(\vec{r}, t)$ which characterizes the density correlations separated by a distance $\vec{r}$ in space and t in time. Another function that is readily measured by experiments is the static structure (form) factor, denoted by $S(\vec{q})$, which is obtained from $S(\vec{q}, \omega)$ as

$$S(\vec{q}) = \int_0^\infty d\omega \, S(\vec{q}, \omega). \qquad (2.43)$$

The static structure factor characterizes the instantaneous density oscillations [36] as can be seen from Eq. (2.43), which is essentially the spectral Fourier transform of $S(\vec{q}, \omega)$ evaluated at $t = 0$ (i.e., instantaneous). If we use Eq. (2.42) in (2.43), we obtain a relation between the static structure factor and the DF as

$$S(\vec{q}) = -\frac{\hbar}{n \pi U^0(\vec{q})} \int_0^\infty d\omega \, \text{Im}\{\frac{1}{\epsilon(\vec{q}, \omega)}\}, \qquad (2.44)$$

which we shall make use of in the following chapter. As another comment, the Eqs. (2.42) and (2.43) are given usually in different forms in the literature, however, the end result, Eq. (2.44) should come out as given here.

There is also an alternative way of calculating the static structure factor, by rotating the frequency integration path from real to imaginary axis [53][11]. The expressions

---

[11] I am grateful to Dr. Bilal Tanatar for suggesting me this alternative method.

are then modified as follows:

$$S(\vec{q}) \;=\; \frac{-\hbar}{\pi\,n}\int_0^\infty d\omega\,\chi(\vec{q},i\omega), \tag{2.45}$$

$$\chi(\vec{q},i\omega) \;=\; \frac{1}{U^0(\vec{q})}\left[\frac{1}{\epsilon(\vec{q},i\omega)}-1\right], \tag{2.46}$$

$$S(\vec{q}) \;=\; \frac{-\hbar}{\pi\,n\,U^0(\vec{q})}\int_0^\infty d\omega\,\left[\frac{1}{\epsilon(\vec{q},i\omega)}-1\right]. \tag{2.47}$$

In our computer code we employ both ordinary and rotated frequency integrations based on their individual benefits.

Finally, from the static structure factor the pair correlation function, $g(\vec{r})$ is obtained (essentially by a Fourier transform) as

$$g(\vec{r}) = 1 + \frac{1}{n}\int\frac{d^D q}{(2\pi)^D}\left[S(\vec{q})-1\right]e^{-i\vec{q}\cdot\vec{r}}, \tag{2.48}$$

where D refers to the dimensionality of the medium (for e.g., in three-dimensions $D=3$). The pair correlation function is a probability[12] that measures the likelihood of finding two electrons separated by a distance $\vec{r}$. The pair correlation function is a handy visual tool for demonstrating the Pauli-Coulomb hole around each electron and is also used for assessing approximate schemes for the DF; most approaches violate the nonnegative property of the pair distribution function.

2.6 Dynamic Local-Field Correction

The RPA density response function (χ^{RPA}) can be corrected by a term called the local-field correction (LFC), denoted by $G(\vec{q},\omega)$, so that, formally the exact density response function (χ) is reached. Stating this in mathematical terms [54]

$$\frac{1}{\chi(\vec{q},\omega)} = \frac{1}{\chi^{RPA}(\vec{q},\omega)} + U^0(\vec{q})\,G(\vec{q},\omega). \tag{2.49}$$

---

[12] Being a probability, this function needs to be nonnegative.

In other words, knowing the *exact* LFC is equivalent to knowing the exact density response function. The problem is that, the determination of the LFC is just as difficult. A resonable question at this step is why to choose a form like this for correcting χ^{RPA}, rather than, for instance

$$\chi(\vec{q},\omega) = \chi^{RPA}(\vec{q},\omega) + C(\vec{q},\omega).$$

The reason is because the form in Eq. (2.49) has the nice feature that the correction term $G(\vec{q},\omega)$ can be attributed a direct physical meaning as its name implies. Namely, $G(\vec{q},\omega)$ has the mission to incorporate the local structure on top of the self-consistent mean-field brought by the RPA. The local structure is due to so-called Pauli and Coulomb holes around each constituent electron of the EL; there exists a neighborhood within which same spin electrons are repelled due to Pauli exclusion principle, furthermore, all electrons are also subject to Coulomb repulsion.

The DF (which is formally exact if the exact LFC is known) becomes

$$\epsilon^{LFC}(\vec{q},\omega) = \frac{1 - U^0(\vec{q})\,\chi^0(\vec{q},\omega)\,[1 - G(\vec{q},\omega)]}{1 + U^0(\vec{q})\,\chi^0(\vec{q},\omega)\,G(\vec{q},\omega)}. \tag{2.50}$$

2.6.1   Static Local-Field Correction

As mentioned above the determination of the dynamic LFC is a formidable problem as the exact many-body solution of the EL itself. The common sense, at this point suggests for approximate schemes led by physical guidence. The fundamental and the most crude approximation done is to neglect the frequency dependence of the LFC, i.e., a static LFC, $G(\vec{q})$. As a matter of fact almost all dielectric formulations of the EL available today are based on a static LFC, and the dynamic case is the challenge for the current front-line researchers [55]. In using a static LFC, basically the inertia

of the Pauli-Coulomb hole is neglected. The particular static LFC that we employ in our work has one appealing feature among the other LFC candidates: the static local-field is determined self-consistently. If we include the fact that the mean-field is also self-consistent, this makes a double self-consistency of the effective field. In the next chapter we elaborate in detail the method we are using.

CHAPTER 3

THREE- AND TWO-DIMENSIONAL

ELECTRON LIQUIDS: FORMULATION

3.1   Introduction

This chapter is complementary to the previous chapter in serving for the formulation. As compared to Chapter 2 containing the general formalism, the present chapter focuses on the explicit expressions for the three- and two-dimensional electron liquid, with the aim of guiding possible future researchers. Before embarking on the specific expressions, however, we first introduce the electron liquid (EL) model. Singwi and coworkers' original derivation for the STLS LFC is revisited for the purpose of presenting a much more detailed account applicable to a general D-dimensional EL. We end this chapter by giving the simplified explicit STLS LFC expressions for the 3D and 2D EL. For the sake of completeness we also include relevant expressions for the quasi-one- dimensional (Q1D) EL.

34

3.2 The Electron Liquid Model

The electron liquid (EL) is a standard model system of many-body quantum mechanics. It contains interacting dynamic electrons and a smeared out (i.e., homogeneous) positive background enabling the charge neutrality of the system. The background is taken to be rigid, nonpolarizable. This model is also named as the *electron gas* in some literature, but we prefer the word *liquid* as the correlations among the electrons are quite significant and short-range order exists as in classical liquids[1]. The long-range Coulomb interaction among the electrons renders impossible, the decoupling of individual electronic motions, and therefore, the EL remained to be the workhorse of many-body physics for the past four decades. More importantly from practical point of view, the EL offers to be the generic model for characterizing the conduction electrons in metals, and especially low-dimensional doped semiconductors such as heterojunctions, quantum wells, and to some extend quantum wires. For this purpose we use as the quantum labels for the constituent electrons of the EL, the spin z-projection (σ), the wave vector ($\vec{k}$) and a valley index (ν) to account for the common case of energetically-degenerate valleys. The electrons are assumed to have an isotropic effective mass, m^* and the dielectric polarization of the bound electrons are incorporated by a background dielectric constant, κ.

The shortcomings of the EL model in representing the real systems are the lack of ionic lattice and disorder effects. The latter is to some extend remedied by introducing a phenomological imaginary part to the Lindhard function. As for the ionic lattice, the dielectric function formalism can be extended to include the Fröhlich electron-phonon coupling [42]. All throughout this text we work in zero-temperature, where

---

[1] Further supports are given in the next chapter within the discussion of the ground-state energy.

the non-interacting Fermi occupation function is of the step form.

3.3   3D Electron Liquid Expressions for a General $G(q)$

We first list the expressions relating electron density (n_{3D}), Fermi wave number (k_F), and r_s for an 3D EL with arbitrary spin and valley degeneracy.

$$n_{3D} = \frac{1}{V} \sum_{\vec{k},\sigma,\nu}^{\vec{k}_F, g_s, g_v} n_{\vec{k},\sigma,\nu} = g_s g_v \frac{k_F^3}{6\pi^2}, \qquad (3.1)$$

where V is the volume terminated by periodic boundary conditions and we introduce an overall degeneracy parameter g_d to represent compactly the spin and valley degeneracies, as $g_d = g_s g_v$. Then k_F depends on n_{3D} as

$$k_F = \left(\frac{6\pi^2 n_{3D}}{g_d} \right)^{1/3}. \qquad (3.2)$$

The most important and actually the only parameter in EL theory is r_s defined as the average electron distance in units of the effective Bohr radius, a_B^* of the system

$$n_{3D} = \frac{1}{\frac{4}{3}\pi(r_s a_B^*)^3}, \qquad (3.3)$$

and

$$k_F = \frac{1}{r_s a_B^*} \left(\frac{9\pi}{2g_d} \right)^{1/3}. \qquad (3.4)$$

The effective Bohr radius is given by

$$a_B^* = \frac{\kappa \hbar^2}{m^* e^2}, \qquad (3.5)$$

where κ is the background dielectric constant and m^* is the (isotropic) effective mass of the electrons as introduced in the previous section. a_B^* is an important length-scale and we shall use it also in 2D EL. The bare $1/R$ Coulomb interaction in reciprocal space is

$$U_{3D}^0(q) = \frac{4\pi e^2}{\kappa q^2}. \qquad (3.6)$$

The dynamo of the DF is still the noninteracting polarization insertion, $\pi^0(q,\omega)$, the Lindhard function. We shall generalize it for an arbitrary degeneracy factor, g_d. In real space its representation becomes

$$\pi^0(x_1,x_2) = \frac{-i}{\hbar} \sum_{\sigma_1,\sigma_2} \sum_{\nu_1,\nu_2} G^0_{\sigma_1\sigma_2,\nu_1\nu_2}(x_1,x_2)\, G^0_{\sigma_2\sigma_1,\nu_2\nu_1}(x_2,x_1), \qquad (3.7)$$

where G^0 denotes the noninteracting propagator and x_1, x_2 denote both space and time variables. For the homogeneous system at hand working in the reciprocal space is suitable via the Fourier transform which yields

$$\pi^0(\vec{q},\omega_q) = \frac{-ig_d}{\hbar} \int \frac{d^3k\, d\omega_k}{(2\pi)^4} G^0(\vec{k},\omega_k)\, G^0(\vec{q}+\vec{k},\omega_q+\omega_k). \qquad (3.8)$$

We state the result for $U^0_{3D}\,\pi^0_{3D}$ as it always occurs in our expressions in this product form

$$\mathrm{Re}\left\{U^0_{3D}(q_n)\,\pi^0_{3D}(q_n,\nu)\right\} = \left(\frac{2g_d^4}{9\pi^4}\right)^{1/3} \frac{r_s}{q_n^2}\left[-1 + \frac{1}{2q_n}(1-\nu_-^2)\ln\left|\frac{1+\nu_-}{1-\nu_-}\right| \right.$$
$$\left. - \frac{1}{2q_n}(1-\nu_+^2)\ln\left|\frac{1+\nu_+}{1-\nu_+}\right|\right], \qquad (3.9)$$

$$\mathrm{Im}\left\{U^0_{3D}(q_n)\,\pi^0_{3D}(q_n,\nu)\right\} = -\frac{r_s\pi}{2q_n^3}\left(\frac{2g_d^4}{9\pi^4}\right)^{1/3}$$

$$\times \begin{cases} (1-\nu_-^2) & \text{for } q_n^2/2 + q_n \geq \nu \geq |q_n^2/2 - q_n| \\ 2\nu & \text{for } q_n \leq 2 \text{ and } q_n - q_n^2/2 \geq \nu \quad (3.10) \\ 0 & \text{otherwise} \end{cases}$$

where we use the reduced units for the wave number and frequency as $q_n = q/k_F$, $\nu = \frac{\hbar\omega}{(2E_F)}$, and

$$\nu_\pm = \frac{\nu}{q_n} \pm \frac{q_n}{2}.$$

We shall also make use of the Lindhard function with imaginary frequency as mentioned in the previous chapter; its form in 3D becomes

$$U_{3D}^0(q_n)\,\pi_{3D}^0(q_n,i\nu) = -\frac{r_s}{q_n^2}\left(\frac{2g_d^4}{9\pi^4}\right)^{1/3}\left\{1 - \frac{\nu}{q_n}\tan^{-1}\left[\frac{q_n(2-q_n)}{2\nu}\right]\right.$$

$$\left. - \frac{\nu}{q_n}\tan^{-1}\left[\frac{q_n(2+q_n)}{2\nu}\right] + \frac{(q_n^2-4)-4(\frac{\nu}{q_n})^2}{8q_n}\ln\left[\frac{(q_n-2)^2+4(\frac{\nu}{q_n})^2}{(q_n+2)^2+4(\frac{\nu}{q_n})^2}\right]\right\}.\quad(3.11)$$

Using Eqs. (3.9) and (3.10) in Eq. (2.50) the expression for the 3D DF, $\epsilon_{3D}(q_n,\nu)$ is reached; we state the static case that will be frequently used

$$\epsilon_{3D}(q_n,0) = \frac{1 + \left(\frac{2g_d^4}{9\pi^4}\right)^{1/3}\frac{r_s}{q_n^2}\left(1 - \frac{4-q_n^2}{4q_n}\ln\left|\frac{2-q_n}{2+q_n}\right|\right)[1-G_{3D}(q_n)]}{1 - \left(\frac{2g_d^4}{9\pi^4}\right)^{1/3}\frac{r_s}{q_n^2}\left(1 - \frac{4-q_n^2}{4q_n}\ln\left|\frac{2-q_n}{2+q_n}\right|\right)G_{3D}(q_n)}.\quad(3.12)$$

As mentioned in the previous chapter, there are two possibilities for the computation of the static structure factor, $S(q)$: integration over the real frequency axis (ω) or over the imaginary frequency axis ($i\omega$). The former contains contributions from the plasmon and electron-hole pair excitations as

$$S_{3D}^{\text{e-h}}(q_n) = -\frac{3q_n^2}{2r_s}\left(\frac{9\pi}{2g_d^4}\right)^{1/3}\int_{\nu_{min}(q_n)}^{\nu_{max}(q_n)}d\nu\,\text{Im}\left\{\frac{1}{\epsilon_{3D}(q_n,\nu)}\right\},\quad(3.13)$$

where $\nu_{max}(q_n) = q_n^2/2 + q_n$ and $\nu_{min}(q_n) = \max\left\{0,\,q_n^2/2 - q_n\right\}$.

$$S_{3D}^{\text{plas}}(q_n) = -\frac{3\pi^2}{2g_d^2}q_n^6\frac{1}{r_s^2}\left(\frac{9\pi}{2g_d}\right)^{2/3}$$

$$\times\frac{\left[1 + U_{3D}^0(q_n)\pi_{3D}^0(q_n,\nu)G_{3D}(q_n)\right]^2}{\left[\nu_-\ln\left(\frac{\nu_--1}{\nu_-+1}\right) + \nu_+\ln\left(\frac{\nu_++1}{\nu_+-1}\right)\right]}\theta(\nu - \nu_{max}(q_n)),\quad(3.14)$$

where ν and $\nu_\pm$ in this equation have to be evaluated at the plasmon frequency ν_p, and $\theta(\cdot)$ denotes the unit step function. Finally, the imaginary frequency integration for $S(q)$ simplifies to

$$S_{3D}(q_n) = \frac{3}{2\pi}\int_0^\infty d\nu$$

$$\frac{\left\{1 - \frac{\nu}{q_n}\tan^{-1}\left[\frac{q_n(2-q_n)}{2\nu}\right] - \frac{\nu}{q_n}\tan^{-1}\left[\frac{q_n(2+q_n)}{2\nu}\right] + \frac{(q_n^2-4)-4(\frac{\nu}{q_n})^2}{8q_n}\ln\left[\frac{(q_n-2)^2+4(\frac{\nu}{q_n})^2}{(q_n+2)^2+4(\frac{\nu}{q_n})^2}\right]\right\}}{1 - U_{3D}^0(q_n)\,\pi_{3D}^0(q_n,i\nu)\,[1-G_{3D}(q_n)]}.$$

$$(3.15)$$

Pair correlation function is the inverse Fourier transform of the static structure factor with the explicit form

$$g_{3D}(r_n) = 1 + \frac{3}{g_d} \int_0^\infty dq_n \frac{q_n}{r_n} \sin(q_n r_n) \left[S_{3D}(q_n) - 1\right], \qquad (3.16)$$

where $r_n = r k_F$. For $r_n = 0$ this expression reduces to

$$g_{3D}(r = 0) = 1 + \frac{3}{g_d} \int_0^\infty dq_n \, q_n^2 \left[S_{3D}(q_n) - 1\right]. \qquad (3.17)$$

Finally, we state the expression for the statically screened interaction in real space which is the inverse Fourier transform of the corresponding interaction in reciprocal space

$$\overline{U}_{3D,scr}(r_n) = \frac{2}{r_n r_s} \left(\frac{9\pi}{2g_d}\right)^{1/3} + \frac{4}{\pi r_s} \left(\frac{9\pi}{2g_d}\right)^{1/3} \int_0^\infty dq_n \frac{\sin(q_n r_n)}{q_n \, r_n} \left[\frac{1}{\epsilon_{3D}(q_n)} - 1\right], \qquad (3.18)$$

in effective Rydberg units designated by an overbar; we add and subtract unscreened Coulomb potential for computational reasons [56].

3.4 2D Electron Liquid Expressions for a General $G(q)$

We shall proceed in the same order of the 3D EL; the expressions relating electron density (n_{2D}), Fermi wave number (k_F), and r_s for an 2D EL with arbitrary spin and valley degeneracy are

$$n_{2D} = \frac{1}{A} \sum_{\vec{k},\sigma,\nu}^{\vec{k}_F, g_s, g_v} n_{\vec{k},\sigma,\nu} = g_d \frac{k_F^2}{4\pi}, \qquad (3.19)$$

where A is the area again terminated by periodic boundary conditions. k_F depends on n_{2D} as

$$k_F = \left(\frac{4\pi n_{2D}}{g_d}\right)^{1/2}. \qquad (3.20)$$

39

The relation between n_{2D} and r_s is

$$n_{2D} = \frac{1}{\pi (r_s a_B^*)^2}, \qquad (3.21)$$

and

$$k_F = \frac{2}{r_s a_B^*} \frac{1}{\sqrt{g_d}}. \qquad (3.22)$$

In these expressions the effective Bohr radius is the same as the 3D case; that is, the average distance for a $1s$ electron of a 3D hydrogen atom. In the 2D EL the interaction potential in reciprocal space is taken to be

$$U_{2D}^0(q) = \frac{2\pi e^2}{\kappa q}. \qquad (3.23)$$

This potential is obtained by taking the 2D Fourier transform of the 3D Coulomb interaction which is $1/R$, R denoting distance in real space (see for e.g., [57]). In fact a strictly 2D solution of Poisson's equation is proportional to $-\ln(R)$ [58] rather than $1/R$ and its 2D Fourier transform is proportional to $1/q^2$ as in 3D EL. However, the $-\ln(R)$ interaction is seldom used [59] due to indication by real physical 2D systems that $1/R$ type of interaction is relevant [60], [61].

Remembering that the 3D polarization insertion is named after Lindhard, it is appropriate to name the 2D zeroth-order polarization insertion as the Stern function in honor of Frank Stern who first worked out its explicit form [62], [63]. Again we state the $U_{2D}^0 \, \pi_{2D}^0$ as it always occurs in our expressions in this product form

$$\mathrm{Re}\left\{ U_{2D}^0(q_n) \, \pi_{2D}^0(q_n, \nu) \right\} = \frac{r_s g_d^{3/2}}{2} \frac{1}{q_n} \left[-1 - \frac{\mathrm{sgn}(\nu_-)}{q_n} \, \Theta(|\nu_-| - 1)\sqrt{\nu_-^2 - 1} \right.$$
$$\left. + \frac{\mathrm{sgn}(\nu_+)}{q_n} \, \Theta(|\nu_+| - 1)\sqrt{\nu_+^2 - 1} \right], \qquad (3.24)$$

$$\mathrm{Im}\left\{ U_{2D}^0(q_n) \, \pi_{2D}^0(q_n, \nu) \right\} = \frac{r_s g_d^{3/2}}{2} \frac{1}{q_n^2} \left[\Theta(1 - |\nu_+|)\sqrt{1 - \nu_+^2} - \Theta(1 - |\nu_-|)\sqrt{1 - \nu_-^2} \right],$$

$$\qquad (3.25)$$

where we use the same definitions for the reduced variables q_n and $\nu_\pm$ as in the previous section, and sgn($\cdot$) denotes the signum (sign) function. The 2D static DF with a general LFC becomes

$$\epsilon_{2D}(q_n,0) = \begin{cases} \dfrac{1 + \dfrac{g_d^{3/2} r_s}{2q_n}\left[1 - G_{2D}(q_n)\right]}{1 - \dfrac{g_d^{3/2} r_s}{2q_n} G_{2D}(q_n)} & \text{for } q_n \leq 2 \\[4em] \dfrac{1 + \dfrac{g_d^{3/2} r_s}{2q_n}\left[1 - \sqrt{1 - (\dfrac{2}{q_n})^2}\right]\left[1 - G_{2D}(q_n)\right]}{1 - \dfrac{g_d^{3/2} r_s}{2q_n}\left[1 - \sqrt{1 - (\dfrac{2}{q_n})^2}\right] G_{2D}(q_n)} & \text{for } q_n > 2 \end{cases} \qquad (3.26)$$

In calculating the static structure factor, $S(q)$ we have two choices, the conventional approach is to separately account for the electron-hole pair and plasmon contributions as

$$S_{2D}^{\text{e-h}}(q_n) = -\frac{4q_n}{\pi r_s g_d^{3/2}} \int_{\nu_{min}(q_n)}^{\nu_{max}(q_n)} d\nu \, \text{Im}\left\{\frac{1}{\epsilon_{2D}(q_n,\nu)}\right\}, \qquad (3.27)$$

where again $\nu_{max}(q_n) = q_n^2/2 + q_n$ and $\nu_{min}(q_n) = \max\{0, \, q_n^2/2 - q_n\}$;

$$S_{2D}^{\text{plas}}(q_n) = -\frac{8q_n^4}{r_s^2 g_d^3} \frac{\left[1 + U_{2D}^0(q_n)\,\pi_{2D}^0(q_n,\nu)\,G_{2D}(q_n)\right]^2}{\left[\dfrac{\nu_+}{\sqrt{\nu_+^2-1}} - \dfrac{\nu_-}{\sqrt{\nu_-^2-1}}\right]} \theta(\nu - \nu_{max}(q_n)), \qquad (3.28)$$

where ν and $\nu_\pm$ in this equation have to be evaluated at the plasmon frequency ν_p; in contrast to 3D case the plasmon dispersion can be obtained in closed form as [64]

$$\nu_p(q_n) = \frac{q_n(z+1)}{2}\left[q_n^2 + \frac{4}{z^2 + 2z}\right]^{1/2}, \qquad (3.29)$$

with z defined as

$$z = \frac{2q_n}{r_s g_d^{3/2}\left[1 - G_{2D}(q_n)\right]}. \qquad (3.30)$$

Eq. (3.29) is valid in the range $[0, q_{n,max}]$ where $q_{n,max}$ satisfies $\nu_p(q_{n,max}) = q_{n,max} + q_{n,max}^2/2$ and outside this region plasmons dissociate to electron-hole pairs so that

41

collective excitations are no longer long-lived. The other alternative for computing $S_{2D}(q_n)$ makes use of the Stern function with imaginary frequency, however, we further apply the so-called Ioriatti-Isihara transformations [66, 65, 61] which greatly simplifies calculation to the form

$$S_{2D}(q_n) = \frac{q_n^2}{\pi} \int_0^{\alpha(q_n)} d\theta \frac{\left[\frac{4}{q_n^2} - \sin^2\theta + \frac{4\cot^2\theta}{q_n^2}\right](1 - \cos\theta)}{\left(\frac{4}{q_n^2} - \sin^2\theta\right)^{1/2}\left[1 + \frac{g_d^{3/2}r_s}{2q_n}(1 - \cos\theta)(1 - G_{2D}(q_n))\right]},$$
(3.31)

where

$$\alpha(q_n) = \begin{cases} \pi/2 & \text{for } q_n \le 2 \\ \\ \sin^{-1}\left(\frac{2}{q_n}\right) & \text{for } q_n > 2 \end{cases}.$$
(3.32)

In the numerical computation one should use

$$\cot^2\theta\,(1 - \cos\theta) \simeq \frac{1}{2}\left(1 - \frac{9}{12}\theta^2\right) \text{ for } 0 \le \theta \le 0.1,$$

where θ is in radians; otherwise the term $\cot^2\theta$ alone will cause a problem for $\theta \to 0$. However, the second approach based on Eq. (3.31) becomes numerically very sensitive and costly for $q_n > 2$, for this reason we switch to ordinary approach (Eq. (3.27)) after the plasmon excitations become Landau-damped.

Finally, the 2D pair correlation function and statically screened interaction in real space are obtained as

$$g_{2D}(r_n) = 1 + \frac{2}{g_d} \int_0^\infty dq_n\, q_n\, J_0(q_n r_n)\left[S_{2D}(q_n) - 1\right],$$
(3.33)

$$\overline{U}_{2D,scr}(r_n) = \frac{4}{r_s\sqrt{g_d}\,r_n} + \frac{4}{r_s\sqrt{g_d}} \int_0^\infty dq_n\, J_0(q_n r_n)\left[\frac{1}{\epsilon_{2D}(q_n)} - 1\right],$$
(3.34)

where J_0 is the zeroth-order cylindrical Bessel function of the first kind.

3.5 STLS: Derivation and Local-Field Correction Expressions

3.5.1 Derivation of the STLS

We follow the pioneering STLS paper [67] for the derivation of the LFC of a *classical liquid*. This is necessary for the understanding of the technique as well as filling the gaps in the original derivation which was written for the experts of the liquid-state physics. As a matter of fact, it can be checked that a one page derivation of the original paper requires highly appreciable and lengthy intermediate steps. For the consistency of this thesis we also make minor modifications in the notation. We consider a classical liquid in the presence of an external field creating the potential energy distribution $U_{ext}(\vec{x}, t)$. The one-particle distribution function $f(\vec{x}, \vec{p}; t)$ is introduced to denote the particle probability density at the $2 \times$ D-dimensional phase space coordinates $(\vec{x}, \vec{p})$ at time t. It should be mentioned that this function does not have a direct quantum mechanical analog due to the well-known uncertainty relation between the noncommuting phase space variables $\vec{x}$ and $\vec{p}$; the closest quantum mechanical function is the so-called Wigner function[2]. The equation of motion (i.e., the time evolution) of the classical one-particle distribution function is governed by

$$\frac{\partial f(\vec{x}, \vec{p}; t)}{\partial t} + \vec{v} \cdot \nabla_{\vec{x}} f(\vec{x}, \vec{p}; t) - \nabla_{\vec{x}} U_{ext}(\vec{x}, t) \cdot \nabla_{\vec{p}} f(\vec{x}, \vec{p}; t)$$

$$- \int \nabla_{\vec{x}} U^0(\vec{x} - \vec{x}') \cdot \nabla_{\vec{p}} f(\vec{x}, \vec{p}; \vec{x}', \vec{p}'|t) \, d\vec{x}' \, d\vec{p}' = 0. \qquad (3.35)$$

---

[2] The appendix of the original STLS paper [67] presents the derivation for the self-consistent LFC for a quantum liquid using the Wigner function. Mahan [42], on the other hand, gives a derivation based on the double commutator of the particle density operator.

43

This is actually a statement of $df(\vec{x}, \vec{p}; t)/dt = 0$ with the total time derivate treated as the hydrodynamic derivative as

$$\frac{df}{dt} = \frac{\partial f}{\partial t} + \underbrace{\frac{d\vec{x}}{dt}}_{\text{velocity}} \cdot \nabla_{\vec{x}} f + \underbrace{\frac{d\vec{p}}{dt}}_{\text{force}} \cdot \nabla_{\vec{p}} f = 0. \tag{3.36}$$

Force has two contributions; one due to external force, $\vec{F}_{ext} = -\nabla_{\vec{x}} U_{ext}(\vec{x}, t)$ and the other due to internal particle interactions, $\vec{F}_{int} = -\nabla_{\vec{x}} U^0(\vec{x} - \vec{x}')$, where $U^0(\vec{x})$ denotes the bare interparticle interaction potential energy. However, to be exact for the internal force we should use the joint two-particle density $f(\vec{x}, \vec{p}; \vec{x}', \vec{p}'|t)$ that tracks the simultaneous densities of the test and perturbation coordinates. Then we must integrate over all possible perturbation coordinates giving

$$\vec{F}_{int} \cdot \nabla_{\vec{p}} f = -\int \nabla_{\vec{x}} U^0(\vec{x} - \vec{x}') \cdot \nabla_{\vec{p}} f(\vec{x}, \vec{p}; \vec{x}', \vec{p}'|t) \, d\vec{x}' \, d\vec{p}',$$

which is just the last term in Eq. (3.35). The equation for the two-particle distribution function is coupled to the three-particle distribution function and so on. Singwi and coworkers close this infinite hierarchy by the following ansatz which is the heart of the STLS technique

$$f(\vec{x}, \vec{p}; \vec{x}', \vec{p}'|t) = f(\vec{x}, \vec{p}; t) \, f(\vec{x}', \vec{p}'; t) \, g(\vec{x} - \vec{x}'), \tag{3.37}$$

where $g(\vec{x})$ is the static equilibrium pair correlation function. Apart from the stringent restrictions of this form, we shall see that the improvement is quite impressive for certain applications. Under the perturbation of the external potential, which is assumed to be small[3] we write the distribution function as

$$f(\vec{x}, \vec{p}; t) = f_0(\vec{p}) + f_1(\vec{x}, \vec{p}; t). \tag{3.38}$$

---

[3] Note again the presence of the linear response assumption.

44

In this equation f_0 denotes the equilibrium distribution which needs to be uniform and with no time evolution, and f_1 shows the deviation from the equilibrium distribution due to external perturbation. The equation of motion (Eq. (3.35)) becomes

$$\frac{\partial f_1}{\partial t} + \vec{v} \cdot \nabla_{\vec{x}} f_1 - \nabla_{\vec{x}} U_{ext}(\vec{x},t) \cdot \nabla_{\vec{p}} \left(f_0 + \overbrace{f_1}^{*} \right)$$

$$- \int \nabla_{\vec{x}} U^0(\vec{x} - \vec{x}') \cdot \nabla_{\vec{p}} \left[f_0(\vec{p}) + \overbrace{f_1(\vec{x},\vec{p};t)}^{*} \right]$$

$$\times g(\vec{x} - \vec{x}') \left[f_0(\vec{p}') + f_1(\vec{x}',\vec{p}';t) \right] d\vec{x}'\, d\vec{p}' = 0. \tag{3.39}$$

We neglect f_1 terms labeled by * which are presumably small compared to the adjacent f_0 terms and thereby linearize the equation. Furthermore, we use $\int d\vec{p}' f_0(\vec{p}') \equiv 0$ due to isotropy of the equilibrium distribution (which amounts to saying that the equilibrium distribution is actually, $f_0(p)$) and get

$$\left[\frac{\partial}{\partial t} + \vec{v} \cdot \nabla_{\vec{x}} \right] f_1(\vec{x},\vec{p};t)$$

$$- \underbrace{\left[\nabla_{\vec{x}} U_{ext} + \int f_1(\vec{x}',\vec{p}';t) g(\vec{x} - \vec{x}') \nabla_{\vec{x}} U^0(\vec{x} - \vec{x}')\, d\vec{x}'\, d\vec{p}' \right]}_{\text{effective force}} \cdot \nabla_{\vec{p}} f_0(\vec{p}) = 0. \tag{3.40}$$

For further progress it is beneficial to split the indicated effective force in the following form

$$\vec{F}_{eff}(\vec{x},t) = \overbrace{-\nabla_{\vec{x}} U_{ext}(\vec{x},t) - \int \nabla_{\vec{x}} U^0(\vec{x} - \vec{x}')\, f_1(\vec{x}',\vec{p}';t)\, d\vec{x}'\, d\vec{p}'}^{\text{mean-force-field used in RPA}}$$

$$\underbrace{- \int \left[g(\vec{x} - \vec{x}') - 1 \right] \nabla_{\vec{x}} U^0(\vec{x} - \vec{x}')\, f_1(\vec{x}',\vec{p}';t)\, d\vec{x}'\, d\vec{p}'}_{\text{local-field correction}}. \tag{3.41}$$

Now we move to the reciprocal space-time by Fourier transforming both sides of Eq. (3.41). For the right hand side of Eq. (3.41) we get

$$\int d\vec{x} \int dt\, \mathrm{e}^{-i\vec{q}\cdot\vec{x}}\, \mathrm{e}^{i\omega t}\, \vec{F}_{eff}(\vec{x},t) \equiv \vec{F}_{eff}(\vec{q},\omega). \tag{3.42}$$

As for the left hand side we have after performing the time transformation

45

$$- \int \left[\nabla_{\vec{x}} U_{ext}(\vec{x}, \omega)\right] e^{-i\vec{q}\cdot\vec{x}} \, d\vec{x} - \int d\vec{p}' \int d\vec{x}' f_1(\vec{x}', \omega; \vec{p}') \int \left[\nabla_{\vec{x}} U^0(\vec{x} - \vec{x}')\right] e^{-i\vec{q}\cdot\vec{x}} \, d\vec{x}$$

$$- \int d\vec{p}' \int d\vec{x}' f_1(\vec{x}', \omega; \vec{p}') \int d\vec{x} \, e^{-i\vec{q}\cdot\vec{x}} \left[g(\vec{x} - \vec{x}') - 1\right] \nabla_{\vec{x}} U^0(\vec{x} - \vec{x}'), \quad (3.43)$$

which simplifies to

$$-i\vec{q} U_{ext}(\vec{q}, \omega) - \int d\vec{p}' \overbrace{\int d\vec{x}' f_1(\vec{x}', \omega; \vec{p}') \, e^{-i\vec{q}\cdot\vec{x}'}}^{f_1(\vec{q}, \omega; \vec{p}')} \, i\vec{q} U^0(\vec{q})$$

$$- \int d\vec{p}' \underbrace{\int d\vec{x}' f_1(\vec{x}', \omega; \vec{p}') \, e^{-i\vec{q}\cdot\vec{x}'}}_{f_1(\vec{q}, \omega; \vec{p}')} \underbrace{\int d\vec{y} \, e^{-i\vec{q}\cdot\vec{y}} [g(y) - 1] \nabla_{\vec{x}} U^0(\vec{y})}_{\text{use convolution property}}; \quad (3.44)$$

using the Fourier transform property that the product of two functions are convoluted in their transforms, we get for this term

$$\int \frac{d\vec{q}'}{(2\pi)^D} \frac{1}{n} \left[S(|\vec{q} - \vec{q}'|) - 1\right] i\vec{q}' U^0(\vec{q}'),$$

where n designates the density of the liquid. The Fourier transform of Eq. (3.41) becomes

$$\vec{F}_{eff}(\vec{q}, \omega) = -i\vec{q} U_{ext}(\vec{q}, \omega) - i\vec{q} U^0(\vec{q}) \int d\vec{p}' f_1(\vec{q}, \omega; \vec{p}')$$

$$- \int \frac{d\vec{q}'}{(2\pi)^D} \frac{1}{n} \left[S(|\vec{q} - \vec{q}'|) - 1\right] i\vec{q}' U^0(\vec{q}') \int d\vec{p}' f_1(\vec{q}, \omega; \vec{p}'). \quad (3.45)$$

We now use the fact that the deviation of the particle density function f_1 from the equilibrium value due to the external perturbation is the induced density,

$$n_{ind}(\vec{q}, \omega) = \int d\vec{p}' f_1(\vec{q}, \omega; \vec{p}'). \quad (3.46)$$

Then,

$$\vec{F}_{eff}(\vec{q}, \omega) = -i\vec{q} U_{ext}(\vec{q}, \omega) - i\vec{q} U^0(\vec{q}) \, n_{ind}(\vec{q}, \omega)$$

$$- n_{ind}(\vec{q}, \omega) \int \frac{d\vec{q}'}{(2\pi)^D} \frac{1}{n} \left[S(|\vec{q} - \vec{q}'|) - 1\right] i\vec{q}' U^0(\vec{q}'). \quad (3.47)$$

As a result the equation of motion in $(\vec{q}, \omega)$ space turns into

$$-i\omega f_1(\vec{q}, \omega; \vec{p}) + i \overbrace{\vec{q} \cdot \vec{v}}^{\vec{q}\cdot\vec{p}/m} f_1(\vec{q}, \omega; \vec{p}) + \vec{F}_{eff}(\vec{q}, \omega) \cdot \nabla_{\vec{p}} f_0(\vec{p}) = 0. \quad (3.48)$$

46

For further progress, we need to identify the density response of a system of non-interacting particles to the external field; we shall use this function to build-up the response of an interacting system.

3.5.1.1 Noninteracting Density Response Function

For the noninteracting case the effective force becomes $\vec{F}_{eff}^0 = -i\vec{q}\ U_{ext}(\vec{q},\omega)$, so Eq. (3.48) becomes

$$-i\omega f_1^0(\vec{q},\omega;\vec{p}) + i\vec{q}\cdot\frac{\vec{p}}{m}f_1^0(\vec{q},\omega;\vec{p}) - i\vec{q}U_{ext}(\vec{q},\omega)\cdot\nabla_{\vec{p}}f_0(\vec{p}) = 0, \qquad (3.49)$$

giving

$$f_1^0(\vec{q},\omega;\vec{p}) = \frac{\vec{q}\cdot\nabla_{\vec{p}}f_0(\vec{p})}{\frac{\vec{p}\cdot\vec{q}}{m}-\omega}\ U_{ext}(\vec{q},\omega). \qquad (3.50)$$

We integrate both sides over $d\vec{p}$ and use Eq. (3.46), yielding

$$n_{ind}^0(\vec{q},\omega) = U_{ext}(\vec{q},\omega)\underbrace{\int d\vec{p}\frac{\vec{q}\cdot\nabla_{\vec{p}}f_0(\vec{p})}{\frac{\vec{p}\cdot\vec{q}}{m}-\omega}}_{\chi^0(\vec{q},\omega)}, \qquad (3.51)$$

where as indicated above the noninteracting density response function for a classical liquid is identified as

$$\chi^0(\vec{q},\omega) = \int \frac{\vec{q}\cdot\nabla_{\vec{p}}f_0(\vec{p})}{\frac{\vec{p}\cdot\vec{q}}{m}-\omega}\ d\vec{p}, \qquad (3.52)$$

by using

$$n_{ind}^0(\vec{q},\omega) = \chi^0(\vec{q},\omega)\ U_{ext}(\vec{q},\omega). \qquad (3.53)$$

3.5.1.2 RPA

Having met with the noninteracting susceptibility ($\chi^0(\vec{q},\omega)$) we can now proceed by including the mean-field term by setting $g(\vec{x},\vec{x}') \equiv 1$ in Eq. (3.41). Before more mathematics, we must observe that in the mean-field approximation any two particles

47

are taken to be uncorrelated, which is surely not the case in reality; there exists a fuzzy forbidden zone around each electron so that $g(|\vec{x}|) < 1$ as $|\vec{x}| \to 0$. The effective force felt by the constituent particles becomes in RPA

$$\vec{F}_{eff}^{RPA}(\vec{q}, \omega) = -i\vec{q}\, U_{ext}(\vec{q}, \omega) - i\vec{q}\, U^0(\vec{q})\, n_{ind}^{RPA}(\vec{q}, \omega). \qquad (3.54)$$

Then Eq. (3.48) yields

$$n_{ind}^{RPA}(\vec{q}, \omega) = \left[U_{ext}(\vec{q}, \omega) + U^0(\vec{q})\, n_{ind}^{RPA}(\vec{q}, \omega) \right] \underbrace{\int \frac{\vec{q} \cdot \nabla_{\vec{p}} f_0(\vec{p})}{\frac{\vec{p} \cdot \vec{q}}{m} - \omega} d\vec{p}}_{\chi^0(\vec{q}, \omega)}, \qquad (3.55)$$

giving

$$n_{ind}^{RPA}(\vec{q}, \omega) = U_{ext}(\vec{q}, \omega)\, \underbrace{\frac{\chi^0(\vec{q}, \omega)}{1 - U^0(\vec{q})\, \chi^0(\vec{q}, \omega)}}_{\chi^{RPA}(\vec{q}, \omega)}, \qquad (3.56)$$

hence, the RPA density response function is obtained as

$$\chi^{RPA}(\vec{q}, \omega) = \frac{\chi^0(\vec{q}, \omega)}{1 - U^0(\vec{q})\, \chi^0(\vec{q}, \omega)}. \qquad (3.57)$$

Note that this is the same as the expression obtained in the previous chapter using the polarization insertion diagrams for the quantum case. Similarly the RPA DF is obtained as

$$\epsilon^{RPA}(\vec{q}, \omega) = \frac{\chi_{scr}(\vec{q}, \omega)}{\chi(\vec{q}, \omega)} = \frac{\chi^0(\vec{q}, \omega)}{\chi^{RPA}(\vec{q}, \omega)} = 1 - U^0(\vec{q})\, \chi^0(\vec{q}, \omega). \qquad (3.58)$$

3.5.1.3 STLS

Finally STLS is reached by retaining $g(\vec{x}, \vec{x}\,')$ as it is

$$\begin{aligned}
\vec{F}_{eff}^{STLS}(\vec{q}, \omega) &= -i\vec{q}\, U_{ext}(\vec{q}, \omega) - i\vec{q}\, U^0(\vec{q})\, n_{ind}^{STLS}(\vec{q}, \omega) \\
&\quad - n_{ind}^{STLS}(\vec{q}, \omega) \int \frac{d\vec{q}\,'}{(2\pi)^D}\, \frac{1}{n} \left[S(|\vec{q} - \vec{q}\,'|) - 1 \right] U^0(\vec{q}\,')\, i\vec{q}\,'. \qquad (3.59)
\end{aligned}$$

Now we concentrate on the last term; particularly $\vec{q}\,'$ can be decomposed as

$$\vec{q}\,' = q_{\parallel}'\, \hat{a}_{\parallel} + q_{\perp}'\, \hat{a}_{\perp},$$

48

defined with respect to the vector $\vec{q}$, and $\hat{a}$ represents a unit vector. The point is that, the integral over the transverse part ($\perp$) will vanish due to the integral

$$\int \frac{d^{D-1}\vec{q}'}{(2\pi)^D} \frac{U^0(\vec{q}')}{n} \left[S\left(\sqrt{\left(q - q'_{\parallel} \right)^2 + q'^2_{\perp}} \right) - 1 \right] iq'_{\perp} \hat{a}_{\perp}.$$

This argument is valid for all dimensions D except for D=1, but the result to be given will trivially hold for D=1 case. As a result the last term reduces the contribution from longitudinal ($\parallel$) part as

$$-n^{STLS}_{ind} \int \frac{d\vec{q}'}{(2\pi)^D} \frac{1}{n} \left[S(|\vec{q} - \vec{q}'|) - 1 \right] U^0(\vec{q}') iq'_{\parallel} \hat{a}_{\parallel}.$$

Also using $q'_{\parallel} \hat{a}_{\parallel} = \vec{q} \frac{\vec{q} \cdot \vec{q}'}{q^2}$ we can express the effective force as

$$\begin{aligned}
\vec{F}^{STLS}_{eff}(\vec{q}, \omega) &= -i\vec{q} \, U_{ext}(\vec{q}, \omega) - i\vec{q} \, U^0(\vec{q}) \, n^{STLS}_{ind}(\vec{q}, \omega) \\
&\times \left\{ 1 + \frac{1}{n} \int \frac{d\vec{q}'}{(2\pi)^D} \frac{\vec{q} \cdot \vec{q}'}{q^2} \frac{U^0(\vec{q}')}{U^0(\vec{q})} \left[S(|\vec{q} - \vec{q}'|) - 1 \right] \right\}.
\end{aligned} \quad (3.60)$$

So, if we define the last term as the local-field correction

$$G(\vec{q}) = -\frac{1}{n} \int \frac{d\vec{q}'}{(2\pi)^D} \frac{\vec{q} \cdot \vec{q}'}{q^2} \frac{U^0(\vec{q}')}{U^0(\vec{q})} \left[S(|\vec{q} - \vec{q}'|) - 1 \right], \quad (3.61)$$

then the effective force becomes

$$\vec{F}^{STLS}_{eff}(\vec{q}, \omega) = -i\vec{q} \left\{ U_{ext}(\vec{q}, \omega) + U^0(\vec{q}) \, n^{STLS}_{ind}(\vec{q}, \omega) \left[1 - G(\vec{q}) \right] \right\}. \quad (3.62)$$

Finally, Eq. (3.62) in Eq. (3.48) leads to the following form for the induced density

$$n^{STLS}_{ind}(\vec{q}, \omega) = \underbrace{\frac{\chi^0(\vec{q}, \omega)}{1 - U^0(\vec{q}) \, \chi^0(\vec{q}, \omega) \left[1 - G(\vec{q}) \right]}}_{\chi^{STLS}(\vec{q}, \omega)} U_{ext}(\vec{q}, \omega). \quad (3.63)$$

From this equation the STLS density response function is identified as indicated above. Using this information in Eq. (2.32) the STLS DF is obtained as

$$\epsilon^{LFC}(\vec{q}, \omega) = \frac{1 - U^0(\vec{q}) \, \chi^0(\vec{q}, \omega) \left[1 - G(\vec{q}) \right]}{1 + U^0(\vec{q}) \, \chi^0(\vec{q}, \omega) \, G(\vec{q})}, \quad (3.64)$$

which is just Eq. (2.50) under a static LFC rather than a dynamic one. Actually these last two equations are applicable for any static LFC; the distinction of the STLS technique lies in Eq. (3.61) which depends on the static form factor, $S(\vec{q})$. $S(\vec{q})$, in turn, depends on the DF through Eq. (2.44). Finally, the DF depends on the LFC as seen in Eq. (3.64). So, there exists a coupled loop of nonlinear integral equations which need to be satisfied simultaneously. This is referred as a self-consistent solution. Having established the STLS LFC for a general D-dimensional case, we present in the following section the explicit expressions for the three-, two-, and quasi-one-dimensions.

3.6 Explicit Expressions for the STLS Local-Field Correction

3.6.1 Three-Dimensions

Eq. (3.61) can be simplified further in 3D by performing the angular integrations analytically [67], and the final form becomes

$$G_{3D}^{STLS}(q_n) = \frac{3}{2\,g_d} \int_0^\infty dp_n\, p_n^2\, [1 - S(p_n)]\, h_{3D}(a), \qquad (3.65)$$

where $a = p_n/q_n$ and

$$h_{3D}(a) = 1 + \frac{1 - a^2}{2a} \ln\left|\frac{a+1}{a-1}\right|. \qquad (3.66)$$

We observe that $h_{3D}(a = 0) = 2$ and $h_{3D}(a = 1) = 1$, so that, it is actually a well-behaved function without singularities. For completeness we would also like to include the expression for the Hubbard LFC for a 3D EL having g_d degeneracy,

$$G_{3D}^H(q_n) = \frac{1}{g_d} \frac{q_n^2}{1 + q_n^2}. \qquad (3.67)$$

The Hubbard LFC [68] approximately accounts for the exchange (Pauli) hole surrounding each electron.

3.6.2 Two-Dimensions

In the 2D case, the polar integral of Eq. (3.61) cannot be expressed in terms of elementary functions, so the computation becomes somewhat more costly. The explicit form is

$$G_{2D}^{STLS}(q_n) = \frac{2}{g_d} \int_0^\infty dp_n \, p_n \, [1 - S(p_n)] \, h_{2D}(a), \tag{3.68}$$

where $a = p_n/q_n$ and

$$h_{2D}(a) = \frac{1}{\pi} \int_0^\pi d\phi \, \frac{a\cos\phi + 1}{\sqrt{1 + a^2 + 2a\cos\phi}}. \tag{3.69}$$

The asymptotical form of $h_{2D}(a)$ is $\frac{1}{2a}$, which can safely be used for $a \geq 10$. To reduce the computational labour, we tabulate the function $h_{2D}(a)$ in the interval $[0, 10]$ using 1000 data points, thereby, the burden of the double integration is circumvented.

Finally, the expression for the Hubbard LFC in 2D case is

$$G_{2D}^H(q_n) = \frac{1}{g_d} \frac{q_n}{\sqrt{1 + q_n^2}}. \tag{3.70}$$

3.6.3 Quasi-One-Dimensions

Even though our goal in this work is to understand and characterize three- and two-dimensional ELs, for completeness it is appropriate to include certain expressions regarding quasi-one-dimesional (Q1D) systems. In the first place it needs to be mentined that the strictly 1D electronic systems have pathological features, which can be cured if the finite spread along the transverse coordinates is incorporated. This is indeed the case in actual systems, like quantum wires. Due to finite extension of the electronic wave function, the bare 1D Coulomb potential is modified[4] by averaging the charge distribution along the transverse plane. Unfortunately, the resultant form

---

[4] For a detailed illustration in Q2D case refer to Chapter 5.

is cross-section dependent and unnecessarily complicated. For a cylindrical quantum wire of radius R, the effective 1D Coulomb interaction in real space can be approximated by [69]

$$U^0_{Q1D}(z) = \frac{e^2}{\kappa} \frac{1}{|z| + \gamma R},$$

(3.71)

where γ is a fitting parameter having a value about $\gamma \simeq 0.3$.

Other expressions for the Q1D EL are also listed below, again for general reference purposes.

$$n_{1D} = \frac{1}{L} \sum_{k=-k_F,\sigma,\nu}^{+k_F,g_s,g_v} n_{k,\sigma,\nu} = g_d \frac{k_F}{\pi},$$

(3.72)

where L is the length terminated by periodic boundary conditions. Similar to 3D and 2D cases we have the relations

$$n_{1D} = \frac{1}{2\, r_s\, a_B^*},$$

(3.73)

and

$$k_F = \frac{\pi}{2\, g_d\, r_s\, a_B^*}.$$

(3.74)

The Lindhard function in 1D including the degeneracy factor g_d becomes

$$\chi^0_{Re}(q_n, \nu) = \frac{g_d\, m}{2\hbar^2 \pi k_F\, q_n} \ln \left| \frac{\nu^2 - \left(\frac{q_n^2}{2} - q_n\right)^2}{\nu^2 - \left(\frac{q_n^2}{2} + q_n\right)^2} \right|,$$

$$\chi^0_{Im}(q_n, \nu) = \begin{cases} -\frac{g_d\, m}{2\hbar^2 q_n k_F}; & \text{if } |\frac{q_n^2}{2} - q_n| < \nu < \frac{q_n^2}{2} + q_n \\ 0; & \text{else} \end{cases}.$$

(3.75)

Note the difference in the zone boundaries of the pair-continuum with respect to 3D and 2D Lindhard expressions.

Finally, the STLS LFC for a Q1D system can be obtained by using the general form in Eq. (3.61) as

$$G_{Q1D}^{STLS}(q_n) = \frac{1}{2\,g_d} \int_{-\infty}^{\infty} dp_n \, \frac{p_n}{q_n} \, \frac{U^0(p_n)}{U^0(q_n)} \left[1 - S(|\vec{q} - \vec{q}'|)\right].$$

(3.76)

We should caution that the debate on the applicability of the EL model (in broad sense, the Fermi liquid model) to low-dimensional systems and especially to Q1D, still continues [70]. We return to this point in the final conclusion chapter.

CHAPTER 4

THREE- AND TWO-DIMENSIONAL

ELECTRON LIQUIDS: RESULTS

4.1 Introduction

In this chapter we would like to gather the results pertaining the formulation given in the previous two chapters. For 3D EL, we compare the STLS results with the recent quantum Monte Carlo (QMC) data released by two groups working in this field [45, 71]. Currently, QMC is believed to yield the most accurate data, however, the agreement between the QMC results produced by independent groups is not satisfactory, and moreover, the computational cost severely restricts the output to a very coarse data grid. Among the exhaustive list of available LFCs [55], the approach due to David Pines, who contributed heavily to this field, and his co-workers [72] deserves special respect and we include in our comparison their pseudopotential formulation [73, 74], which renders our treatment more interesting and complete. Our results indicate that STLS, with its comparatively low computational cost and apart from some drawbacks to be mentioned, offers to be a good alternative to QMC.

54

The 2D EL is given a special emphasis in this work due to its technological importance. Again we compare the 2D STLS results with the QMC data produced by two independent groups [75, 76]. This time we also have the opportunity to test the spin-polarized STLS results with the QMC data of Tanatar and Ceperley [75]. Again our comparison is supplemented by the pseudopotential approach which was pursued for 2D EL by Iwamoto [57]. We present an analytical fitting for the normal-state 2D LFC which was available in the literature for the 3D case, but the 2D counterpart was lacking until the appearance of our work [63]. In addition to the formulation presented in the previous chapters, we also include the computation of the correlation energy (equivalently the ground-state energy) and the compressibility of the 2D EL. These two are one of the most demanding calculations in this work as we do not resort here to any simplifications such as curve fitting. Furthermore, we gain a valuable information about a physical issue, the so-called compressibility sum rule, where STLS is criticised to be poor. Our findings also comply with this common belief that was mainly established in 3D [42]. Finally, we bring into foreground the provocative subject of overscreening, which has been very poorly investigated in the literature. We explore the driving mechanism of this effect.

4.2   3D Electron Liquid Results

Our reference in comparing the STLS DF will be the QMC data recently produced by two independent groups [45, 71]. This choice is due to the currently existent confidence on the QMC data. As a matter of fact, our investigation will not only question STLS but the QMC results as well, by comparing the agreement of the data produced by these two independent groups. We shall not make use of the full strength

of the formulation developed in the previous chapters; the comparison will involve only the normal-state of the single-valley EL $(g_d = 2)$, due to lack of QMC data for other degeneracy factors. However, the chapter on the Mott transition makes an exhaustive use of the degeneracy factor.
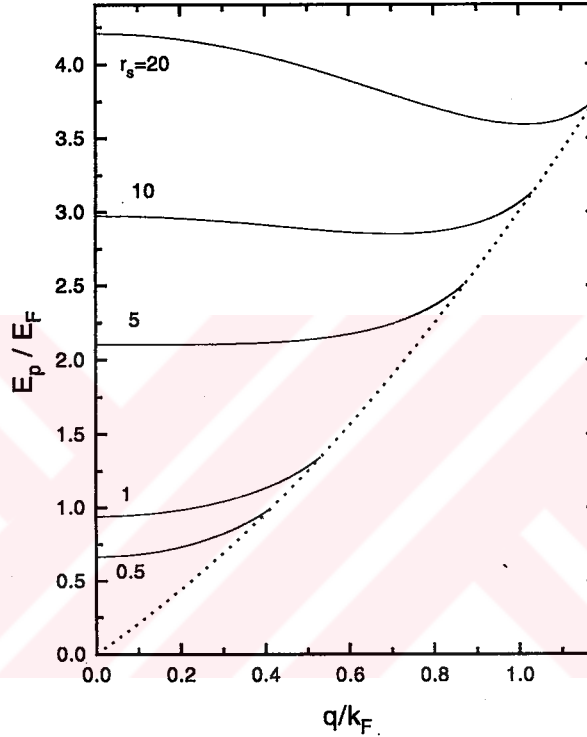
Figure 4.1: Plasmon energy (E_p) normalized to Fermi energy (E_F) versus q/k_F, of the 3D EL based on STLS. The dotted line marks the onset of particle-hole continuum.

The longitudinal plasmon dispersion extracted from the zeros of the STLS DF is shown in Fig. 4.1 for several r_s values. In this figure, the plasmon energy is normalized to Fermi energy and the wave number is normalized to Fermi wave number. The plasmon dispersion curves are mainly included to assist future researchers for comparing their own data. The plasmon curves are shown till the dotted line which marks the onset of the single electron-hole pair production. Within this region, the imaginary

part of the DF is not zero, however, the zeros of the real part of the DF can still be traced, even though, the plasmon will not be a long-lived elementary excitation due to Landau-damping. It needs to be mentioned that most of the techniques including STLS, out of the single- pair continuum, predict undamped plasmons. However, experiments indicate a finite lifetime possibly due to two effects that are ususally omitted: multipair excitations which are not restricted to the single-pair continuum zone, and the interaction of the electrons with the periodic lattice potential [77].

Bowen *et al.* [45] reported their QMC data on the static DF for the 3D EL at the densities $r_s = 1$, 4, 6 and 10. Soon afterwards, Moroni *et al.* [71] announced their QMC results on the static LFC of the 3D EL, computed at the r_s values 2, 5 and 10. First, we extract $G(q)$ (actually $G(q, 0)$) data from the tabulated $\epsilon^{-1}(q, 0)$ data of Bowen *et al.* by means of the equation

$$G(\vec{q}, \omega) = \frac{1}{1 - \epsilon(\vec{q}, \omega)} - \frac{1}{U^0(\vec{q}) \, \chi^0(\vec{q}, \omega)}. \tag{4.1}$$

We should note that this equation is exact. Thereby, we can compare $G(q)$ of STLS with the two QMC data, as shown in Fig. 4.2. In these figures we also include the LFC based on Pines and Iwamoto's pseudopotential theory [73][1]. In adapting the liquid Helium formulation to EL problem, Iwamoto and Pines (IP) essentially constrained the static LFC, so that certain static response functions of the EL coincide with the "accurate" QMC data. In particular, they fitted their static LFC to the long-wavelength limit ($q \to 0$) of the compressibility and spin susceptibility QMC data of Ceperley and Alder [79]. The resultant form of the LFC can be named as a generalized

---

[1] David Pines can be described as the most credited scientist in the many-body physics. He is the author of more than three authoritive research books in this field and he can be named as the person for constructing the language of correlated electron systems. In 1980's he revisited the EL problem after developing a powerful theory for the liquid Helium towards the end of 1970's together with Aldrich [78].

Hubbard LFC, as it also incorporates the correlation among spin antiparallel($\uparrow\downarrow$) electrons as well as the parallel spin ($\uparrow\uparrow$) ones,

$$G_{3D}^{IP}(q_n) = \underbrace{\frac{q_n^2}{2\left(q_n^2 + q_{\uparrow\uparrow}^2\right)}}_{\text{Exchange}} + \underbrace{\frac{q_n^2}{2\left(q_n^2 + q_{\uparrow\downarrow}^2\right)}}_{\text{Ex.-Corr.}} . \tag{4.2}$$

We should mention that the ordinary Hubbard LFC is obtained from this form by setting $q_{\uparrow\uparrow} \to \infty$ (i.e., no correlation) and $q_{\uparrow\downarrow} \to 1$ (exchange part). However, IP's LFC reduces for $r_s \to 0$ (exchange dominant regime) to the form [73]

$$G_{3D}^{IP \to H}(q_n) = \frac{1}{2}\frac{q_n^2}{q_n^2 + 2}; \tag{4.3}$$

This is nothing but the form suggested by Geldart and Vosko [80] by correcting Hubbard's original LFC. The values for $q_{\uparrow\uparrow}$ and $q_{\uparrow\downarrow}$ are tabulated by IP in the density range $r_s = 1\text{-}20$.

Having made this introduction for the pseudopotential theory of IP we can make the following observations about the Fig. 4.2: i) STLS and the QMC data due to Bowen *et al.* denoted by *QMC (1)* have a reasonable agreement for all r_s values given. $G(q)$ due to *QMC (1)* is observed to be consistently lower than that of the STLS values. ii) The QMC data of Moroni *et al.* which will be represented by *QMC (2)* is reported for $q_n = q/k_F$ values larger than 1. The agreement of $G(q)$ with STLS is especially poor for $q_n > 2$ for all r_s values. We believe this to be an artifact of STLS in accounting for the short-range correlations. However, we would like to draw attention to the case $r_s = 10$, where a direct comparison of the two QMC data is possible. There, we observe that *QMC (2)* increasingly disagrees with *QMC (1)* for large q_n values. The IP LFC fitted to QMC data in the long-wavelength, as expected agrees with QMC in the $q_n \to 0$ region much better than STLS. However, this picture quickly changes; for the intermediate q_n values STLS is superior to IP.
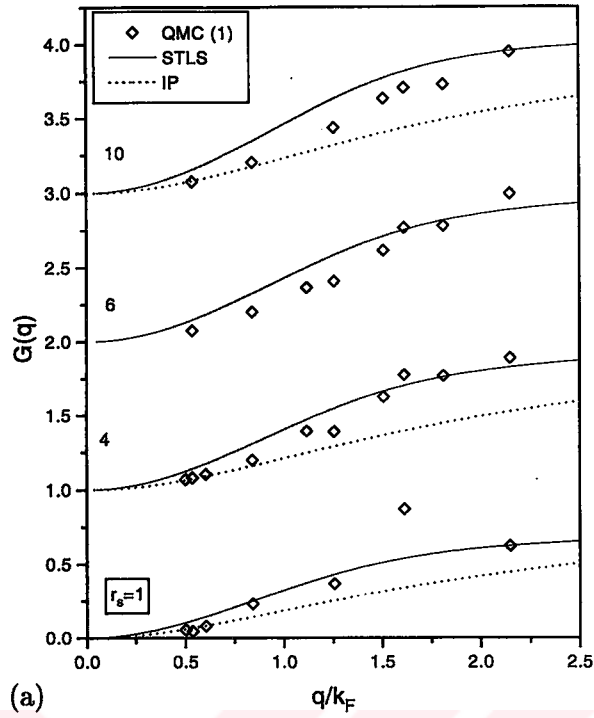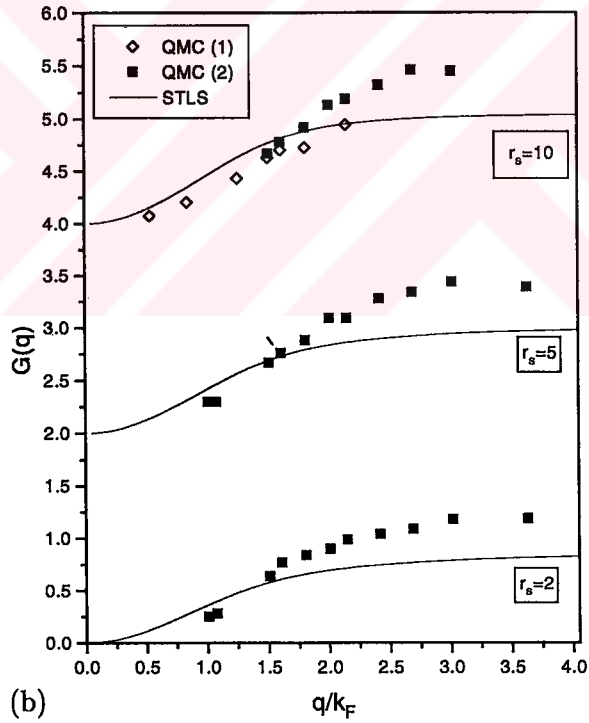
Figure 4.2: $G(q)$ versus q/k_F. (a) Diamonds show QMC data extracted from the work of Bowen and co-workers, dotted lines refer to Iwamoto and Pines' (IP) LFC, (b) solid squares show the QMC data of Moroni and co-workers. The upper curve also compares the two independent QMC results and STLS, where solid lines indicate STLS results. The curves in (a) and (b) are vertically offset by 1 and 2 units respectively for clarity.

59

Fig. 4.3 illustrates the inverse static DFs of the STLS and the QMC. The agreement of STLS with *QMC (1)* is good for $r_s = 1$ and 4 values, but for the case of $r_s = 6$ and especially for $r_s = 10$, there is a disagreement for the long wavelengths $q_n \leq 1.5$. In this region STLS shows an exaggerated *overscreening* (i.e., $\epsilon < 0$) as compared to QMC. Even though, formally both of the techniques are to be questioned, we again blame STLS due to its violation of the compressibility sum rule [67, 42], which is manifested in the long wavelength behavior of the static DF. We shall elaborate more on this subject while analyzing the 2D EL. Another interesting point is that the sizeable disagreement of STLS and QMC in the $G(q)$ data for $r_s = 10$ and $q_n > 2$ values is not reflected on $\epsilon^{-1}(q)$ results, where this time an excellent agreement is recorded for $q_n \geq 1.5$ between the two. In Fig. 4.3 (b) the RPA result is also included to show its failure for all practical wave numbers. IP again shows a good agreement with the QMC data only in the extreme long-wavelength limit; for $r_s = 6$, IP results are not included in the comparison as $q_{\uparrow\uparrow}$ and $q_{\uparrow\downarrow}$ values are not supplied by IP at this r_s value. Finally, the disagreement of the two independent QMC data and the few number of data points available due to computational cost of the simulation, lead us to conclude that QMC is still premature, and in 3D, STLS seems to be a better alternative for practical screening applications together with its limitations. The IP pseudopotential approach shows a complementary performance to that of STLS, where only in the long-wavelength limit a good agreement with QMC is registered.
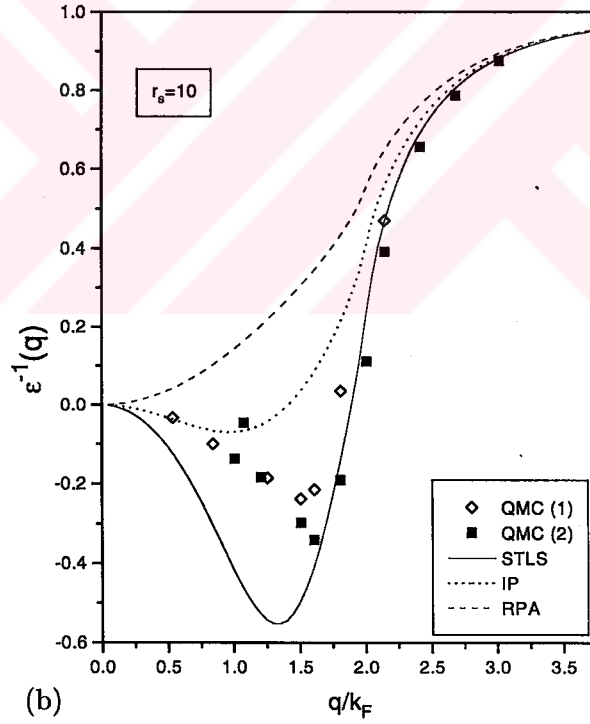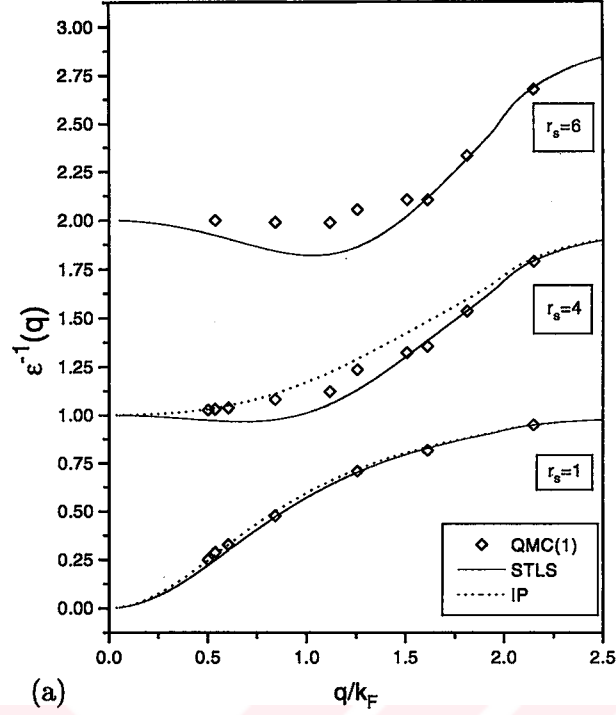
Figure 4.3: Inverse static DF versus q/k_F. (a) Diamonds show QMC data of Bowen and co-workers and solid lines indicate STLS results for r_s=1, 4, 6. (b) Comparison of the static DF for $r_s = 10$. Additionally, solid squares show the results extracted from the QMC data of Moroni and co-workers and dashed line indicates the RPA result. The dotted lines refer to Iwamoto and Pines' (IP) LFC. The upper curves in (a) are vertically offset by 1 unit for clarity.

61

4.3 2D Electron Liquid Results

Our assessment of the DFs for the 2D EL is more comprehensive than the 3D case. Our comparison again includes the STLS, QMC and the pseudopotential theory which was undertaken by Iwamoto for the 2D EL. For the QMC data we have two independent simulations due to Tanatar and Ceperley (TC) [75] (to be abbreviated by QMC-TC) and very recently by Senatore [81, 76] (QMC-S). The former is among the most cited works in EL theory due to the exhaustive and accurate treatment, moreover, we have the opportunity to make use of our general formulation by comparing the spin-polarized EL as well.

In Figs. 4.4 and 4.5 we first compare the STLS $g(r)$ and $S(q)$ data with QMC-TC in the density range $r_s = 1 - 20$ for both the normal ($g_d = 2$) and spin-polarized ($g_d = 1$) states of the EL. If we first concentrate on the QMC data, and compare the effect of the degeneracy factor g_d on $g(r)$ and $S(q)$, we observe that for $r_s = 1$ and 5 the differences are marginal, apart from $g(0)$ values, where the spin-polarized state goes to zero even for $r_s = 1$ case as expected. Another observation is that the spin-polarized state has a more pronounced structure for $r_s = 10$ and 20 values. For both states STLS results are in excellent agreement with the QMC-TC for $r_s = 1$ and 5. However, especially for $r_s = 20$ the peaks signifying an approach towards crystallization are very much underestimated by the STLS. So, in the search for the Wigner solid, which is predicted to be around $r_s \simeq 37$ [75], STLS falls far short[2], which requires a very strong coupling theory. However, such r_s values are well beyond the practical region utilized by electronic devices and materials. We also indicate in $S(q)$ curves for $g_d = 2$, the plasmon contribution for $r_s = 1$; observe that in the long-wavelength limit $S(q)$ is

---

[2] See also our work for further supports [63].

62
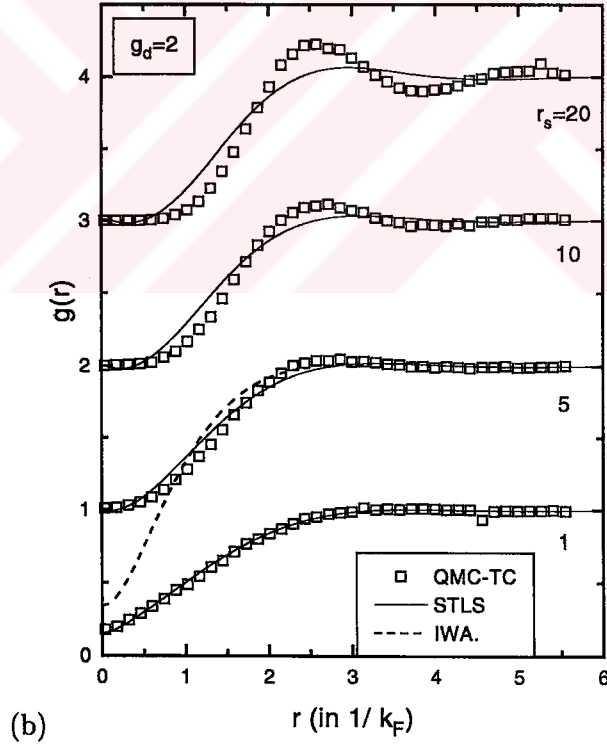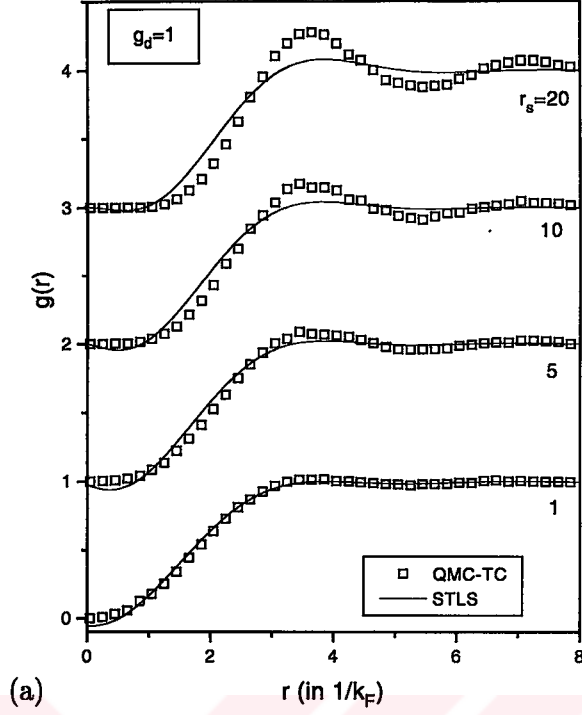
Figure 4.4: Pair-correlation function versus distance for $r_s = 1 - 20$. Hollow squares indicate the QMC data of TC, solid curves are STLS results for a) spin-polarized EL ($g_d = 1$). Upper curves are successively shifted vertically by one unit for clarity. Dotted curve on the right shows Iwamoto's result for $r_s = 5$.

63
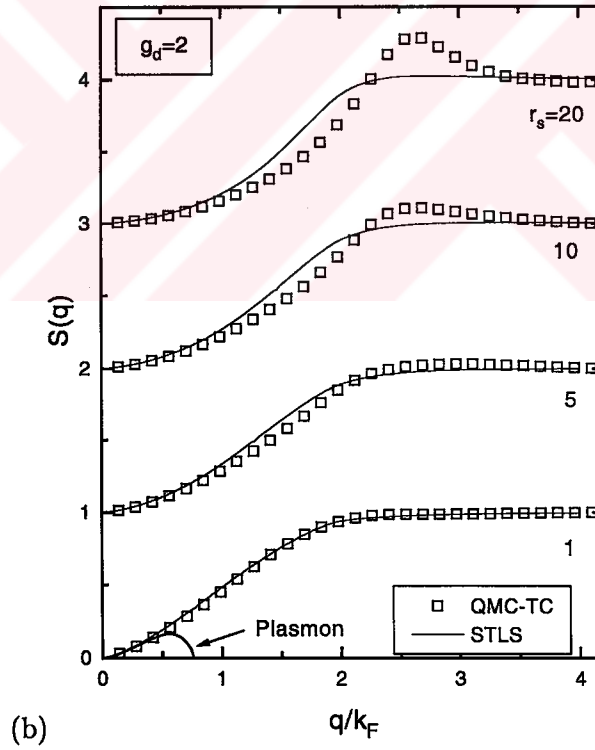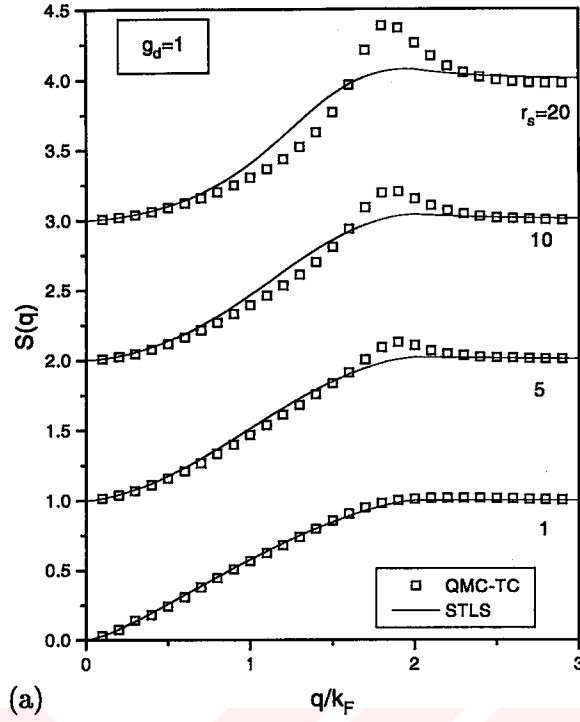
Figure 4.5: Static form factor versus normalized wave number for $r_s = 1 - 20$. Hollow squares indicate the QMC data of TC, solid curves are STLS results for a) spin-polarized EL ($g_d = 1$). Upper curves are successively shifted vertically by one unit for clarity. The STLS plasmon contribution to the overall form factor is indicated on the right for the $r_s = 1$ case.
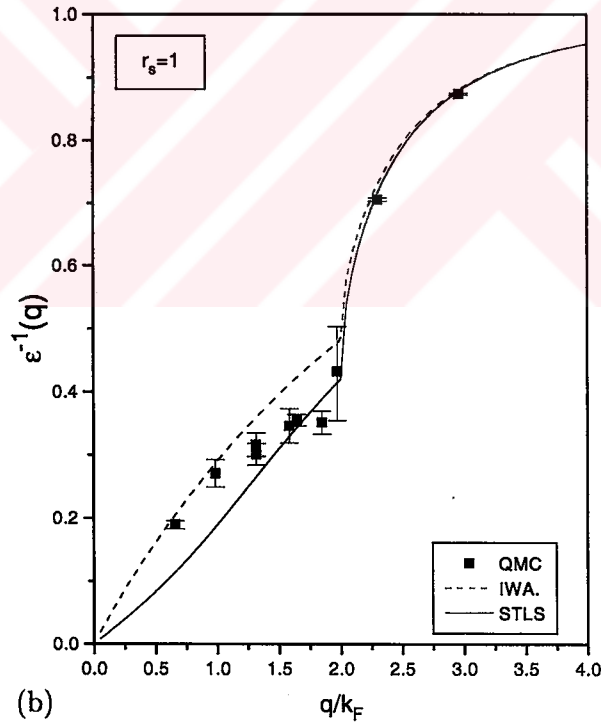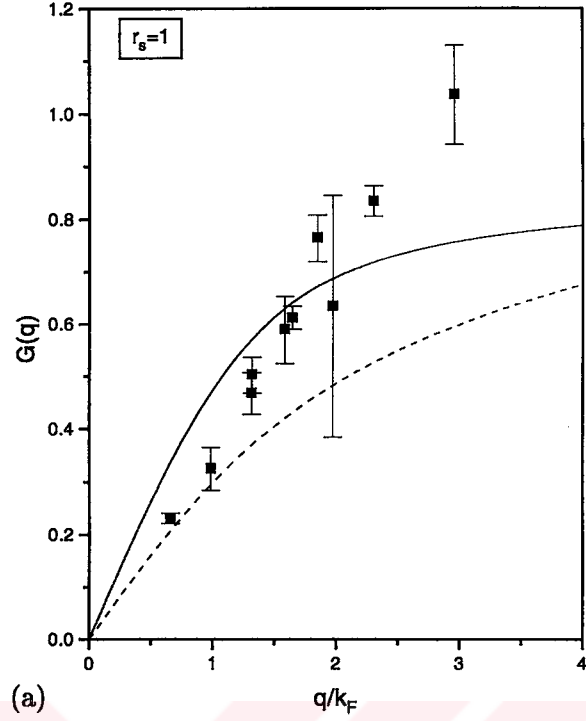
Figure 4.6: Comparison of STLS (solid lines), QMC-S (squares) and pseudopotential approach of Iwamoto (dashed lines) for the a) LFC and b) inverse static DF of a 2D EL with $g_d = 2$ at $r_s = 1$.

65
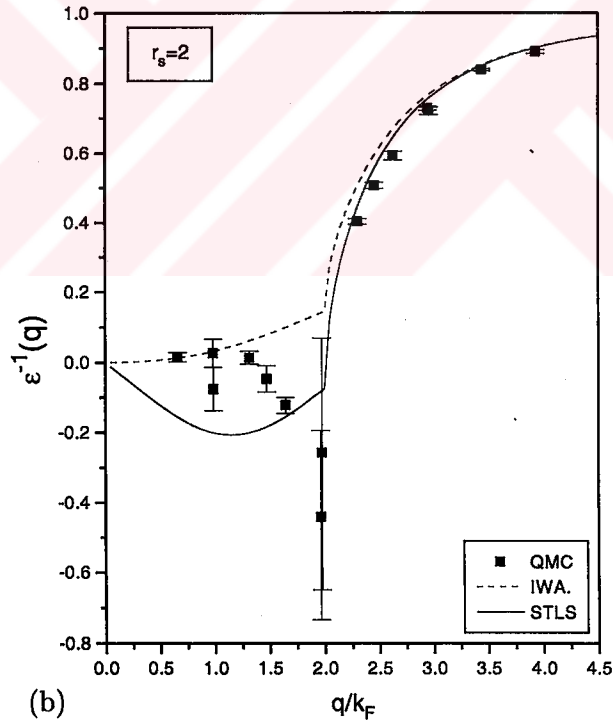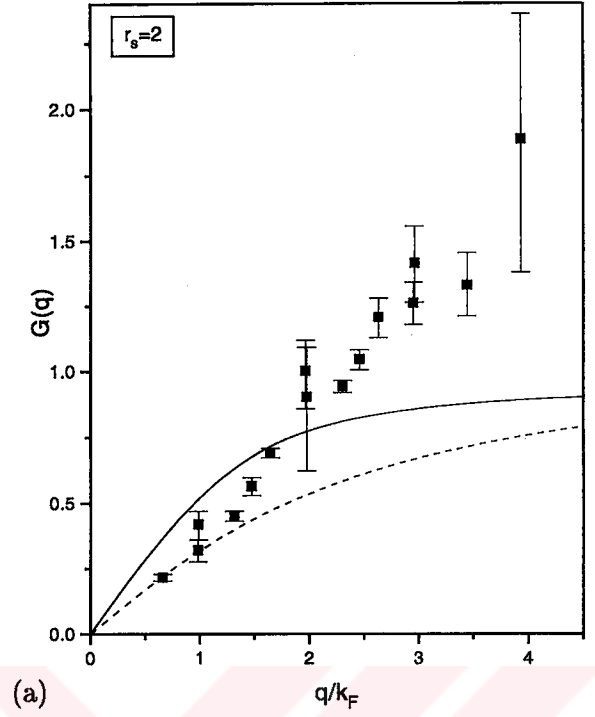
Figure 4.7: Same as the previous figure but at $r_s = 2$.
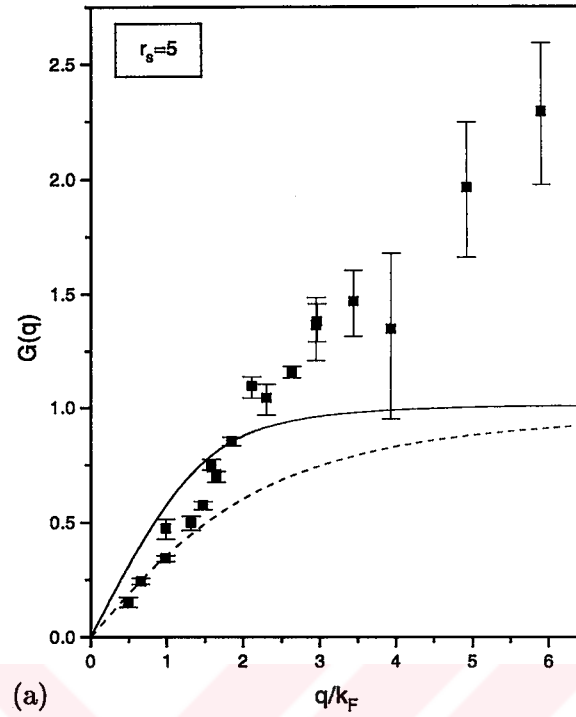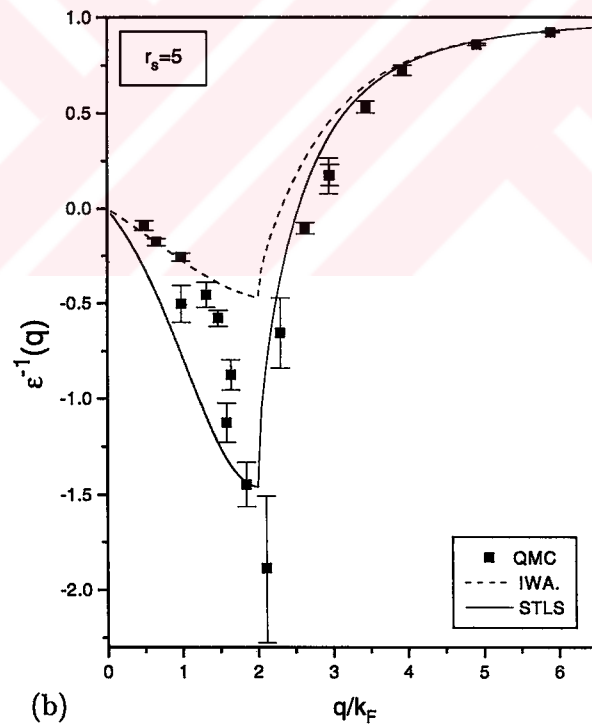
Figure 4.8: Same as the previous two figures but at $r_s = 5$.

dominated by the plasmon contribution as compared to single-pair and multi-pair contributions.

Figs. 4.6 to 4.8 compare LFC and static DF for STLS, QMC-S (Senatore) and pseudopotential approaches. Iwamoto fitted the 2D LFC to the long-wavelength behavior of the compressibility and spin susceptibility data of QMC-TC[3]. The resultant form of the Iwamoto's LFC is again a generalization of the Hubbard LFC in 2D as,

$$G_{2D}^I(q_n) = \underbrace{\frac{q_n}{2\sqrt{q_n^2 + q_{\uparrow\uparrow}^2}}}_{\text{Exchange}} + \underbrace{\frac{q_n}{2\sqrt{q_n^2 + q_{\uparrow\downarrow}^2}}}_{\text{Ex.-Corr.}}. \tag{4.4}$$

The values for $q_{\uparrow\uparrow}$ and $q_{\uparrow\downarrow}$ are tabulated by Iwamoto in the density range r_s=1-40.

The bottleneck about the *static* LFCs has been emphasized in another work of Iwamoto [82]; namely the compressibility sum-rule and the third-frequency moment sum rule [55] cannot be satisfied simultaneously by *static* LFCs. So, depending on the particular application at hand, one should choose a suitable static LFC which performs well for that specific physical quantity of interest. Iwamoto's LFC is appealing for our considerations as it is fitted to the long-wavelength compressiblity of the QMC data where STLS is known to be very weak. Our following investigation illuminates this dark spot by comparing the two extreme static LFCs by the QMC data. On one side we have STLS that violates the compressibility sum rule but has an impressive pair correlation function due to the built-in self-consistency and on the other hand the pseudopotential approach that presumably behaves just the opposite way.

Our observations about Figs. 4.6 to 4.8 can be listed as follows: i) Iwamoto's pseudopotential approach only agrees with the QMC-S in the long-wavelengths, where

---

[3] The seven-year gap between the appearance of 3D and 2D pseudopotential forms is due to the absence of QMC data for the latter, until TC reported their work.
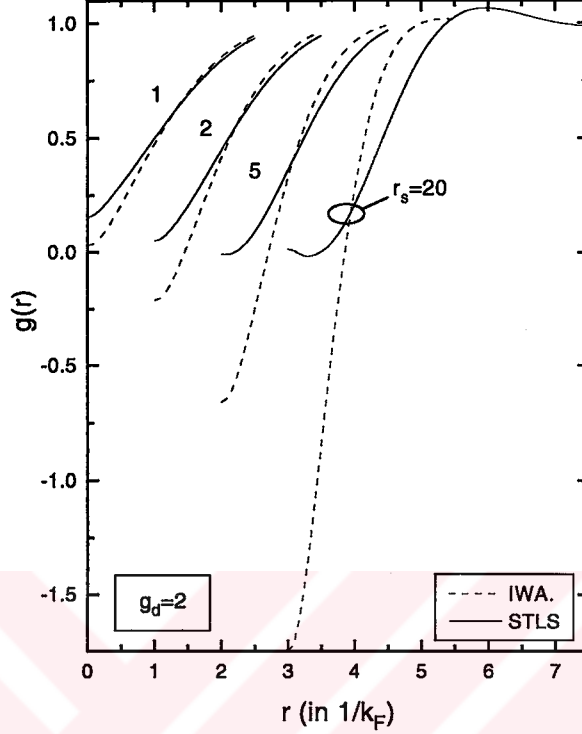
Figure 4.9: Comparison of the pair-correlation functions of the STLS (solid lines) and the pseudopotential appproach of Iwamoto (dashed lines) for several densities of the 2D EL with $g_d = 2$. Curves are successively shifted horizontally by one unit to the right for clarity.

STLS is observed to be in disagreement, ii) for intermediate wave numbers STLS and QMC-S agree very well apart from the fluctuations of the latter, ii) for large wave numbers QMC-S and STLS disagree for $G(q)$ data, where STLS saturates but QMC continues to grow. However, this disagreement is not reflected to the static DF data which shows a good agreement of the two. As a matter of fact, we had similar observations about the static performances of these three aprroaches in 3D case.

Both Iwamoto-Pines [73] and Iwamoto Fig. 4.9 papers do not present any quantitative assessment of their pair-correlation function. We explore this for the 2D case in Fig. 4.9 by comparing $g(r)$ of STLS and Iwamoto; also see $r_s = 1$ curve in Fig. 4.4 (b).

$g(r)$ for small r values as calculated from Iwamoto's LFC is seen to be increasingly negative for increasing r_s values; STLS practically preserves its nonnegative property for all r_s values. In summary, STLS, apart from its deteriorated long-wavelength behavior has several appealing features: i) good agreement with QMC for intermediate and large q values for the static DF over all realistic r_s values, ii) almost nonnegative pair-correlation function, and the most important of all, iii) self- consistent scheme which does not require any fitting to experimental or simulation data (in contrast to pseudopotential approach). This last property makes STLS a highly preferred technique for characterizing quantum liquids with arbitrary geometrical constraints such as heterojunctions, quantum wells, quantum wires and etc., where QMC data is not available.

4.4 An Analytical Fitting to 2D STLS Local-Field Correction

To enable a widespread use of the STLS technique in 2D EL we propose an analytical expression having two fitting parameters [63]. We are led to this effort by the availability of a similar work in 3D EL by Singwi and co-workers [83, 84, 42]. As in the 3D counterpart we restrict our fitting only to the normal-state, single-valley EL (i.e., $g_d = 2$).

To propose a fitting function for the LFC its asymptotic forms must be known. In the small argument case, as $q \to 0$, $G(q) \sim \gamma\, q_n$ and $\gamma = \frac{1}{2} \int_0^\infty dp[1 - S(p)]$. In other words, $G(q)$ depends linearly on q. γ is an important parameter which is related to the compressibility [42], [55]. For the large argument behavior, i.e., as $q \to \infty$, $G(q) \sim 1 - g(0)$, where $g(0)$ is the pair correlation function at interparticle distance

$r = 0$. We propose an interpolating function between these two limiting cases as

$$G(q) = A\left(1 - e^{-q_n \frac{B}{A}}\right),$$ (4.5)

in which A and B are the fitting parameters[4]. If A equals $1 - g(0)$ and B equals γ then the limiting cases will be exactly satisfied, however, to optimize the agreement for all q values, A and B deviate from these values. Table 4.1 lists the fitting parameters as a function of r_s from 0.1 to 6. Both A and B depend smoothly on r_s and one can use a linear interpolation for those r_s values not contained in Table 4.1. For r_s values larger than 6, the electron liquid approaches towards crystallization and a peak begins to appear in $G(q)$. However, the functional form of Eq. (4.5) cannot accommodate this peak and therefore it leads to poor agreement, especially, beyond $r_s = 10$.

Table 4.1: Fitting parameters A and B (see Eq. (4.5)) as a function of r_s for the characterization of the 2D electron liquid. The small (i.e., γ) and the large argument (i.e., G_∞) behavior of the exact STLS $G(q)$ are also shown for completeness.

r_s	0.1	0.5	1	2	3	4	5	6
A	0.5513	0.7036	0.8128	0.9214	0.9752	1.0004	1.0165	1.0296
B	0.6310	0.6804	0.7322	0.8075	0.8585	0.9121	0.9444	0.9583
G_∞	0.5531	0.7260	0.8406	0.9409	0.9813	0.9989	1.0096	1.0130
γ	0.4491	0.5063	0.5472	0.5910	0.6157	0.6317	0.6432	0.6515

In Fig. 4.10 (a) we present our self-consistent STLS results for $G(q)$ and compare them with the fitted form. The value of γ as calculated by the STLS turns out to be larger than the correct value γ_0 which results in the violation of the compressibility sum rule. It must be mentioned that the fitted form has $B > \gamma$ in the r_s range considered. This in turn, will lead to an even degraded compressibility value for the fitted form. To further assess the performance of the fitting, in Fig. 4.10 (b), the

---

[4] Even though, we use the same symbols for the fitting parameters as in Singwi and co-workers' expressions, note the difference in the structure. We made this change to attribute to A and B direct physical meanings; see also Table 4.1.
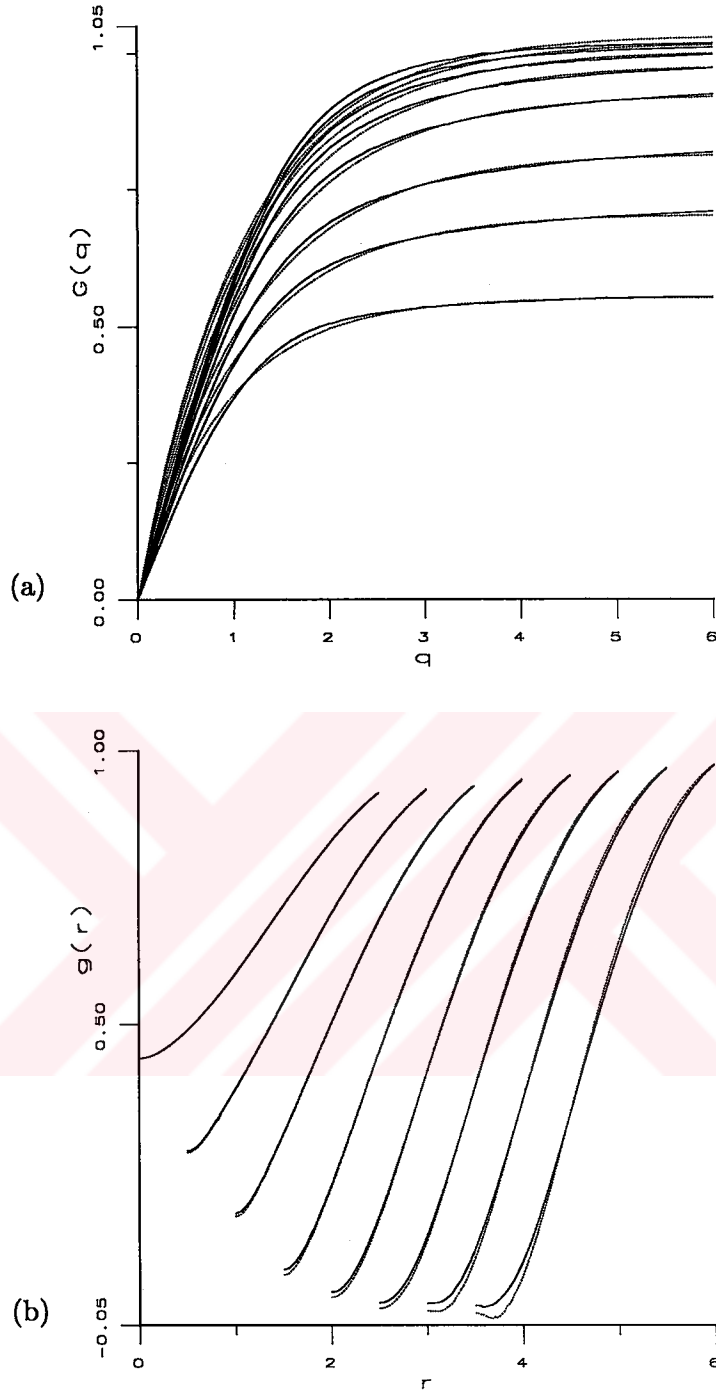
Figure 4.10: Comparison of the exact STLS (solid lines) and the fitted form (dotted lines) for $r_s = 0.1, 0.5, 1, 2, 3, 4, 5, 6$: a) LFC, b) pair-correlation function (curves are shifted horizontally for clarity).

STLS pair correlation function is plotted together with that obtained using the fitted expression(i.e., Eq. (4.5)) for $G(q)$, excellent agreement can be observed.

Knowing $G(q)$, both the dynamic and the static DF of the 2D EL is easily obtained. In particular, the static DF under the fitted form for the LFC becomes[5]

$$
\epsilon^{STLS}(q_n, \omega = 0) = \begin{cases} \dfrac{1 + \dfrac{\sqrt{2}r_s}{q_n}\left[1 - A(1 - e^{-q_n B/A})\right]}{1 - \dfrac{\sqrt{2}r_s}{q_n}A(1 - e^{-q_n B/A})} & \text{for } q_n \leq 2 \\[4em] \dfrac{1 + \dfrac{\sqrt{2}r_s}{q_n}\left[1 - \sqrt{1 - (\dfrac{2}{q_n})^2}\right]\left[1 - A(1 - e^{-q_n B/A})\right]}{1 - \dfrac{\sqrt{2}r_s}{q_n}\left[1 - \sqrt{1 - (\dfrac{2}{q_n})^2}\right]A(1 - e^{-q_n B/A})} & \text{for } q_n > 2 \end{cases}
$$

$$(4.6)$$

4.5 Charge Density Screening in Real Space

One of the direct applications of the DF is to calculate the response of the system under a spatially and/or temporally varying charge distribution. The formulation is easier in the reciprocal space $(\vec{q}, \omega)$, however, we shall eventually obtain the real space/time response by a Fourier transform. For instance, an external charge distribution $\varrho_{ext}(\vec{r}, t)$ has the form in $(\vec{q}, \omega)$ space as

$$
\rho_{ext}(\vec{q}, \omega) = \int \int d^2r \, dt \, e^{-i\vec{q}\cdot\vec{r}} \, e^{i\omega t} \, \varrho_{ext}(\vec{r}, t). \tag{4.7}
$$

If, in particular, the external charge has no time dependence (i.e., static) then

$$
\rho_{ext}(\vec{q}, \omega) = 2\pi \, \delta(\omega) \underbrace{\int d^2r \, e^{-i\vec{q}\cdot\vec{r}} \, \varrho_{ext}(\vec{r})}_{\rho_{ext}(\vec{q})}. \tag{4.8}
$$

---

[5] This expression was changed by the editorial office of the Physical Review B for stylistic reasons and unfortunately, published with a minor mistake in the Ref. [63]. The form given here is correct.

73

The system's response to $\rho_{ext}(\vec{q}, \omega)$ is in the form of an induced charge density, which is also related to the DF and the total screened charge density ρ_{scr} through

$$\rho_{scr}(\vec{q}, \omega) = \rho_{ind}(\vec{q}, \omega) + \rho_{ext}(\vec{q}, \omega) = \frac{\rho_{ext}(\vec{q}, \omega)}{\epsilon(\vec{q}, \omega)},\tag{4.9}$$

so that,

$$\rho_{ind}(\vec{q}, \omega) = \left[\frac{1}{\epsilon(\vec{q}, \omega)} - 1 \right] \rho_{ext}(\vec{q}, \omega).\tag{4.10}$$

The induced charge density distribution in real space-time under a dynamic external perturbation becomes

$$\varrho_{ind}(\vec{r}, t) = \int \frac{d^2 q}{(2\pi)^2} \int \frac{d\omega}{2\pi} \left[\frac{1}{\epsilon(\vec{q}, \omega)} - 1 \right] \rho_{ext}(\vec{q}, \omega)\, e^{i\vec{q}\cdot\vec{r}}\, e^{-i\omega t}.\tag{4.11}$$

For a static external charge $\varrho_{ext}(\vec{r})$, this expression becomes

$$\varrho_{ind}(\vec{r}) = \int \frac{d^2 q}{(2\pi)^2} \left[\frac{1}{\epsilon(\vec{q}, 0)} - 1 \right] \rho_{ext}(\vec{q})\, e^{i\vec{q}\cdot\vec{r}}.\tag{4.12}$$

We shall consider two static external charge density profiles. The first one will be a disk-shaped uniform distribution as

$$\varrho_{ext}(\vec{r}) = \begin{cases} \rho_0 & , |\vec{r}| \leq a \\ \\ 0 & , |\vec{r}| > a \end{cases}.\tag{4.13}$$

The corresponding form in reciprocal space becomes

$$\rho_{ext}(\vec{q}) = 2\pi\rho_0\, \frac{a}{q}\, J_1(a\, q),\tag{4.14}$$

where J_n is n-th order cylindrical Bessel function of the first kind. Then using Eq. (4.12) the induced charge density in real space becomes

$$\varrho_{ind}(\vec{r}) = a\rho_0 \int_0^\infty dq\, J_1(a\, q) J_0(q\, r) \left[\frac{1}{\epsilon(\vec{q}, 0)} - 1 \right].\tag{4.15}$$

This expression must be evaluated numerically for a given DF. The total induced charge is determined simply as

$$N_{ind} = \int d^2r \, \varrho_{ind}(\vec{r}) = 2\pi \int_0^\infty dr \, r \, \varrho_{ind}(r). \qquad (4.16)$$

If we repeat the same analysis for a localized (point) external impurity, i.e., $\varrho_{ext}(\vec{r}) = \delta(\vec{r})$, then we get

$$\varrho_{ind}(\vec{r}) = \int_0^\infty \frac{dq}{2\pi} \, q \left[\frac{1}{\epsilon(\vec{q}, 0)} - 1 \right] J_0(q \, r). \qquad (4.17)$$

The results of these two test cases, namely the disk-shaped positive static impurity with $\rho_0 = 1/(\pi \, a^2)$ and a chosen as $2/k_F$ and the point impurity are shown in Fig. 4.11 for $r_s = 0.5$ and 4 values [85]. For comparison purposes the RPA is also included as well as the STLS results. The latter is observed to have a stronger screening and the discrepancy with the RPA is more pronounced in the distributed (disk-shaped) external charge density case. The oscillations of the induced charge density (which are barely visible in this scale) of the point-charge screening are known as the Friedel oscillations [51, 42].

4.6 Correlation Energy of the 2D Electron Liquid

Wigner defined the correlation energy *per electron* of the EL as

$$E_{corr} = E_g - E_g^{HF}, \qquad (4.18)$$

where E_g is the ground-state energy (per electron) of the EL and E_g^{HF} is the ground-state energy (per electron) in Hartree-Fock (HF) approximation. The difference between the two lies in the many-body wave functions that characterize the ground-state

75
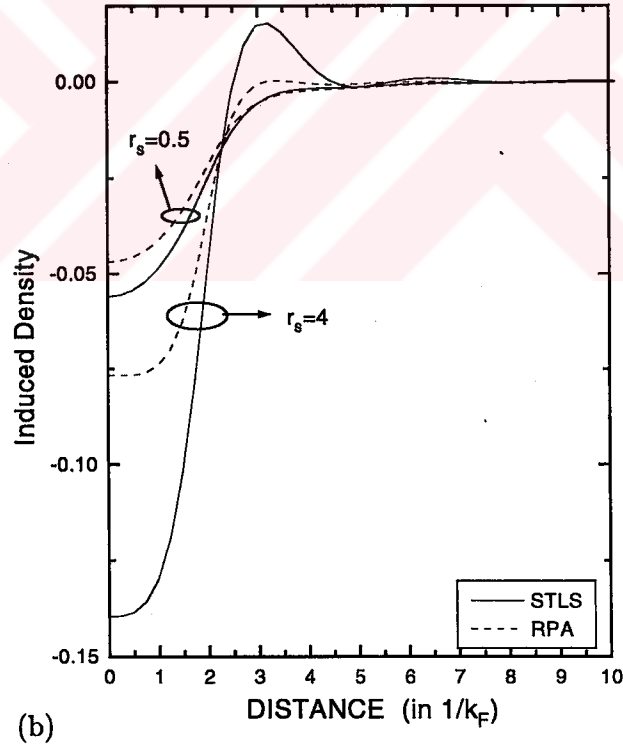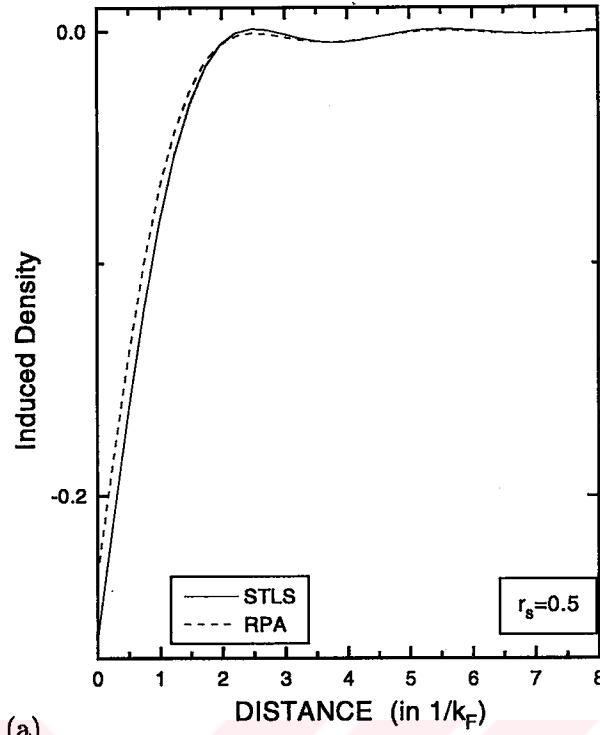
Figure 4.11: Comparison of STLS (solid lines) and RPA (dashed lines) for the induced charge density versus distance in real space for a) a positive point impurity, b) a positive disk-shaped impurity (see the text). Normal-state EL ($g_d = 2$) is assumed.

of the EL: the former considers the *exact* ground-state, $|\Psi_g\rangle$, i.e., $E_g = \langle\Psi_g|H = \hat{T} + \hat{U}|\Psi_g\rangle$ and the latter assumes the ground-state of the EL to be that of the *non-interacting* EL, which is the filled Fermi sea, $|\mathrm{F}\rangle$, i.e., $E_g^{HF} = \langle\mathrm{F}|H|\mathrm{F}\rangle$. E_g^{HF} can be splitted into the kinetic and potential energy terms as

$$E_g^{HF} = \langle\mathrm{F}|\hat{T}|\mathrm{F}\rangle + \langle\mathrm{F}|\hat{U}|\mathrm{F}\rangle = E_{kin}^{HF} + E_{ex}^{HF}. \qquad (4.19)$$

The potential energy for the filled Fermi sea is the Coulomb interaction between equal spin electrons and for this reason it is abbreviated as *ex* standing for exchange.

The correlation energy is calculated by treating the Hamiltonian artificially as $\hat{H}(\lambda) = \hat{T} + \lambda\hat{U}$ and performing an integration over the coupling constant λ and subtracting the HF exchange energy. That is,

$$E_{corr} = \int_0^1 \frac{d\lambda}{\lambda}\, E_{int}(\lambda) - E_{ex}^{HF}, \qquad (4.20)$$

where

$$E_{int}(\lambda) = \langle\Psi_g(\lambda)|\lambda\hat{U}|\Psi_g(\lambda)\rangle. \qquad (4.21)$$

We do not include the details of the calculation[6], but present the final form for the correlation energy of the 2D EL having $g_d = 2$.

$$E_{corr,2D} = \underbrace{-\frac{2\sqrt{2}}{r_s^2}\int_0^{r_s} dr_s'\,\gamma(r_s')}_{\text{Exchange-correlation En.}} + \underbrace{\frac{8\sqrt{2}}{3\,\pi\,r_s}}_{-E_{ex,2D}^{HF}}, \qquad (4.22)$$

where

$$\gamma(r_s') = \frac{1}{2}\int_0^{\infty} dq_n\,\left[1 - S_{r_s'}(q_n)\right]. \qquad (4.23)$$

Note that to determine the correlation energy at a density r_s, we need to know the static form factor at all intermediate r_s' values between 0 to r_s. For this reason the

---

[6] For the details Mahan's book can be referred for the 3D El [42] and Iwamoto's paper includes both 3D and 2D ELs [82].
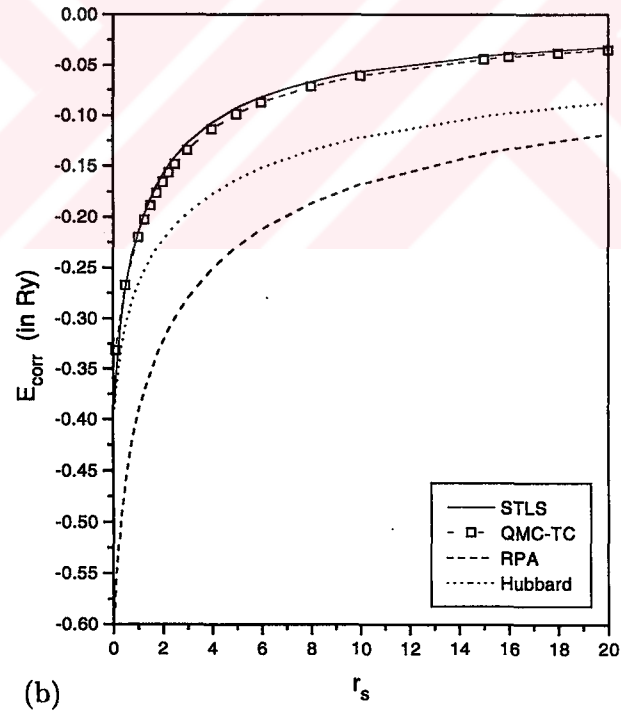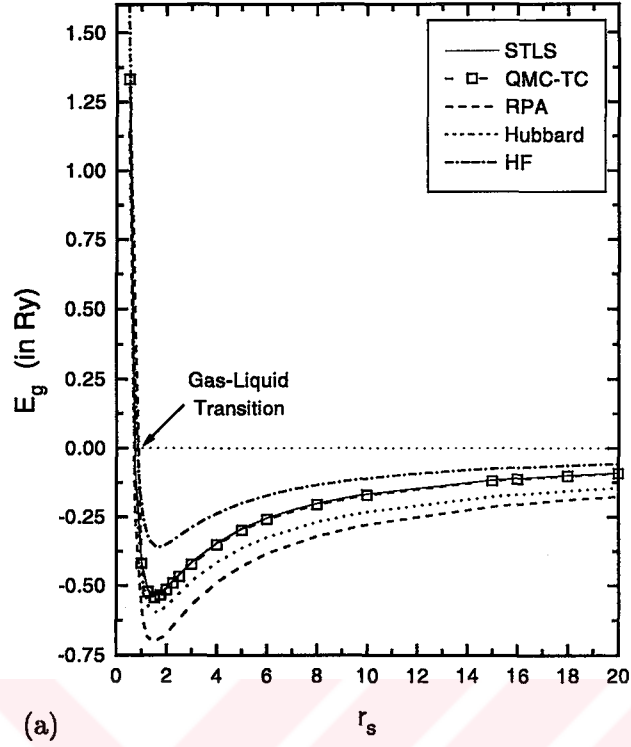
Figure 4.12: a) the ground-state energy and b) the correlation energy (both in Rydbergs) of the 2D EL with $g_d = 2$ versus r_s using several techniques as indicated.

computation of the correlation energy and therefore the compressibility (see the next section) of the EL becomes a costly task. To reduce this cost, we could have made use of the fitted $G(q)$ data, however, we avoid this simplification and present the correlation energy results of the 2D EL in Table 4.2. This table also contains the results of several other references for comparison. Fig. 4.12 (a) and (b) illustrate the ground-state energy and the correlation energy of the 2D EL again under several approaches. Notably, we indicate in Fig. 4.12 (a) the gas-liquid transition density as the point where the ground-state energy becomes negative. Having made this choice which is somewhat arbitrary (see Isihara [61]), all approaches (including the Hartree-Fock) yield a value about $r_s = 0.7$ for this transition density, however, in this work we use the word *liquid* for all densities without discrimination.

4.7 Isothermal Compressibility of the 2D Electron Liquid

For the electrical engineers or even for device engineers, the word isothermal compressibility may sound something of only academic concern or highly irrelevant for the electronic operation. This turns out to be a simplistic approach, actually every effect is highly electronic in origin. Isothermal compressibility is a thermodynamic quantity; it describes an important macroscopic property of the system. Our system is the EL; imagine now that we want to compress this system, keeping the temperature (i.e., isothermal) and particle number inside constant. We must overcome basically two kinds of forces: one is the pressure exerted on the bounding walls of the system due to the kinetic energy of the electrons, the other is the interparticle Coulomb and exchange forces that resist to compression. To explain the latter just recall that equal-spin particles do not like to get closer in space, which the compression wants

79

Table 4.2: Correlation energy (in absolute value) of the 2D EL with $g_d = 2$ using several techniques: STLS (our results), QMC-TC ([75]), STLS-M (Mahan '85 [64]), STLS-J (Jonson '76 [86]), Freeman's diagrammatic calculations CCLAD (Freeman '83 [87]), and Ring (Freeman '78 [88]).

r_s	STLS	QMC-TC	STLS-M	STLS-J	CCLAD	Ring
0.0					0.39	0.393
0.5	0.270	0.268	0.275	0.250	0.28	0.274
1	0.216	0.220	0.224	0.211	0.22	0.231
1.25	0.197	0.203				
1.50	0.182	0.189	0.192			
1.75	0.169	0.177				
2	0.159	0.166	0.170	0.155	0.16	0.185
2.25	0.149	0.157				
2.5	0.141	0.148				
3	0.127	0.135				
4	0.107	0.114		0.108	0.11	0.141
5	0.093	0.099				
6	0.082	0.088				
7	0.074					
8	0.067	0.072		0.066	0.064	0.103
9	0.061					
10	0.057	0.061				
15	0.041	0.044				
16	0.039	0.042		0.038	0.037	0.072
17	0.037					
18	0.036	0.038				
19	0.034					
20	0.033	0.035				

to achieve.

Again we do not include the intermediate steps but present only the final expression for the compressiblity of the 2D EL (see the previous footnote).

$$\frac{K_{2D}^0}{K_{2D}} = 1 - \frac{\sqrt{2}r_s}{\pi} + \frac{1}{8}\left[-r_s^3\frac{\partial E_{corr,2D}}{\partial r_s} + r_s^4\frac{\partial^2 E_{corr,2D}}{\partial r_s^2}\right], \qquad (4.24)$$

where $E_{corr,2D}$ in this expression should be in Rydberg units, and K_{2D}^0 is the isothermal compressibility of the 2D free Fermi gas, which is used for normalization purposes. We consider the *inverse* compressiblity (just as in the inverse static DF case) due to the ease in plotting this quantity rather than the reciprocal. Observe that, having determined the correlation energy, we additionally require a double differentiation with respect to r_s to get the compressibility expression.

There is an alternative method of determining the isothermal compressibility which is much easier to compute once the static DF is known. At this point we quote Iwamoto [82]: "The requirement that the response of the system to a static long-wavelength perturbation (a uniform compression) must give the compressibility which is obtained thermodynamically from the ground-state energy provides a constraint on the long-wavelength behavior of the static screened response function and hence $G(q)$". There is an *exact* relation between the compressiblity and the long-wavelength limit of the static DF as [42]

$$\lim_{q\to 0}\epsilon(q,0) = 1 + U^0(q)\,n^2\,K, \qquad (4.25)$$

where n is the particle density, and this relation is valid for any dimensions. The normalized compressibility in terms of the static DF for 2D EL becomes

$$\frac{K_{2D}}{K_{2D}^0} = \lim_{q\to 0}\left\{\frac{q}{q_{TF}}[\epsilon(q,0) - 1]\right\}, \qquad (4.26)$$

where $q_{TF} = 2/a_B^*$ is the Thomas-Fermi wave number for 2D EL (with $g_d = 2$). We now list the specific forms of the normalized inverse compressibility for the choices of RPA, Hubbard and STLS:

$$\left(\frac{K_{2D}^0}{K_{2D}}\right)_{RPA} = 1, \tag{4.27}$$

$$\left(\frac{K_{2D}^0}{K_{2D}}\right)_{Hub.} = 1 - \frac{r_s}{\sqrt{2}}, \tag{4.28}$$

$$\left(\frac{K_{2D}^0}{K_{2D}}\right)_{STLS} = 1 - \sqrt{2}\, r_s\, \gamma(r_s), \tag{4.29}$$

where $\gamma(r_s) = \frac{1}{2}\int_0^\infty dq_n\,[1 - S(q_n)]$. Also note that the RPA static DF in the long-wavelength limit behaves just like the noninteracting Fermi gas so that the ratio comes out as unity.

In summary, we have two choices for computing the compressibility of the EL and they should yield the same result; this requirement is called the *compressibility sum-rule*. The inevitably approximate nature of the DFs cause the violation of this rule by most of them. We illustrate this point in Fig. 4.13 by calculating the normalized inverse compressiblity using the energy and the long-wavelength static DF approaches. As in the 3D EL case [42] STLS violates the compressibility sum-rule which was in fact, reflected in the poor agreement with the QMC data in the long- wavelengths.

4.8   Overscreening

Fig. 4.13 illustrates that all of the techniques (other than RPA via static DF) agree upon the fact that eventually the compressibility of the 2D EL becomes *negative*; their
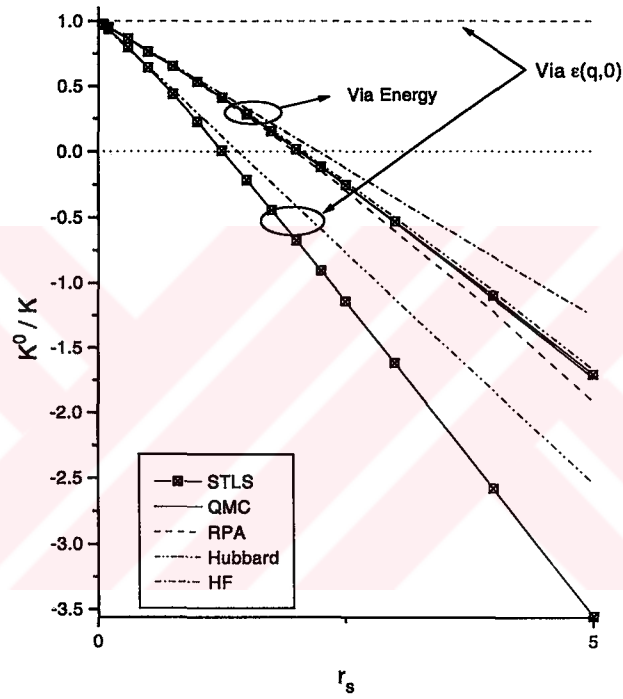
Figure 4.13: The isothermal compressibility of the 2D EL with $g_d = 2$ versus r_s using several techniques. Two alternative approaches, the energy differentiation and long-wavelength static DF are used as indicated.

discrepancy is about the critical density at which this occurs. A negative compressibility has a very drastic physical consequence: the system wants to get compressed without any need for an external force. Obviously such a system cannot be structurally stable; it should collapse beyond this critical density. The stability of real systems (such as metals, semiconductors) is established by the positive background [75]; recall that in the EL model we assume the positive background to be rigid, which cannot respond to any perturbation. For this reason, we can call this peculiar effect as the negative *electronic* compressibility, to spare room for the ionic contribution. The speculative nature of this subject has recently changed, by the announcement of Eisenstein and co-workers about the measurement of a negative electronic compressiblity of a 2D quantum well, which is actually a quasi-2D structure [89]. Very recently, Cambridge group also reported their results [90] on the compressibility of the quantum wells, confirming the previous experiment, but claimed to be with better accuracy[7]. Furthermore, it is pointed out that, for the compressibility of quantum wells with large well widths, the contribution of the Hartree band bending term is sizeable. As a matter of fact, the theoretical predictions of Gold and Calmels' [91] on the compressibility of quasi-2D quantum wells ignoring this term is shown to be in large disagreement with the experimental data [90].

Negative compressibility is intimately related to the negative long-wavelength static DF. Figs. 4.6, 4.8 (b) indicate the negative q-zone of the static DF. As Dolgov *et al.* [92] have pointed, a negative static DF does not contradict with the causality, as a matter of fact, this feature is shared by most of the techniques beyond the RPA including the QMC. The physical consequence of a negative static DF is that

---

[7] We are thankful to Prof. B. Tanatar for informing us about this work.

an external impurity can be screened by more than the equal amount of opposite charge. This effect is sometimes named as *anti-screening* (see, for instance, Ref. [93]), however, here we prefer the word *overscreening*. A curious point that has not been addressed in the literature is the driving mechanism of this effect, which we recently raised in a previous work [85]. To illuminate this point, we first investigate different physical systems that show an overscreening. First of all overscreening is not limited to i) 2D ELs, it exists in 3D EL as well (see, for instance, Fig. 4.3 (b)), moreover, ii) this effect is present also in Bose liquids [94], furthermore, iii) classical liquids show overscreening too [95]. These diverse examples reveal that overscreening is not due to a i) dimensionality effect, or to a ii) quantum statistical effect, or to a iii) quantum mechanical effect, respectively. A common feature in all these example cases is that overscreening is observed for low particle densities where the strong potential energy dominates the system behavior, which leads us to conclude that overscreening is driven by a liquid-solid transition. This subject is still premature and an important initial step is to determine the phase diagram in the density-temperature plane of the "normal" electron liquid.

CHAPTER 5

QUASI-TWO-DIMENSIONAL ELECTRON LIQUID:

HETEROJUNCTIONS

Research in 2D electronic systems has been driven mainly by the technologically important structures such as silicon-inversion layers which actually forms the basis of the metal-oxide semiconductor field effect transistors (MOSFETs) and modulation-doped field effect transistors (MODFETs or also named as HEMTs) [96]. The geometrical and physical parameters that define the actual realization of these 2D structures also bring additional challenges to their characterizations. In addition to these highly important transistor structures, in 2D, novel physical effects have recently been observed such as high T_c superconductivity in Copper Oxide layers, and the integer and fractional quantum Hall effects [97, 61, 3, 98, 99].

In this part of the thesis, our aim is to present an accurate and systematic characterization of the dielectric properties of the quasi-2D (Q2D) EL in real heterojunctions where the electron distribution can penetrate to both sides of the interface. The charge distribution is based on a variational approach proposed by Bastard

[100, 101, 102]. The accurate characterization of the Q2D EL is formed by two steps. The first step is the variational determination of the confined electron energy states and the associated wave functions; this requires a self-consistency as the confinement potential is in part, due to trapped electrons[1]. In mathematical terms, we simply have a coupling between the Possion's equation and the Schrödinger equation, so that both have to be satisfied simultaneously. As a matter of fact, most of the solid-state problems are defined by coupled equations and need a self-consistent solution. The second step utilizes the single-electron wave functions to obtain the Coulomb form factor which determines how much the bare Coulomb interaction differs from its strictly 2D value, due to the extension of the electrons along the confinement direction. The image charges arising due to background dielectric constant mismatches at the material boundaries need to be included as well. The Coulomb form factor is the key ingredient for an accurate DF of the Q2D EL. The DF of the Q2D EL, which is our main result, is restricted to the so-called electrical quantum limit (EQL), where only the lowest subband along the confinement direction is populated[2]. To assess the validity region of the EQL and the influences of higher subband populations on the Coulomb form factor, we actually consider a two-subband populated case. In the following section we begin by presenting the general framework of the variational self-consistent treatment of the Q2D EL for any number of filled subbands. Choosing the GaAs/AlGaAs heterojunction as the candidate Q2D system, we give the DF for wide ranges of electron and ionized acceptor densities. We also fit analytical expressions to our data for the efficient use of these results by other researchers [110]. The

---

[1] The self-consistent potential produced by these electrons is commonly called the Hartree potential.

[2] We refer to a very recent work [103], discussing somewhat formally, the effects of higher subbands on the DF.

87

variational expressions for a heterojunction with two occupied subbands are deferred
to the appendix section.

5.1 General Framework for the Self-Consistent Variational Characterization of the Q2D Electronic Structure

Our aim is to determine, for a given 2D free carrier density (n_{2D}), the subband wave
functions $(\varsigma_i$'s), and the Fermi energy E_F. Strictly speaking this requires a full 3D
numerical characterization. We rather, follow a variational approach that is sim-
pler but yet highly accurate. However, this variational approach becomes extremely
cumbersome for more than two populated subbands.

As in any problem in quantum mechanics we first need to introduce the Hamilto-
nian (within the single-band effective mass approximation):

$$H = -\frac{\hbar^2}{2m^*(z)}\nabla_t^2 - \frac{\hbar^2}{2}\frac{d}{dz} + U_{ID}(z) + U_{e-e}(z) + U_{bar}(z) \qquad (5.1)$$

where ∇_t^2 is the transverse Laplacian, U_{ID} is the potential energy due to ionized
dopants, U_{e-e} is the so-called Hartree potential produced by the subband electrons
and U_{bar} is the barrier potential energy resulting from the conduction band offset at
the heterojunction. As seen from this Hamiltonian the electron is free to move in the
$x-y$ plane, so the transverse eigenstates are 2D plane waves forming a continuum and
the correct enumeration requires the 2D density of states (DOS). The confinement
along the $z-$direction gives rise to subbands along the z direction.

$$H\,\Psi_{i,k_x,k_y}(x,y,z) = \left[E_i + \frac{\hbar^2}{2m^*}\left(k_x^2 + k_y^2\right)\right]\Psi_{i,k_x,k_y}(x,y,z), \qquad (5.2)$$

$$\Psi_{i,k_x,k_y}(x,y,z) = \frac{e^{i(k_x x + k_y y)}}{\sqrt{A}}\,\varsigma_i(z), \qquad (5.3)$$

where A is the normalization area in the $x-y$ plane.

88

Now we concentrate on the z–problem and apply a variational strategy. The self-consistency actually comes into play when more than one subband is populated (i.e., beyond the EQL), so, for generality we relax the EQL approximation. We now outline the formulation for a *fixed* 2D electron density, with N_{sub} subbands being occupied. As a matter of fact, we do not know in advance N_{sub}, neither the density of electrons $(n_{2D,i})$ in each subband. But formally we can write,

$$n_{2D} = \sum_{i=1}^{N_{sub}} n_{2D,i}, \tag{5.4}$$

$$n_{2D,i} = \int_{E_i}^{E_F} D_{2D}(E) \, \Theta(E_F - E_i) \, dE, \tag{5.5}$$

where D_{2D} is the 2D density of states including the standard spin degeneracy [104]

$$D_{2D}(E) = \frac{m^*}{\pi \hbar^2}, \tag{5.6}$$

so that

$$n_{2D,i} = \frac{m_i^*}{\pi \hbar^2} \, (E_F - E_i) \, \Theta(E_F - E_i), \tag{5.7}$$

where m_i^* is the *subband* effective mass to be disclosed later.

The first step in the variational procedure is to choose appropriate variational subband wave functions $\varsigma_i(z, \lambda_i)$ with λ_i being the variational parameter. For notational simplicity we shall assume each subband wave function to have one variational parameter -λ, but in our implementation this will be more than one. These subband wave functions must satisfy the following orthonormality condition

$$\int_{-\infty}^{+\infty} \varsigma_n^*(z) \, \varsigma_m(z) \, dz = \delta_{n,m} \,, \tag{5.8}$$

for all subbands n, m, where $\delta_{n,m}$ is the Kronecker delta.

The potential energy term $U_{bar}(z)$ in the Hamitonian reminds us that there are interfaces (physical discontinuties) in the geometry. For illustration purposes we

89

assume that we have an interface along $z = z_b$. In general, this forces us to specify different forms for $\varsigma_i(z)$ on both sides of the interface. Then, we need to impose the following two continuity conditions at the interface

$$\varsigma_i(z)\big|_{z_b^-} = \varsigma_i(z)\big|_{z_b^+}, \tag{5.9}$$

$$\frac{1}{m_i^*(z)}\frac{d}{dz}\varsigma_i(z)\bigg|_{z_b^-} = \frac{1}{m_i^*(z)}\frac{d}{dz}\varsigma_i(z)\bigg|_{z_b^+}, \tag{5.10}$$

where the first one ensures the single-valuedness of the probability and the second guarantees the continuity of the particle current.

Having disciplined the variational wave functions with these conditions we can now outline the recipe for the self-consistent loop for a given n_{2D}.

- First we guess N_{sub} and subband energy levels E_i^{old} for $i = 1, \cdots, N_{sub}$. (Successfull guesses can be made if the process is first initiated from densities where EQL holds and gradually increasing the density keeping track of the energy levels.)

- Fermi energy and subband populations are then determined as

$$E_1 + \frac{\pi\hbar^2}{m_1^*}\,n_{2D,1} = E_F, \tag{5.11}$$

$$\vdots$$

$$E_{N_{sub}} + \frac{\pi\hbar^2}{m_{N_{sub}}^*}\,n_{2D,N_{sub}} = E_F, \tag{5.12}$$

and

$$n_{2D,1} + n_{2D,2} + \cdots + n_{2D,N_{sub}} = n_{2D}. \tag{5.13}$$

These constitute $(N_{sub} + 1)$ equations for the same number of unknowns.

- Then we determine the *total system* energy *per particle* as the sum of the kinetic and potential energy terms, which are

$$\langle T \rangle_{sys} = \frac{1}{n_{2D}}\sum_{i=1}^{N_{sub}} n_{2D,i}\,\langle \varsigma_i|\hat{T}|\varsigma_i \rangle, \tag{5.14}$$

$$\langle U_{TOT} \rangle_{sys} \quad = \quad \frac{1}{n_{2D}} \sum_{i=1}^{N_{sub}} n_{2D,i} \, \langle \varsigma_i | U_{ID} + U_{bar} + \frac{1}{2} U_{e-e} | \varsigma_i \rangle, \qquad (5.15)$$

where the 1/2 term in front of the U_{e-e} term is to avoid the double counting of the electron-electron interaction in the *total* system energy.

- Now we minimize the *total system* energy per particle and determine the variational parameters λ_i's accordingly.

$$E_{sys}(\lambda_1, \cdots, \lambda_{N_{sub}}) = \langle T \rangle_{sys} + \langle U_{tot} \rangle_{sys}. \qquad (5.16)$$

We denote the particular λ_i values that minimize E_{sys} as $\lambda_{i,min}$.

- Knowing $\lambda_{i,min}$'s now we determine the subband energies E_i^{new} as

$$E_i^{new} = \langle \varsigma_i(\lambda_{i,min}) | \hat{T} + U_{ID} + U_{bar} + U_{e-e} | \varsigma_i(\lambda_{i,min}) \rangle, \qquad (5.17)$$

where U_{e-e} actually depends on all variational parameters, λ_i's.

This loop has to be iterated till subband energies converge, that is to say

$$\frac{1}{N_{sub}} \sum_{i=1}^{N_{sub}} |E_i^{new} - E_i^{old}| < \epsilon, \qquad (5.18)$$

where ϵ is a suitable small positive threshold number. The common suggestion in any recursive algorithm is to use a mixture of the n'th and $(n-1)$'th iteration results to assure convergence at the expense of longer execution time. For this reason, we can mix the subband energies as

$$\frac{1}{2} E_i^{new} + \frac{1}{2} E_i^{old}.$$

Finally as promised we mention the subband effective mass which is actually a wave function-weighted sum of the two region masses as

$$m_i^* = \left[\int_{-\infty}^{z_b} dz \, \frac{|\varsigma_i(z)|^2}{m_B^*} + \int_{z_b}^{+\infty} dz \, \frac{|\varsigma_i(z)|^2}{m_A^*} \right]^{-1}, \qquad (5.19)$$

where m_B^* (m_A^*) is the conduction band effective mass for the material that resides in the region $z < z_b$ $(z > z_b)$.

5.2 Variational Wave Functions for a Penetrable-Barrier Heterojunction

The electrons from ionized donors in the barrier side of a modulation doped hetero-junction are trapped in a wedge-like well formed by a step barrier due to conduction band edge discontinuity on one side, and the potential due to presence of the transferred electrons and ionized acceptors on the other [105]. The one-dimensional quantum confinement gives the Q2D nature to the system and behaves remarkably different than ideal 2D and 3D systems. In handling the many-body effects in hetero-junctions we avoid some critical simplifications that have been used in the past such as infinite barrier height [106], [107], [108] (which is a reasonable approximation only for Si inversion layers) and no ionized acceptors within the channel [109] (which is in fact not the case in practise). For an accurate account of the electronic distribution in heterojunctions, we use Bastard's variational approach that was tested previously in determining the subband energies [102]. We do not mention the particular assumptions and the solution of the Poisson's equation but refer for these to Bastard's work [101].

5.2.1 Electric Quantum Limit

Bastard proposed the following variational form for the lowest subband $\varsigma_1(z)$ allowing penetration to the barrier region, $(z < 0)$ [101]

$$
\varsigma_1(z) = \begin{cases} M_1 e^{\kappa_{b1} z/2}, & \text{for } z \leq 0 \\ \\ N_1(z + z_0)e^{-bz/2}, & \text{for } z \geq 0 \end{cases} \quad . \tag{5.20}
$$

92

Invoking the continuity of $\varsigma_1(z)$ and $m^{-1}(z)\frac{d}{dz}\varsigma_1(z)$ at $z = 0$ and the normalization of $\varsigma_1(z)$, $\int_{-\infty}^{+\infty} dz |\varsigma_1(z)|^2 = 1$, yields the following three equations,

$$M_1 = N_1 z_0, \tag{5.21}$$

$$z_0 = \frac{2}{b + \kappa_{b1}\frac{m_A}{m_B}}, \tag{5.22}$$

$$N_1 = \sqrt{\frac{b^3}{2\left[1 + bz_0 + \frac{b^2 z_0^2}{2}\left(1 + \frac{b}{\kappa_{b1}}\right)\right]}}. \tag{5.23}$$

Bastard also set $\kappa_{b1} = 2\sqrt{2m_B U_b/\hbar^2}$ and used b as the only variational parameter. Here U_b is the barrier height (conduction band offset), i.e., $U_{bar}(z) = U_b \Theta(-z)$. We tested this claim at two different densities $n_{2D} = 2 \times 10^{11}$ and 7×10^{11} cm^{-2} by keeping κ_{b1} both as fixed (at the suggested value) and as a variational parameter. The results are listed in Table 5.1. First note that when κ_{b1} is treated as an additional variational parameter, the total energy per particle, E_{sys} is further lowered which is the natural characteristic of variational approaches. We observe that Bastard's choice is reasonable for the EQL, however, especially at $n_{2D} = 7 \times 10^{11}$ cm^{-2} the subband energy deviates more than 1 meV if this parameter is also optimized. Note

Table 5.1: The effect of κ_{b1} on several energies. (O) designates that the parameter is optimized, and (F) means that the paramater is kept fixed at that value.

n_{2D} (cm^{-2})	2×10^{11}		7×10^{11}	
b_{min}	0.0148 (O)	0.0149 (O)	0.0208 (O)	0.0205 (O)
κ_{b1}	0.0763 (F)	0.0800 (O)	0.0763 (F)	0.0694 (O)
E_F (meV)	39.543	39.557	84.662	84.361
E_1 (meV)	32.717	32.730	60.826	62.771
E_{sys} (meV)	24.165	24.158	41.143	41.084

that M_1, N_1 and z_0 also depend on b through Eqs.(5.21)-(5.23). b is determined by minimizing the *total* system energy. A closed form representation of b is not possible,

unlike the Si-inversion layer [105], however, the minimization can easily be achieved numerically.

5.2.2 First-Excited Subband

The EQL breaks down for the GaAs/AlGaAs system beyond the density $7 \times 10^{11} \text{cm}^{-2}$, so we now include the first-excited subband in our treatment, to explore higher densities. The commonly used variational form for the first-excited subband allowing penetration to barrier region is

$$\varsigma_2(z) = \begin{cases} M_2 e^{\kappa_{b2} z/2}, & \text{for } z \leq 0 \\ \\ N_2(z + z_1)(z + z_2)e^{-cz/2}, & \text{for } z \geq 0 \end{cases} . \qquad (5.24)$$

Here c is the variational parameter, similarly κ_{b2} can either be kept as an additional variational parameter or fixed at the suitable value $\sqrt{2m_B U_b/\hbar^2}$. Refer to the appendix section for the lenghty variational energy expression. We compare in Fig. 5.1 the ground-state and first-excited state wave functions at the density $n_{2D} = 2 \times 10^{12} \text{ cm}^{-2}$ for the cases of two parameter (b, c) and four parameter $(b, c, \kappa_{b1}, \kappa_{b2})$ optimizations. The difference can be observed in the barrier region. In the same figure, the lower plot shows the subband energies and the Fermi energy as function of the electron density. Note that beyond the critical density marked by an arrow, E_2 falls below the Fermi energy and begins to be populated. We also show the predictions of the EQL on E_1 and E_F; the latter is seen to be represented reasonably well to higher densities than the former.

94
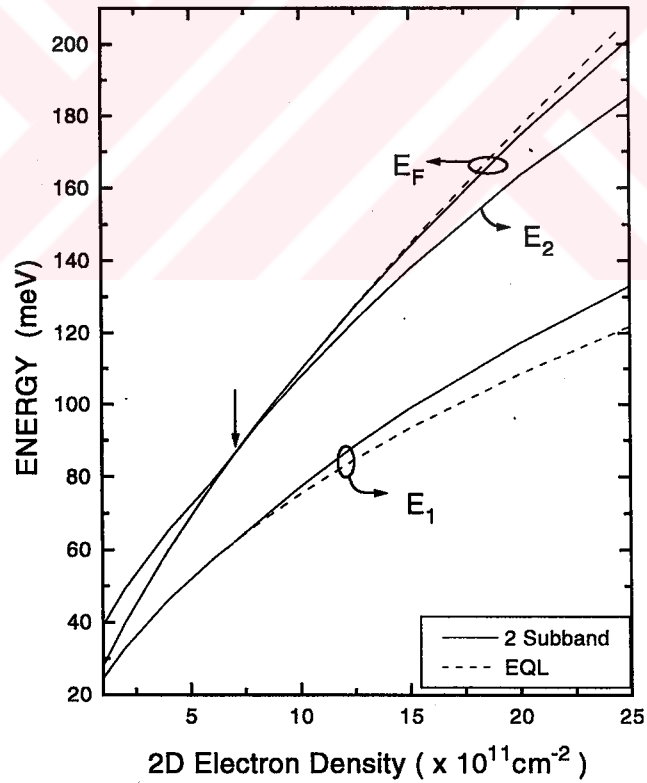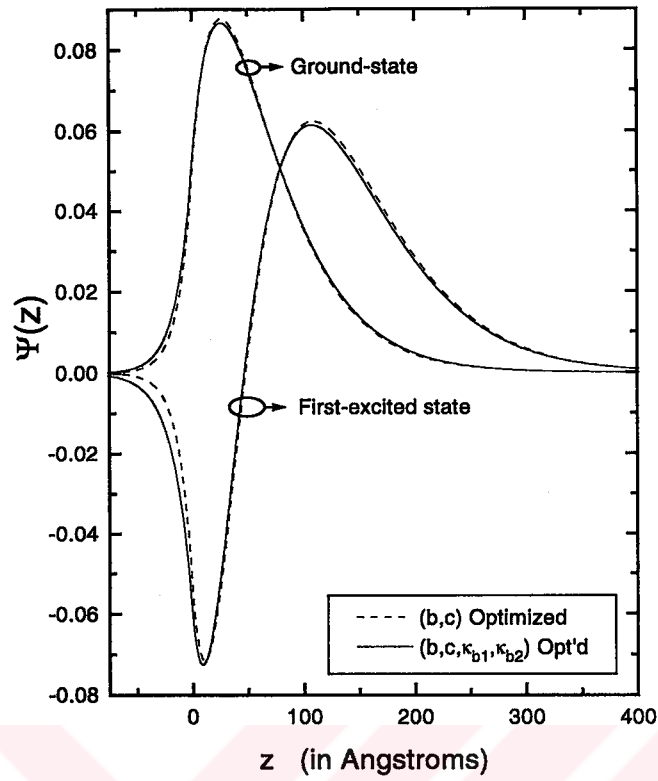
Figure 5.1: The upper plot illustrates the ground-state and the first-excited state wave functions. The lower plot shows the density variation of subband and Fermi energies.

5.3 Coulomb Form Factor for a Penetrable Heterojunction

In the 2D EL the interaction potential in reciprocal space is taken to be $2\pi e/q$, where q is the wave number. This potential is obtained by taking the 2D Fourier transform of the 3D Coulomb interaction which is $1/R$, R denoting distance in real space [57]. For the case of a Q2D system the charge distribution along the third dimension modifies the effective 2D interaction from $2\pi e/q$ to $F(q)\,2\pi e/q$ (to be shown later). $F(q)$ is the Coulomb form factor describing the effect of the finite spread of the charge distribution along the confinement direction over a region where the background dielectric constant is discontinous due to different materials on both sides.
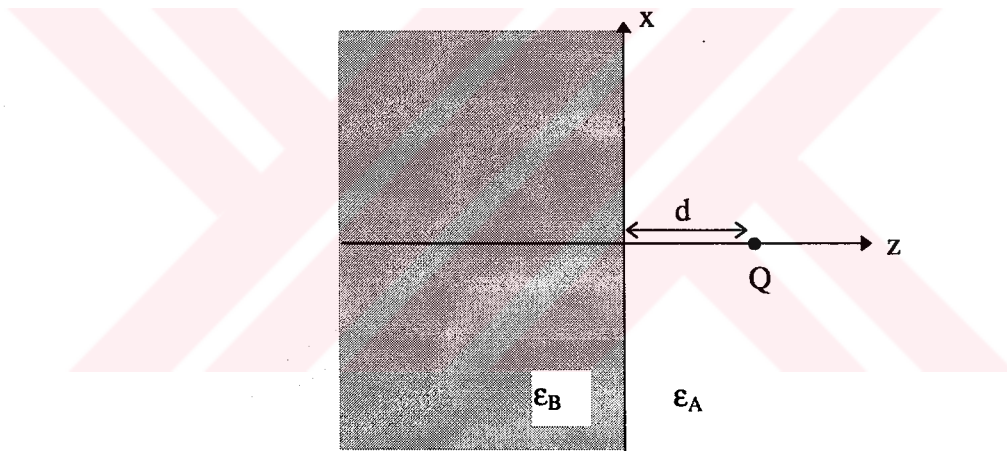
Figure 5.2: The geometry for the Poisson's equation.

Following the approach in the previous section we use the variational charge distribution that can leak into the barrier region and calculate the function $F(q)$ accordingly. We first recall the electrostatic potential due to a point charge Q, at a distance d (along the z-axis) from the interface formed by two semi-infinite dielectric media with permittivities ϵ_A and ϵ_B (see Fig. 5.2). Solution of the Poisson's equation subject to continuity requirements at the interface, $z = 0$ results in an electrostatic

96

potential of the form [48],

$$\Phi(\vec{R}, z) = \begin{cases} \frac{1}{\epsilon_A}\left(\frac{Q}{\sqrt{R^2+(d-z)^2}} + \frac{\epsilon_A-\epsilon_B}{\epsilon_A+\epsilon_B}\frac{Q}{\sqrt{R^2+(d+z)^2}}\right), & z \geq 0 \\ \\ \frac{2}{\epsilon_A+\epsilon_B}\frac{Q}{\sqrt{R^2+(d-z)^2}}, & z \leq 0 \end{cases} \tag{5.25}$$

This result will now be used in constructing the effective 2D Coulomb interaction energy between two (charge) distributions $n(\vec{R}, z)$ and $n(\vec{R}', z')$

$$U_{Q2D}(\vec{R}-\vec{R}') =$$

$$\frac{e^2}{\epsilon_A}\left\{\int_0^\infty dz \int_0^\infty dz' \left[\frac{n(\vec{R},z)\,n(\vec{R}',z')}{\sqrt{|\vec{R}-\vec{R}'|^2+(z-z')^2}} + \frac{\epsilon_A-\epsilon_B}{\epsilon_A+\epsilon_B}\frac{n(\vec{R},z)\,n(\vec{R}',z')}{\sqrt{|\vec{R}-\vec{R}'|^2+(z+z')^2}}\right]\right\}$$

$$+\frac{e^2}{\epsilon_B}\left\{\int_{-\infty}^0 dz \int_{-\infty}^0 dz' \left[\frac{n(\vec{R},z)\,n(\vec{R}',z')}{\sqrt{|\vec{R}-\vec{R}'|^2+(z-z')^2}} + \frac{\epsilon_B-\epsilon_A}{\epsilon_A+\epsilon_B}\frac{n(\vec{R},z)\,n(\vec{R}',z')}{\sqrt{|\vec{R}-\vec{R}'|^2+(z+z')^2}}\right]\right\}$$

$$+\frac{2e^2}{\epsilon_A+\epsilon_B}\left\{\int_0^\infty dz \int_{-\infty}^0 dz'\frac{n(\vec{R},z)\,n(\vec{R}',z')}{\sqrt{|\vec{R}-\vec{R}'|^2+(z-z')^2}}\right.$$

$$\left.+\int_{-\infty}^0 dz \int_0^\infty dz'\frac{n(\vec{R},z)\,n(\vec{R}',z')}{\sqrt{|\vec{R}-\vec{R}'|^2+(z-z')^2}}\right\}$$

$$\tag{5.26}$$

The first two terms in Eq. (5.26) represent direct and image interaction of the charge distributions on the right side of the interface ($z > 0$). Third and fourth terms represent the same interactions for $z < 0$ region. The last two terms which are in fact equal, represent the direct interaction between charge distributions on opposite sides of the interface.

The charged-particle distribution is $n(\vec{R}, z) \equiv n(z) = |\varsigma_1(z)|^2$, where $\varsigma_1(z)$ is given in Eq. (5.20). The 2D Fourier transform of $U_{Q2D}(\vec{R}-\vec{R}')$ is easily obtained using the result

$$\int d^2r \frac{e^{-i\vec{q}\cdot\vec{r}}}{\sqrt{r^2+a^2}} = \frac{2\pi}{q}e^{-|a|q} \tag{5.27}$$

97

as

$$U_{Q2D}(q) = \frac{2\pi e^2}{q\epsilon_A}\left(I_1 + \frac{\epsilon_A - \epsilon_B}{\epsilon_A + \epsilon_B}I_2\right) + \frac{2\pi e^2}{q\epsilon_B}\left(I_3 + \frac{\epsilon_B - \epsilon_A}{\epsilon_A + \epsilon_B}I_4\right) + \frac{8\pi e^2}{q(\epsilon_A + \epsilon_B)}I_5, \quad (5.28)$$

with,

$$I_1 = \int_0^\infty dz \int_0^\infty dz' N^4 (z + z_0)^2 (z' + z_0)^2 e^{-bz} e^{-bz'} e^{-|z-z'|q}, \quad (5.29)$$

$$I_2 = \int_0^\infty dz \int_0^\infty dz' N^4 (z + z_0)^2 (z' + z_0)^2 e^{-bz} e^{-bz'} e^{-(z+z')q}, \quad (5.30)$$

$$I_3 = \int_{-\infty}^0 dz \int_{-\infty}^0 dz' M^4 e^{\kappa_b(z+z')} e^{-|z-z'|q} \quad (5.31)$$

$$I_4 = \int_{-\infty}^0 dz \int_{-\infty}^0 dz' M^4 e^{\kappa_b(z+z')} e^{(z+z')q} \quad (5.32)$$

$$I_5 = \int_0^\infty dz \int_{-\infty}^0 dz' M^2 N^2 e^{\kappa_b z'} (z + z_0)^2 e^{-bz} e^{-(z-z')q}. \quad (5.33)$$

These integrals are straightforward and the Coulomb form factor is obtained as

$$F(q) = \frac{1}{2}\left(1 + \frac{\epsilon_B}{\epsilon_A}\right)I_1 + \frac{1}{2}\left(1 - \frac{\epsilon_B}{\epsilon_A}\right)I_2 + \frac{1}{2}\left(1 + \frac{\epsilon_A}{\epsilon_B}\right)I_3 + \frac{1}{2}\left(1 - \frac{\epsilon_A}{\epsilon_B}\right)I_4 + 2I_5, \quad (5.34)$$

where,

$$\begin{aligned}
I_1 = \ & 2N^4 \left\{ \frac{1}{2b}\left[\frac{z_0^4}{(b+q)} + \frac{2z_0^3}{(b+q)^2} + \frac{2z_0^2}{(b+q)^3}\right] \right. \\
& + \frac{1}{(2b)^2}\left[\frac{4z_0^3}{(b+q)} + \frac{6z_0^2}{(b+q)^2} + \frac{4z_0}{(b+q)^3}\right] + \frac{1}{(2b)^3}\left[\frac{12z_0^2}{(b+q)} + \frac{12z_0}{(b+q)^2} + \frac{4}{(b+q)^3}\right] \\
& \left. + \frac{1}{(2b)^4}\left[\frac{24z_0}{(b+q)} + \frac{12}{(b+q)^2}\right] + \frac{1}{(2b)^5}\frac{24}{(b+q)} \right\},
\end{aligned} \quad (5.35)$$

$$I_2 = N^4 \left[\frac{z_0^2}{(b+q)} + \frac{2z_0}{(b+q)^2} + \frac{2}{(b+q)^3}\right]^2, \quad (5.36)$$

$$I_3 = \frac{M^4}{\kappa_b(\kappa_b + q)}, \quad (5.37)$$

$$I_4 = \frac{M^4}{(\kappa_b + q)^2}, \quad (5.38)$$

$$I_5 = \frac{M^2 N^2}{(\kappa_b + q)}\left[\frac{z_0^2}{(b+q)} + \frac{2z_0}{(b+q)^2} + \frac{2}{(b+q)^3}\right]. \quad (5.39)$$

In Eq. (5.34) ϵ_A and ϵ_B are the background dielectric constants of the well-acting

and the barrier-acting materials respectively. The bare electron-electron interation

potential energy for this Q2D system becomes

$$U_{Q2D}(q) = \frac{2\pi e^2}{\bar{\epsilon} \, q} F(q), \qquad (5.40)$$

where $\bar{\epsilon} = (\epsilon_A + \epsilon_B)/2$ and q is the 2D wave number associated with the spatial

variation along the 2D sheet.
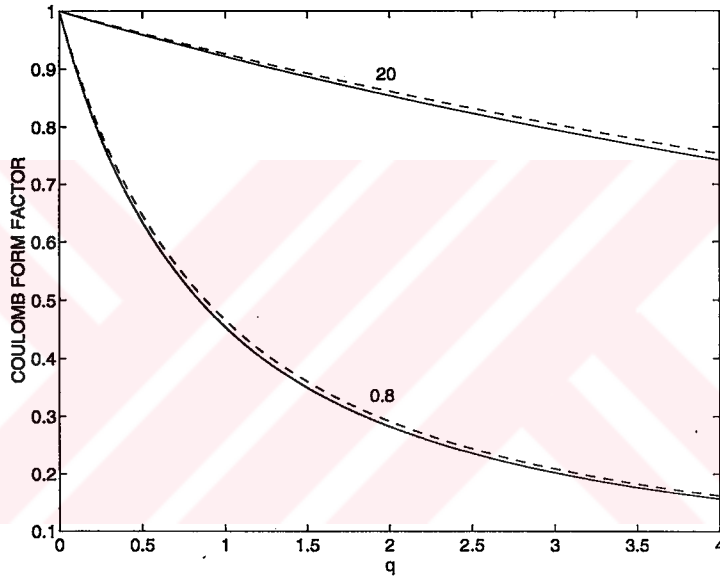
Figure 5.3: The Coulomb form factor F and the effect of the image terms as a function of wave number q (in units of k_F) for the electronic densities r_s=0.8 and 20. The full lines apply to GaAs/AlGaAs heterostructure having ϵ_A=13 and ϵ_B=12.1. The dashed lines refer to the same system but with $\epsilon_A = \epsilon_B$=12.55 so that no image term appears.

The terms containing I_2 and I_4 in Eq. (5.34) represent the image interaction re-

sulting from the different permittivities on both sides. Their effects decrease when

the permittivity contrast diminishes; an example is the GaAs/AlGaAs system con-

sidered in Fig. 5.3 for two different electron densities (see the following section for

the material parameters used). The Coulomb form factor becomes more important in

99

high electron densities (see Fig. 5.3) where the in-plane particle separation is comparable to the extension of the charge distribution along the confinement direction. The expression for $F(q)$ in Eq. (5.34) will especially be useful for heterojunctions with a high permittivity difference and a low barrier height.

Finally, we consider some limiting cases: the effective 2D interaction $U_{Q2D}(\vec{R} - \vec{R}')$ must reduce to ideal 2D case as $|\vec{R} - \vec{R}'| \to \infty$

$$\lim_{|\vec{R}-\vec{R}'|\to\infty} U_{Q2D}(\vec{R} - \vec{R}') = \frac{e^2}{\epsilon_A |\vec{R} - \vec{R}'|} \left(1 + \frac{\epsilon_A - \epsilon_B}{\epsilon_A + \epsilon_B} \right) \left[\int_0^\infty dz \, n(z) \right]^2 + \frac{e^2}{\epsilon_B |\vec{R} - \vec{R}'|}$$
$$\left(1 + \frac{\epsilon_B - \epsilon_A}{\epsilon_A + \epsilon_B} \right) \left[\int_{-\infty}^0 dz \, n(z) \right]^2 + \frac{4e^2}{(\epsilon_A + \epsilon_B)|\vec{R} - \vec{R}'|} \int_0^\infty dz \, n(z) \int_{-\infty}^0 dz' \, n(z').$$

$$(5.41)$$

Using $\int_0^\infty n(z)\, dz = 1 - \int_{-\infty}^0 n(z')\, dz'$ in Eq. (5.41) leads to the desired result,

$$\lim_{|\vec{R}-\vec{R}'|\to\infty} U_{Q2D}(\vec{R} - \vec{R}') = \frac{e^2}{|\vec{R} - \vec{R}'|} \frac{2}{\epsilon_A + \epsilon_B}. \qquad (5.42)$$

As a consequence the Fourier transform gives

$$\lim_{q\to 0} U_{Q2D}(q) = \frac{2\pi e^2}{q\, \bar{\epsilon}}, \qquad (5.43)$$

so that $\lim_{q\to 0} F(q) = 1$ as can be observed in Fig. 5.3. This also indicates that all of the interactions are properly accounted for in Eq. (5.28).

5.4 Q2D STLS

We discussed the STLS technique for the strictly 2D case in Chap. 3; in going from 2D to Q2D the only modification (within the EQL) is the replacement of the 2D Coulomb interaction energy by the effective 2D interaction due to finite extension of the charge distribution along the confinement direction. The LFC in the case of Q2D

STLS reads

$$G_{Q2D}(q) = \iint \frac{d^2 p_n}{2\pi} \frac{F(p)}{F(q)} \frac{\vec{q_n} \cdot \vec{p_n}}{q_n\, p_n} \left[1 - S(|\vec{p} - \vec{q}|)\right].$$ (5.44)

A change of variables leads to a substantial improvement in the execution speed of

the STLS algorithm. Using $\vec{t_n} = \vec{p_n} - \vec{q_n}$ in Eq. (5.44) leads to

$$G_{Q2D}(q) = \frac{1}{\pi\, F(q)} \int_0^\infty dt_n\, t_n \left[1 - S(t)\right] \int_0^\pi d\phi\, F\left(q\sqrt{1 + a^2 + 2a\cos\phi}\right) \frac{a\cos\phi + 1}{\sqrt{1 + a^2 + 2a\cos\phi}},$$
(5.45)

where $a = t_n/q_n$.
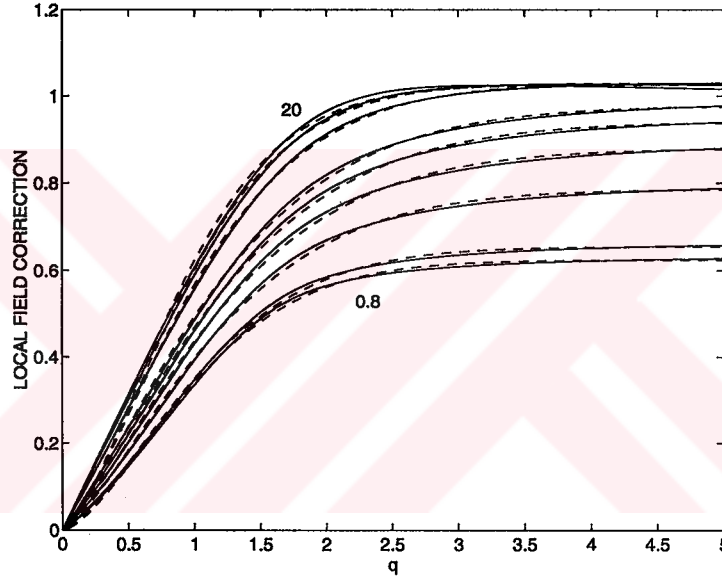
Figure 5.4: $G_{Q2D}(q)$ of Q2D EL versus wave number q (in units of k_F) for r_s values 0.8, 1, 2, 3, 4, 5, 10, 15, and 20. Solid lines: STLS and dashed lines: calculation using the fitted form for $G_{Q2D}(q)$; see Eq. (5.53) with the values from Table 5.2.

In Fig. 5.4 we present the self-consistent STLS $G_{Q2D}(q)$ results for a wide range

of electronic densities given in terms of r_s. r_s is the effective interparticle spacing

defined as $r_s = 1/a_B^*\sqrt{\pi n_{2D}}$ where n_{2D} is the 2D electronic density and a_B^* is the

effective Bohr radius given by $a_B^* = \frac{\bar{\epsilon}}{m^*}\frac{\hbar^2}{e^2}$, $\bar{\epsilon}$ is the background average static dielectric

constant and m^* is the effective mass of the electrons considered, and the free electron

mass is denoted by m_0. We consider GaAs/AlGaAs heterojunction as the physical

system with the parameters $m_A = 0.07m_0$, $m_B = 0.088m_0$, $\epsilon_A = 13$, $\epsilon_B = 12.1$ and $U_b = 0.3\,\text{eV}$ (corresponding to an Al mole fraction of 0.3) which were used by Stern and Das Sarma [111]. For a_B^* we used $\bar{\epsilon} = 12.55$ and $m^* = 0.07\,m_0$, giving $a_B^* = 9.49\,\text{nm}$. The conduction band offset, U_b was measured by some groups to be around $0.225\,\text{eV}$ (in contrast to $0.3\,\text{eV}$) [112, 113, 114]. We have observed that our results are not sensitive to the deviation of U_b in this range. In Fig. 5.4 the interval $r_s = 0.8 - 20$ is shown with an ionized acceptor density of $N_{depl} = 0.46 \times 10^{11}\,\text{cm}^{-2}$. For $r_s < 0.8$ the higher subbands start to be populated which was not taken into our analysis.

For the 2D EL, STLS $G(q)$ becomes proportional to q as $q \to 0$ [63] whereas in 3D case it is proportional to q^2 (see, for instance, Ref. [115]). In the Q2D case we observe that (see Fig. 5.4) for low r_s values small-q behavior is close to quadratic and as r_s increases this behavior goes towards a linear one indicating an approach to a 2D character.

Gold and Calmels also reported their results on $G_{Q2D}(q)$ for GaAs/AlGaAs heterostructure [109]. Their treatment is based on STLS but with essential discrepancies compared to ours. They imposed the local-field correction for 2D and Q2D to be of the form

$$G_{Q2D}^{GC}(x) = r_s^{2/3} \frac{1.402\,x}{[2.644\,C_{12}^2(r_s) + x^2 C_{22}^2(r_s)]^{1/2}} \qquad (5.46)$$

where $x = \frac{q}{k_F} \frac{1}{\sqrt{2}r_s^{1/3}}$ and the coefficients C_{12} and C_{22} were tabulated [109]. They assumed no penetration to barrier region in the Coulomb form factor and also neglected the presence of ionized acceptors in the well-acting region. Especially, the form used in Eq. (5.46) enabled them to reduce the computational effort appreciably, however, their results are in strong disagreement with ours for $r_s \geq 1$ and $q \simeq 2k_F$ both in
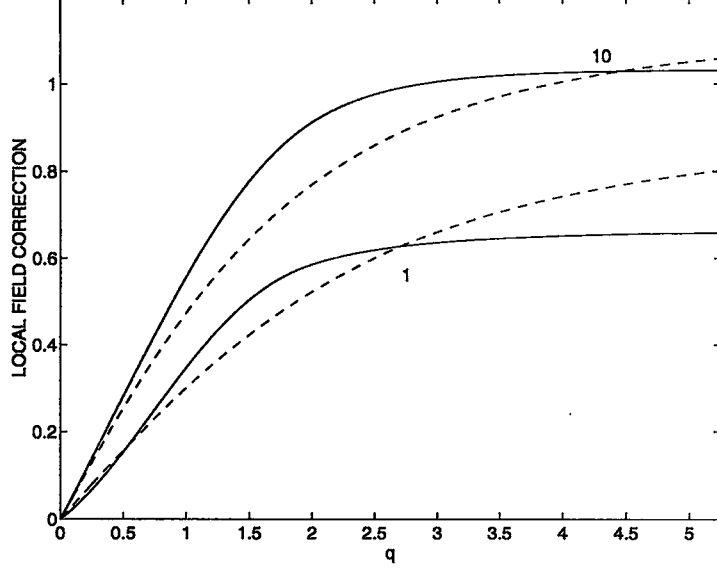
Figure 5.5: The comparison of the full STLS Q2D local-field correction (solid lines) with that of Gold and Calmels' (dashed lines) given by Eq. (5.46) as a function of wave number q (in units of k_F) for $r_s=1$ and 10.

2D [63] and Q2D [110] as can be seen in Fig. 5.5. The form in Eq. (5.46) cannot accommodate the full STLS $G(q)$ leading to a poor DF and screening properties. The ionized acceptors in the well region play a primary role and need to be included in the treatment.

5.5 Q2D Dielectric Function

The function of practical importance is the wave number- and frequency-dependent (longitudinal) DF, $\epsilon(q,\omega)$ that not only determines the response to a weak external perturbation but also possesses information on the many-body dynamics of the system. With the knowledge of the LFC, $\epsilon(q,\omega)$ is given as

$$\epsilon_{Q2D}^{STLS}(q,\omega) = \frac{1 - U_{Q2D}(q)\,\pi^0(q,\omega)\,[1 - G_{Q2D}(q)]}{1 + U_{Q2D}(q)\,\pi^0(q,\omega)\,G_{Q2D}(q)}, \qquad (5.47)$$

where $\pi^0(q,\omega)$ is the 2D zeroth-order polarization insertion, the Stern function [62], [63]. Apart from π^0, 2D and Q2D quantities behave differently. This is illustrated

103

in Fig. 5.6 showing inverse static DF, $\epsilon^{-1}(q,0)$ within RPA and STLS for both 2D and Q2D cases. To assess the effect of penetration of the charge distribution into the barrier region, we compare $U_b = 0.1\,\mathrm{eV}$ case with $U_b \to \infty$ in Fig. 5.7 at $r_s = 0.8$. It is observed that for GaAs/AlGaAs-like heterojunctions, this penetration has a minor effect on the static DF. In Fig. 5.8 the inverse static DF of GaAs/AlGaAs heterojunction is plotted in the density range $r_s = 0.8 - 20$ and for $N_{depl} = 0.46 \times 10^{11}\,\mathrm{cm}^{-2}$. Notably, the GaAs/AlGaAs heterostructure shows an overscreening effect (i.e., $\epsilon < 0$) for $r_s \geq 3$. The onset of overscreening shifts to higher electron densities for the strictly 2D case [63], due to enhanced particle correlations in lower dimensions. As mentioned in the previous chapter, the negative DF suggests a negative compressibility of the Q2D EL [42] and in fact, recently this has been experimentally observed on a GaAs quantum well structure [89].
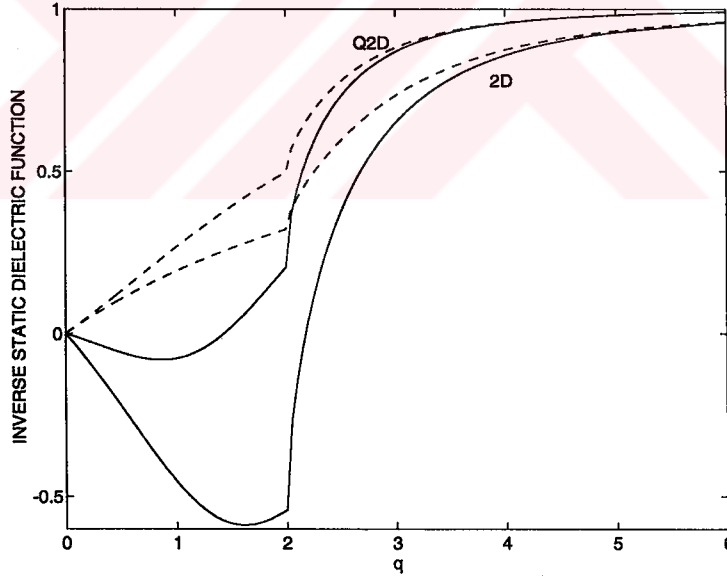
Figure 5.6: Comparison of ideal 2D and Q2D inverse static dielectric function, $1/\epsilon(q,0)$ as a function of wave number q (in units of k_F) for $r_s{=}3$. Solid lines: STLS, dashed lines: RPA. For Q2D EL, GaAs/AlGaAs heterostructure is used with $N_{depl} = 0.46 \times 10^{11}\,\mathrm{cm}^{-2}$.

We would like to include some necessary remarks about this DF. The expression in
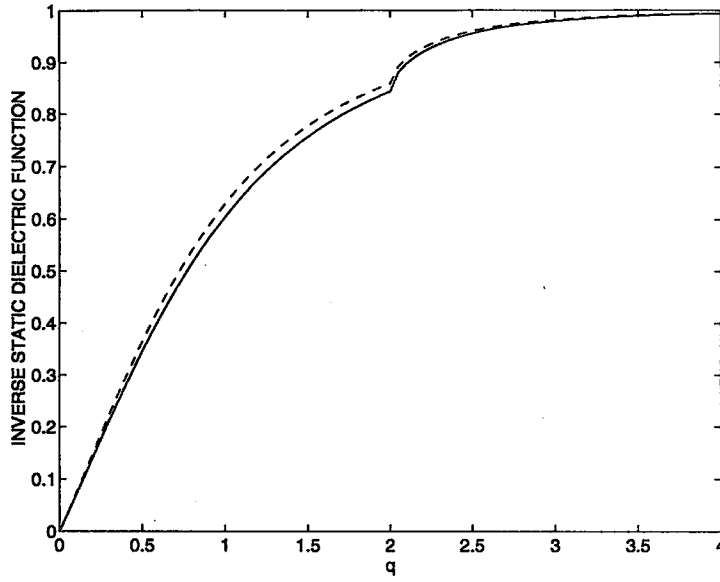
Figure 5.7: The effect of the barrier height, U_b on the inverse static dielectric function, $1/\epsilon(q,0)$ as a function of wave number q (in units of k_F) for $r_s = 0.8$. Solid line: $U_b = 0.1\,\text{eV}$, dashed line: $U_b \to \infty$. Other parameters for the heterostructure are given in the text.
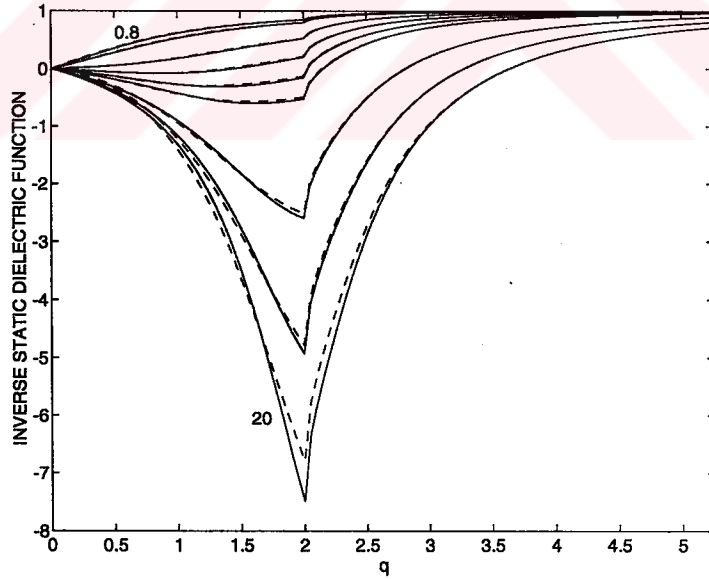
Figure 5.8: The inverse static dielectric function of Q2D EL, $1/\epsilon(q,0)$ as a function of wave number q (in units of k_F) for r_s values 0.8, 1, 2, 3, 4, 5, 10, 15, and 20. Solid lines: STLS and dashed lines: calculation using the fitted forms for $G_{Q2D}(q)$ given by Eq. (5.53) and $F(q)$ given by Eq. (5.55) with the values in Table 5.2.

105

Eq. (5.47) only gives the Q2D EL DF. The total screened electron-electron interaction is

$$U_{Q2D,scr}(q,\omega) = F(q)\frac{2\pi e^2}{\bar{\epsilon} q}\frac{1}{\epsilon_{Q2D}^{STLS}(q,\omega)}. \qquad (5.48)$$

The dielectric responses of the polar lattice and the valence electrons are contained in the average background dielectric constant $\bar{\epsilon}$. Here we have used the *static* dielectric constant (see, for instance, our definition of a_B^* in this chapter), hence, it is assumed that the polar lattice can follow the external excitations. Obviously this limits the validity range of this work to $\omega \ll \omega_{TO}$, with ω_{TO} being the transverse optical phonon frequency. This limitation is relaxed if the background lattice does not have a polar character. For the particular system that we are considering , the DF is expected to be valid up to about 1 THz. In principle, however, the static nature of the LFC of the STLS technique can further limit this upper frequency.
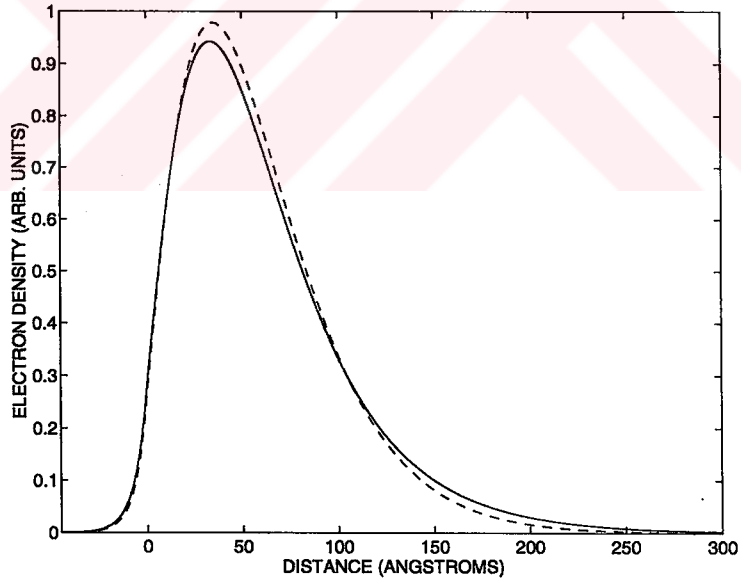
Figure 5.9: The electron distribution along the confinement direction in arbitrary units. The total electron density is $1 \times 10^{12}\,\mathrm{cm}^{-2}$. Other parameters are as given in the text. Solid line refers to the two subband populated calculation and the dashed line is based on the EQL.

Finally, the DF given by Eq. (5.47) takes into account the polarization of the

electrons in the lowest subband. Even though the presently available experiments on GaAs/AlGaAs systems mainly fall into this regime [116], [117], the technological trend aims to populate the higher subbands to increase the amount of current carried in modulation doped field effect transistors by using different materials such as InGaAs/InAlAs (for a review see [118]). When the higher subbands are occupied the DF should necessarily be a tensor of the form $\epsilon_{ij}(q, \omega)$, where $i = j$ terms account for the intrasubband polarizations and $i \neq j$ terms represent intersubband couplings. To assess the performance of the presented approach regarding the electrical quantum limit, we extended the variational wave function technique to include lowest two subbands and determined the subband populations by invoking self-consistency between Poisson and Schrödinger equations. In Fig. 5.9 we show the charge distributions along the confinement direction for a density of $1 \times 10^{12}\,\mathrm{cm}^{-2}$. The solid curve represents the correct charge distribution containing contributions from the lowest and first-excited subbands. The dashed curve, on the other hand, sticks to the electrical quantum limit which actually breaks down beyond $N_{2D} = 7 \times 10^{11}\,\mathrm{cm}^{-2}$. It is important to observe that the difference between the two curves is quite marginal. This is simply because the percentage of the first-excited subband electrons is 4.7% at this density.

5.6   Plasmon Dispersion

The elementary excitations in electron liquids are electron-hole pair creations and collective excitations knowns as plasmons [53]. The latter can be characterized with the knowledge of the wave number and frequency-dependent DF, $\epsilon(q, \omega)$. Particularly, the plasmon dispersion relation, $\omega_p(q)$ is available through the zeros of the dielectric

function;

$$\epsilon(q, \omega_p(q)) = 0. \qquad (5.49)$$

Inserting the expression for $\epsilon(q, \omega)$ from Eq. (5.47) leads to the following closed form expression for the plasmon dispersion

$$\nu_p(q) = \frac{q_n(z+1)}{2} \sqrt{q_n^2 + \frac{4}{z^2 + 2z}}, \qquad (5.50)$$

where

$$z = \frac{q_n}{\sqrt{2} r_s F(q) [1 - G_{Q2D}(q)]}, \qquad (5.51)$$

and

$$\nu_p(q) = \frac{\hbar \omega_p(q)}{2E_F} = \frac{m \omega_p(q)}{\hbar k_F^2}. \qquad (5.52)$$

which is valid in the range $[0, q_{n,max}]$ where $q_{n,max}$ satisfies $\nu_p(q_{n,max}) = q_{n,max} + q_{n,max}^2/2$ and outside this region plasmons dissociate to electron-hole pairs so that collective excitations are no longer long-lived. The Eq. (5.50) reduces to the ideal 2D result [64] when $F(q) \to 1$. Fig. 5.10 shows the plasmon dispersion for GaAs/AlGaAs heterostructure with $N_{depl} = 0.46 \times 10^{11} \text{cm}^{-2}$ and for several r_s values. Even though the plasmon dispersion can be experimentally probed, such as, through far infrared spectroscopy [116], the available experimental results pertain to high electronic densities and small wave numbers ($q < k_F$). Therefore the effects of the LFC have not yet been verified.

5.7 Analytical Expressions

In this section, we present our fitted expressions to $G_{Q2D}(q)$ and $F(q)$ applicable to GaAs/AlGaAs heterojunction in the density range $r_s = 0.8 - 20$. As a fit to $G_{Q2D}(q)$

108
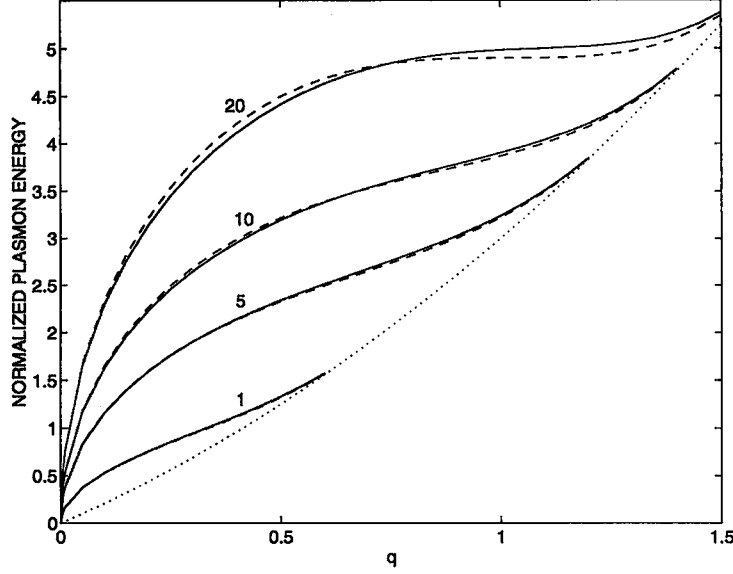
Figure 5.10: The normalized plasmon energy $(E_p/E_F \equiv 2\nu_p)$ as a function of wave number q (in units of k_F) for r_s values 1, 5, 10, and 20. Solid lines: STLS and dashed lines: calculation using the fitted forms for $G_{Q2D}(q)$ given by Eq. (5.53) and $F(q)$ given by Eq. (5.55) with the values in Table 5.2. The dotted line marks the onset of the electron-hole continuum.

(shown in Fig. 5.4 by solid lines), we tried a simple form containing three fitting parameters,

$$G_{Q2D}^{fit}(q) = A \left(1 - \exp \left[-\frac{B}{A} q_n^C \right] \right), \tag{5.53}$$

where A, B and C are the fitting parameters. The optimized values are tabulated in Table 5.2 for $N_{depl} = 0.46 \times 10^{11} \, \text{cm}^{-2}$. The third parameter, C is introduced based on our observations on the long-wavelength behavior of $G_{Q2D}(q)$. In ideal 2D, C was equal to one and in 3D case C was equal to two. Optimized C values in Table 5.2 show this interpolation between $r_s = 0.8$ to 5, but then this trend is lost to enable a good fit for the whole q values. The fitted expressions are plotted in Fig. 5.4 by the dotted lines. To assess the quality of the fitting we use the following error estimate between a target vector, $T(i)$ and the fitted vector $T_{fit}(i)$:

$$error(\%) = \frac{1}{N} \sum_{i=1}^{N} \left| \frac{T(i) - T_{fit}(i)}{T(i)} \right| 100. \tag{5.54}$$

109

Accordingly the deviation of the fitting in Fig. 5.4 is less than 2.5%.

Table 5.2: Fitting parameters A, B, C, and D used in Eqs. (5.53) and (5.55) as a function of r_s for the characterization of the Q2D EL in a GaAs/AlGaAs heterostructure. The ionized acceptor density is $N_{depl} = 0.46 \times 10^{11}\,\mathrm{cm}^{-2}$. See text for the other parameters used for GaAs/AlGaAs system.

r_s	A	B	C	D
0.8	0.6243	0.4923	1.5462	1.2750
1.0	0.6549	0.5005	1.5079	1.1542
1.5	0.7250	0.5274	1.4342	0.9285
2.0	0.7857	0.5519	1.3950	0.7690
2.5	0.8380	0.5763	1.3644	0.6497
3.0	0.8794	0.5999	1.3512	0.5571
4.0	0.9405	0.6461	1.3274	0.4321
5.0	0.9779	0.6855	1.3264	0.3494
6.0	1.0012	0.7209	1.3356	0.2922
8.0	1.0225	0.7792	1.3683	0.2197
10	1.0294	0.8223	1.4097	0.1752
12	1.0305	0.8597	1.4545	0.1454
15	1.0295	0.9007	1.5014	0.1158
20	1.0257	0.9555	1.5185	0.0863

The Coulomb form factor, $F(q)$ also requires a laborious work for GaAs/AlGaAs system. This function can be fitted by a simple expression

$$F_{fit}(q) = \frac{1}{1 + Dq_n}, \tag{5.55}$$

containing a single fitting parameter D which is tabulated in Table 5.2 for the same N_{depl} value.

The knowledge of $G_{Q2D}^{fit}(q)$ and $F_{fit}(q)$ is sufficient for representing the DF (see Eq. (5.47)). The performance of fitting for $\epsilon^{-1}(q,0)$ is available from Fig. 5.8 (shown by dotted lines) where the error, using the estimate in Eq. (5.54) is less than 1%. Similarly in Fig. 5.10 the plasmon dispersions with the use of the fitted forms are shown in dashed lines, the fitting error being much less than 0.1%.

110

Table 5.3: The constants used in Eqs. (5.56)-(5.59) for different ionized acceptor densities, N_{depl} in cm^{-2}. The parameters characterizing the heterostructure are chosen suitable to the GaAs/AlGaAs system.

N_{depl} ($\times 10^{11}$)	a_1	a_2	a_3	b_1	b_2	b_3	c_1	d_1	d_2
0.146	0.6384	0.2213	0.5555	0.3023	4.9907	-0.0435	0.6891	4.3194	2.4659
0.46	0.6770	0.2794	0.6372	0.2575	2.6283	0.1623	0.7914	2.7325	1.3674
1.47	0.6953	0.2302	0.6888	0.2253	1.4913	0.3043	1.1675	1.6566	0.6898
4.69	0.6887	0.1802	0.7418	0.1978	0.6977	0.4195	1.5437	1.0004	0.3518

We have observed that taking the barrier height $U_b = 0.225\,\mathrm{eV}$ does not significantly affect the parameters A, B, C, and D. However, N_{depl} takes an important part in both $G(q)$ and $F(q)$, so we repeated the self-consistent Q2D STLS technique for $N_{depl} = 0.146$, 1.47, 4.69 $\times 10^{11}\,\mathrm{cm}^{-2}$ and performed again fittings. Rather than specifying these results in tabular form we present below fitted *functions* of r_s for A, B, C, and D.

$$A_{fit} = 1.02 \left[1 - a_1 r_s^{a_2} e^{-a_3 r_s} \right], \qquad (5.56)$$

$$B_{fit} = b_1 \ln(b_2 r_s) + b_3, \qquad (5.57)$$

$$C_{fit} = 0.42 r_s^{-c_1} + 1.03\, r_s^{0.12}, \qquad (5.58)$$

$$D_{fit} = \frac{d_1}{d_2 + r_s^{1.15}}, \qquad (5.59)$$

the constant parameters contained in these expressions are tabulated in Table 5.3 for the considered range of N_{depl} values. With the expressions in Eqs. (5.56)-(5.59), inverse static DF can be generated to an accuracy of about 1% except $r_s = 2$ case having an error about 9%. Similarly with these equations plasmon dispersion can be recovered to an error much less than 0.1%.

CHAPTER 6

MOTT TRANSITION AND IMPURITY BINDING

ENERGIES IN THREE- AND TWO-DIMENSIONAL

ELECTRON LIQUIDS

6.1 Introduction

One of the long-standing problems of the condensed matter physics is the metal-nonmetal (MNM) transition [119, 120] introduced by Mott [121]. An important sub-class of MNM transition consists of the so-called quantum phase transition, which is a continuous phase transition that occurs at zero temperature, driven by non-thermal effects with changing some parameter in the Hamiltonian of the system [122][1]. On the theoretical side of the problem, three major lines of thought have dominated: i) Mott's original idea based on the overlap of outer shell electronic wave functions

---

[1] "This parameter might be the charging energy in Josephson-junction arrays (which controls their superconductor-insulator transition), the magnetic field in a quantum-Hall sample (which controls the transition between quantized Hall plateaus), doping in the parent compound of a high-T_c superconductor (which destroys the antiferromagnetic spin order), or disorder in a conductor near its metal-insulator transition (which determines the conductivity at zero temperature)" [123].

[121], referred to as Mott transition ii) Hubbard's approach based on his famous tight-binding Hamiltonian with hopping between the sites [124] known as Mott-Hubbard transition, and iii) Anderson's wave function localization due to disorder [125, 126] referred to as Anderson transition. The first two transitions are driven by many-body effects, whereas the last one predicts MNM transition by considering a single electron over a sufficiently strong random potential. However, it has not been possible to assess the individual role played by many-body and disorder effects on the observed MNM transitions in real systems [119, 120]. Another aspect of the MNM transition is the role of dimensionality on the transition. The scaling theory of localization claimed that there should be no true metallic states of a strictly 2D electronic system with arbitrary amount of disorder [127]. This result has recently been challenged by both theoretical [128] and experimental [129, 130, 131, 132] works. The latter attribute the disagreement between the two to the absence of many-body effects in the scaling theory of localization.

Our aim in this work [133] is to assess the many-body and in particular exchange effects on the MNM transition, both qualitatively and quantitatively in three-dimensional (3D) and two-dimensional (2D) electronic systems based on the electron liquid model. We proceed along the lines of Mott's original idea as opposed to Hubbard's tight-binding Hamiltonian. This path has also been followed by other researchers [134, 135, 136, 137, 138, 139, 140] and their works can be grouped as variational [134, 135, 136, 137] and numerical [138, 139, 140] treatment of the bound-electron wave functions. The former is appealing due to its simplicity but may not be suitable to use in problems such as the Mott transition as the resultant binding energy will inevitably be higher than the true ground-state energy. Martino *et*

113

al. [138] have shown this to be the case by comparing Krieger and Nightingale's [134] variational hydrogenic wave function treatment with their numerical method. Nevertheless, 3D Mott transition has still been dealt with variational techniques by replacing the trial wave functions with the Hulthén's form [141], resulting in a better agreement with Ref. [138]. In all these works several forms of dielectric screening have been employed such as Thomas-Fermi [134, 135, 136], Random Phase Approximation (RPA) [134, 135, 136, 137], and Hubbard-Sham [138, 135, 139]. Very recently Borges *et al.* [142] dealt with 3D Mott transition using STLS dielectric function, with Hulthén variational wave function. In our work we employ the numerical approach due to mentioned drawbacks of the variational techniques, and consider the 2D Mott transition as well.

We observe that Friedel oscillations [51, 42] associated with the screening of an impurity potential play an important role in the Mott transition and impurity binding energies. Appreciable differences are seen between our numerical approach based on the computationally-efficient solution of an integral equation and the standard hydrogenic variational treatments. These results will have implications on the accurate characterization of impurities as well as excitons [69] under the presence of free carrier screening. Furthermore, to the best of our knowledge, exchange effects have not been studied elaborately in regard to MNM transition, especially in 2D. The full strength of our formulation can now be utilized; especially, by means of the degeneracy parameter of the EL, the exchange effects are investigated in the spectrum ranging from spin-polarized and single-valley EL to six valley EL. In 2D, the existence of the Mott transition is observed to be controlled by the degeneracy parameter, where no Mott transition exists for the spin-polarized and the normal-state single-valley EL.

6.2 Theoretical Approaches

In dealing with MNM transition, the electron-electron interactions are treated start-
ing from two opposite limits [119]: in one method the dielectric formulation [36] is
used assuming that donor impurity electrons form an almost free EL, whereas the
other considers electrons tightly bound to a lattice of impurities with nearest neighbor
hopping leading to an impurity band formation; as mentioned in the previous section
these two approaches are discriminated by the names Mott and Mott-Hubbard tran-
sitions respectively. We focus on the Mott transition and consider a single neutral
impurity[2] being immersed into an EL, and monitor the binding energy of a bound
electron to the ion as the density of the screening electrons making up the EL is
changed. The reasoning behind this standard model is that for doped semiconduc-
tors, the valence electrons of each donor impurity will also screen other impurity
sites so that effectively an EL will be formed; so, we investigate whether an impurity
can trap an electron with the screening of the EL present. In some systems such as
quasi-2D modulation doped heterostructures the impurity and the free carrier con-
centrations within the active 2D channel are not equal and/or the impurity scattering
on the electronic motion is important. There, our model will not be applicable and
we refer to the relevant work of Serre *et al.* [143]. The Mott transition in the model
we are using is controlled by three effects: i) the attractive bare Coulomb interaction
of the ion that enhances the binding, ii) the kinetic energy of the bound electron
that tries to overcome the binding and iii) the screening of the bare interaction by
the "free" carriers of the EL that weakens the binding of the electron. The Mott
transition under this picture, is driven by the winning of the last two over the first

---

[2] The chemical identity of the impurity does not play a role in our treatment.

as the concentration of the free carriers in the EL is increased.

It seems appropriate to stress once again that, we work at zero temperature, and for the 2D case, aiming for general results, we assume no extension along the third dimension (i.e., strictly 2D), where electrons still interact with Coulomb $1/R$ potential [61]. We mainly use 3D effective Rydbergs (Ry*) for the energies and denote them with an overbar. Also we introduce length-related reduced variables by scaling with the effective Bohr radius, a_B^* and denote them by the subscript r such as $a_r \equiv a/a_B^*$, $q_r \equiv a_B^* q$, for variables having length and reciprocal length dimensions respectively.

6.2.1 Variational Expressions

For completeness we first list the expressions for the hydrogenic variational approach. In 3D case Krieger and Nightingale [134] used a variational approach for the Mott transition based on a hydrogenic $1s$ trial wave function for the bound electron as

$$\psi_0(r) = \frac{1}{\sqrt{\pi a^3}} \, e^{-r/a}, \tag{6.1}$$

with a being the variational parameter, whereas Panat and Paranjape [56] used the same form in 2D with radial variable r being replaced by the polar radial variable ρ as

$$\psi_0(\rho) = \sqrt{\frac{2}{\pi a^2}} \, e^{-\rho/a}. \tag{6.2}$$

The corresponding binding energies are given as

$$\overline{E}_0(a_r) = \frac{1}{a_r^2} - \frac{4}{\pi} \left\{ \int_0^\infty \frac{dq_r}{\left[(\frac{a_r q_r}{2})^2 + 1 \right]^2} \left[\frac{1}{\epsilon_{3D}(q_r)} - 1 \right] \right\} - \frac{2}{a_r}, \tag{6.3}$$

in 3D and

$$\overline{E}_0(a_r) = \frac{1}{a_r^2} - 2 \left\{ \int_0^\infty \frac{dq_r}{\left[(\frac{a_r q_r}{2})^2 + 1 \right]^{3/2}} \left[\frac{1}{\epsilon_{2D}(q_r)} - 1 \right] \right\} - \frac{4}{a_r}, \tag{6.4}$$

116

in 2D case, where bare interaction is added and subtracted to achieve faster decaying integrand as suggested in Ref. [56].

6.2.2 Integral Equation Formulation

In contrast to simplicity of the variational techniques, they must be used with care in problems such as the Mott transition, where the variational energy only yields an upper bound for the true ground-state energy. As a better alternative, we present below an approach that leads to an integral equation for which we also develop computationally-efficient operator techniques.

6.2.2.1 Formulation for 3D

The bound electron feels a centrally symmetric radial potential, and for the lowest $1s$ state, Schrödinger equation in 3D becomes

$$\frac{1}{r_r^2}\frac{d}{dr_r}\left(r_r^2\frac{d\psi_0(r_r)}{dr_r}\right) + \left[\overline{E}_0 - \overline{U}_{3D,scr}(r_r)\right]\psi_0(r_r) = 0. \tag{6.5}$$

$\overline{U}_{3D,scr}(r_r)$ is the screened potential energy due to a singly-ionized attractive impurity in real space to be computed as

$$\overline{U}_{3D,scr}(r_r) = -\frac{2}{r_r} + \frac{4}{\pi}\int_0^\infty dq_n \frac{\sin\left(q_n\frac{r_r}{r_s}\left[\frac{9\pi}{2g_d}\right]^{1/3}\right)}{q_n r_r}\left[1 - \frac{1}{\epsilon_{3D}(q_n)}\right], \tag{6.6}$$

where r_r is the reduced distance in real space; again we add and subtract unscreened Coulomb potential for computational reasons [56].

The principal problem in the numerical solution is the infinite domain of the wave function. As a remedy, Martino *et al.* [138] noting the difference with the hydrogen atom problem due to the presence of screening, set $\overline{U}_{3D,scr}(r)$ to zero for distances greater than some large value R. Then, for $r > R$ the wave function for bound states

117

becomes [139]

$$\psi_0(r) \sim \frac{e^{-\kappa r}}{r} \text{ with } \kappa = \sqrt{\frac{2m^*}{\hbar^2}|E_0|}, \tag{6.7}$$

upto a normalization constant. The continuity of the wave function together with its derivative at $r = R$, or equivalently, the continuity of the logarithmic derivative of the wave function yields

$$\left. \frac{d\ln\psi_0(r)}{dr} \right|_{r=R} = -\kappa - \frac{1}{R}. \tag{6.8}$$

Eq. (1.5) is a two-value differential equation problem dealt with shooting type numerical techniques [145]. We, rather, prefer to convert the radial Scrödinger equation to an integral equation as

$$\Gamma(r_r) = S(r_r) - \frac{1}{r_r}\int_0^{r_r} dr' \, \Gamma(r')^2, \tag{6.9}$$

where

$$S(r_r) = \frac{1}{r_r}\int_0^{r_r} dr' r'^2 \, \overline{U}_{3D,scr}(r'_r) + \frac{r_r^2}{3}|\overline{E}_0|, $$

and

$$\Gamma(r_r) = r_r \frac{d\ln\psi_0(r_r)}{dr_r}. \tag{6.10}$$

The energy eigenvalue is determined from $\Gamma(R_r) = -R_r\sqrt{|\overline{E}_0|} - 1$. In our work we extracted the energy eigenvalue $\overline{E}_0$ from the above equation by sampling the wave function in the 5% neighborhood of $R_r = 10$. Eq. (1.9) is a nonlinear integral equation of the Volterra type in the fixed-point form (refer to, for e.g., Ref. [146]). However, we observed very slow convergence of the standard techniques; for this purpose we first express the Eq. (1.9) as an operator equation as

$$P\left[\Gamma(r_r)\right] = \Gamma(r_r) - S(r_r) + \frac{1}{r_r}\int_0^{r_r} dr' \, \Gamma(r')^2 = 0 \tag{6.11}$$

118

and resort to operator form of the Newton's method [147] which requires the inverse

operator of the derivative (Fréchet derivative [147])[3] of the operator P evaluated at

the function $\Gamma(r_r)$. This inverse operator acting on $\Gamma(r_r)$ is given as

$$\{P'\left[\Gamma(r_r)\right]\}^{-1} = \sum_{n=0}^{\infty}(-1)^n\frac{2}{r_r}\int_0^{r_r}dr'\Gamma(r')\frac{2}{r'}\int_0^{r'}dr''\Gamma(r'')\cdots\frac{2}{r^{(n-1)}}\int_0^{r^{(n-1)}}dr^{(n)}\Gamma(r^{(n)});$$

(6.12)

here the prime on the left hand side designates a derivative, whereas, the primes on

the right hand side are used to produce dummy variables. We retain the first two

terms and approximate the final equation as

$$\Gamma_{new}(r_r) = \Gamma_n(r_r) - P\left[\Gamma_n(r_r)\right] + \frac{2}{r_r}\int_0^{r_r}dr'\,\Gamma_n(r')P\left[\Gamma_n(r')\right],$$

(6.13)

where Γ_n denotes Γ at the nth iteration; we determine Γ_{n+1} by mixing Γ_{new} and Γ_n.

The final form, then offers a rapidly converging algorithm, once we initiate the process

at low densities (like $r_s = 20$) using the variational wave function as the initial guess

and gradually increase the density towards the Mott transition point.

6.2.2.2 Formulation for 2D

2D Schrödinger equation for the ground-state wave function reads

$$\frac{1}{\rho_r}\frac{d}{d\rho_r}\left(\rho_r\frac{d\psi_0(\rho_r)}{d\rho_r}\right) + \left(\overline{E}_0 - \overline{U}_{2D,scr}(\rho_r)\right)\psi_0(\rho_r) = 0.$$

(6.14)

The expression for the screened potential energy due to a singly-ionized attractive

impurity in real space, which shows Friedel oscillations is

$$\overline{U}_{2D,scr}(\rho_r) = -\frac{2}{\rho_r} + \frac{4}{r_s\sqrt{gd}}\int_0^{\infty}dq_n\,J_0\left(q_n\frac{2}{r_s\sqrt{gd}}\rho_r\right)\left[1 - \frac{1}{\epsilon_{2D}(q_n)}\right],$$

(6.15)

---

[3] I would like to thank Prof. M. Kuzuoğlu for suggesting me to use Newton's technique in operator form and Prof. K. Leblebicioğlu for helping me with the Fréchet derivative and refering me to useful literature.
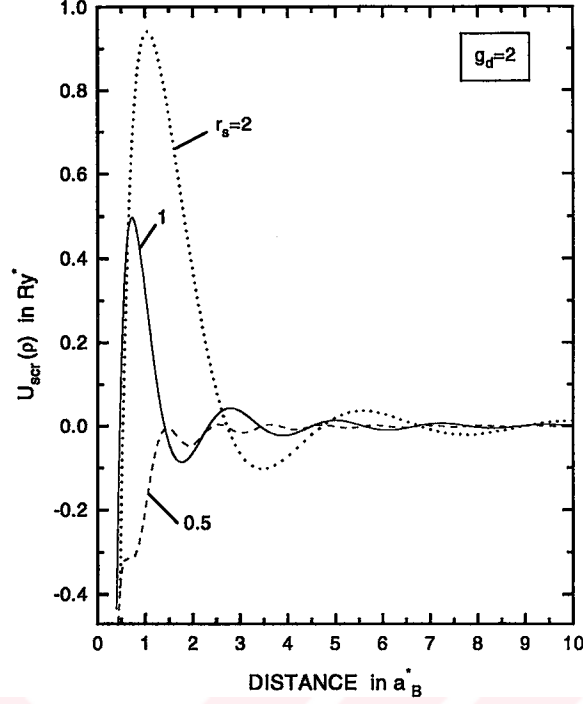
Figure 6.1: Potential energy distribution due to a screened, singly-ionized attractive impurity versus distance. A normal-state, single-valley EL is considered ($g_d = 2$) at several densities.

where ρ_r is the reduced 2D radial coordinate and J_0 is the zeroth-order cylindrical Bessel function of the first kind. See Fig. 1.1 for the screened potential energy at several values of the 2D electronic density; also note the evolution of the Friedel oscillations as the density decreases. As in 3D, we work with the function $\Gamma(\rho_r) = \rho_r d \ln \psi_0 / d\rho_r$, rather than with the wave function itself; in this way an exponentially decaying function is mapped to a linearly decreasing one. The nonlinear integral equation satisfied by Γ becomes

$$\Gamma(\rho_r) = S(\rho_r) - \int_0^{\rho_r} d\rho' \frac{\Gamma(\rho')^2}{\rho'}, \qquad (6.16)$$

where

$$S(\rho_r) = \int_0^{\rho_r} d\rho' \rho' \, \overline{U}_{2D,scr}(\rho') + \frac{\rho_r^2 |\overline{E}_0|}{2}, \qquad (6.17)$$

120

which is to be computed with very high precision. A nonlinear equation needs to be solved for the bound-state energy eigenvalue, of the form

$$\Gamma(R_r) = -R_r\sqrt{|E_0|}K_1(R_r\sqrt{|E_0|})/K_0(R_r\sqrt{|E_0|}),\qquad(6.18)$$

where K_n is the n'th order modified Bessel function of the second kind.

To achieve much faster convergence than the fixed-point form, the operator P is introduced as

$$P\left[\Gamma(\rho_r)\right] = \Gamma(\rho_r) - S(\rho_r) + \int_0^{\rho_r} d\rho'\frac{\Gamma(\rho')^2}{\rho'} = 0\qquad(6.19)$$

We give the final form of the iterative equation we use in 2D which closely resembles the 3D case

$$\Gamma_{new}(\rho_r) = \Gamma_n(\rho_r) - P\left[\Gamma_n(\rho_r)\right] + 2\int_0^{\rho_r} d\rho'\frac{\Gamma_n(\rho')}{\rho'}P\left[\Gamma_n(\rho')\right].\qquad(6.20)$$

6.3 Results

6.3.1 3D Electron Liquid Results

We investigate the transition of the binding energy of the impurity electron from bound to unbound state to estimate the Mott transition density. In Fig. 1.2 we plot the variational (hydrogenic) and integral equation solutions for the binding energy; the deviation is clearly visible towards the transition point. In Table 1.1, we list the so-called Mott constant defined by $a_B^* n_{3D}^{1/3}$, as a function of the degeneracy parameter g_d from spin-polarized electrons to six valley degeneracy as in the conduction band of silicon. It can be seen that for g_d greater than 4 the exchange effects do not lead to appreciable changes in the Mott constant. The spin-polarized EL ($g_d = 1$) has the highest Mott constant, which is due to poor screening of the impurity potential by the participating electrons having large Pauli holes around them.

121

Table 6.1: Critical Mott transition density, r_{sc} of the 3D EL. The corresponding Mott constants, defined as $a_B^* n_{3D}^{1/3}$ are indicated in parentheses. The numerical results based on the integral equation solution are more reliable (see text).

Degeneracy factor: g_d	1 (spin pol.)	2 (1-valley)	4 (2-valley)	8 (4-valley)	12 (6-valley)
Variational-(H): r_{sc}	2.25	3.57	4.11	4.13	4.05
(Mott Cons.)	(0.275)	(0.174)	(0.151)	(0.150)	(0.153)
Numerical: r_{sc}	1.44	2.70	3.62	3.80	3.75
(Mott Cons.)	(0.430)	(0.230)	(0.171)	(0.163)	(0.166)
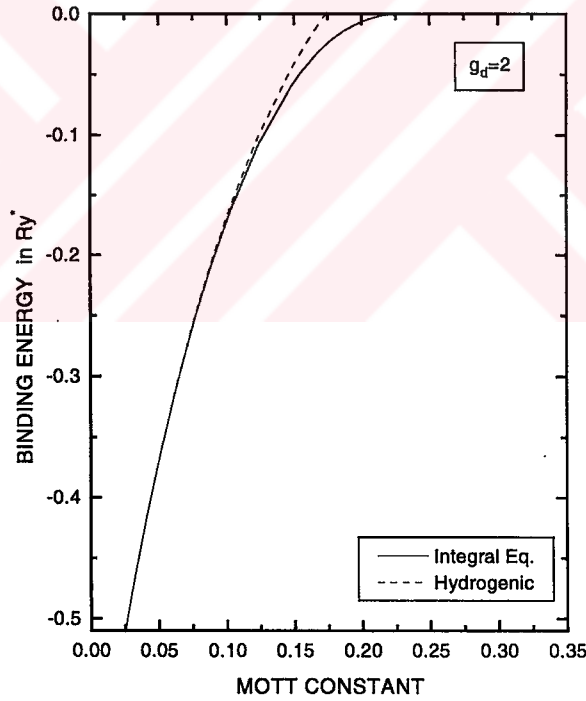
Figure 6.2: Binding energy of a bound impurity electron within a normal-state, single-valley ($g_d = 2$) 3D EL versus the Mott constant, defined as $a_B^* n_{3D}^{1/3}$. Solid line refers to integral equation solution which gives a lower energy than the variational treatment based on the hydrogenic wave function denoted by the dashed lines.

There is also a large amount of experimental data in the 3D MNM transition; see, for instance, the compilation by Ref. [148]. The differences between our results and the experimental data are due to our simplifications as disorder-free electronic system and the isotropic effective mass for the bound and screening electrons. The latter is predominantly effective in multi-valley materials such as silicon and germanium. We refer to other works considering the mass anisotropy problem [136, 137, 142]. However, in single-valley systems the conduction band effective mass is close to isotropic such as the $Al_xGa_{1-x}As$ system. Katsumoto *et al.* [149] using an n-doped $Al_{0.3}Ga_{0.7}As$ system measured the Mott constant as 0.21 which is somewhat close to our estimate of 0.23. We think that the difference is due to disorder apparently effective in this system. Gold and Ghazali [140] have also dealt with 3D Mott transition using STLS type screening and numerical solution for the bound electron wave function. They reported for the same 3D Mott constant the value 0.25. We attribute the difference between our and their results to the fact that these authors enforced Hubbard-like form for the local-field correction which differs from the exact STLS local-field correction leading to a discrepancy in the dielectric function.

6.3.2   2D Electron Liquid Results

The dimensionality plays a crucial role in almost all electronic properties and the Mott transition is of no exception [119]. Particularly, the role of Friedel oscillations is enhanced in 2D; see Fig. 1.1. However, quite commonly the in-plane wave function for (quasi) 2D bound impurities [56, 150, 151, 152] in the presence of free carriers (i.e., screening) has been chosen to be of $e^{-\rho/\lambda}$ type where λ is the variational parameter. In Fig. 1.3 the hydrogenic variational probability distribution is compared with that

123

of the integral equation solution. The screened attractive potential energy is also added in this figure to aid the comparison. The probability distribution obtained by integral equation solution is lower in the first repulsive part of the potential energy and higher in the neighboring attractive region than the variational solution; in turn, the electron is expected to be more tightly bound. This is seen to be the case in Fig. 1.4 showing the 2D impurity binding energy for the spin-polarized and normal states respectively. Furthermore, Mott transition is not observed for these two cases at zero temperature. For $g_d = 4$, the variational approach predicts a Mott transition in the range $r_s = 0.38$-1.81. The integral equation solution suggests that this window is narrower and situated around $r_s = 1$ as can be seen in Fig. 1.5(a). For $g_d=8$ and 12 Mott transitions are observed (see Fig. 1.5(b)) like the 3D cases at the r_s values 1.52 and 1.48 respectively based on the integral equation solution; the variational approach again leads to higher values. From these three figures we can also conclude that the hydrogenic variational technique is successful for the small values of the degeneracy factor, g_d.

Fig. 1.4 shows an interesting strengthening of binding at the high density limit, $r_s \to 0$. The screened interactions for several values of g_d at $r_s = 0.02$ are plotted in Fig. 1.6. In this limit, the Friedel oscillations diminish and the screening is determined by the exchange effects. Hence, for the spin polarized case ($g_d = 1$), the screening electrons cannot approach to the ion due to their mentioned Pauli holes resulting in poor screening of the ion potential and enhanced binding. As the degeneracy parameter, g_d is increased to 12, the exchange effects and the Pauli hole lose their importance and the screening is more effective than the spin-polarized EL, which leads to the existence of the Mott transition. Fig. 1.7 compares the effect of

124
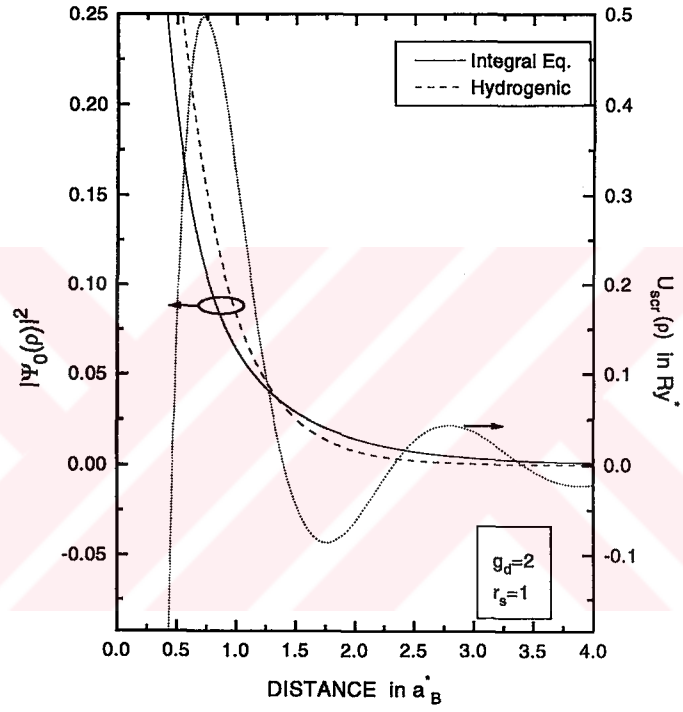
Figure 6.3: Probability distribution of the bound electron wave function within a 2D EL having $r_s = 1$ and $g_d = 2$. Solid line is based on the integral equation solution and dashed line refers to 2D hydrogenic wave function, i.e., Eq. (1.2). Also shown by dotted lines is the screened potential energy experienced by the bound electron.

125
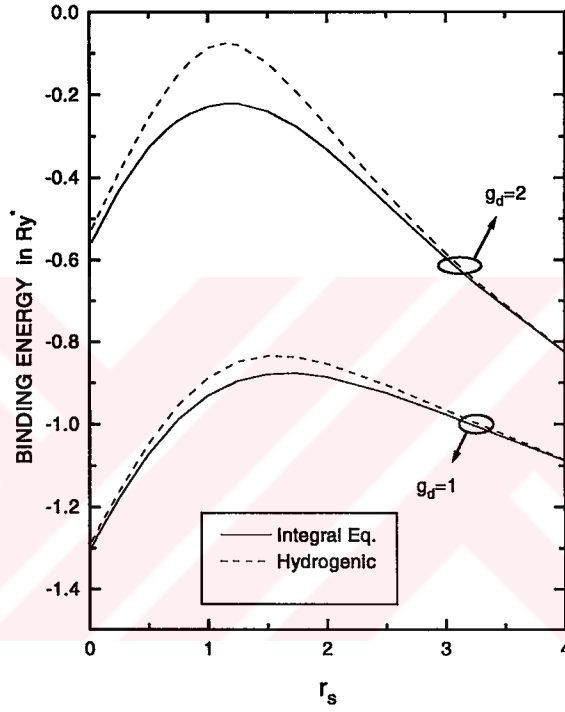
Figure 6.4: Binding energy of a bound electron within a 2D EL versus r_s. Calculations are based on the integral equation solution (solid lines) and 2D hydrogenic variational wave function (dashed lines). No mott transition is observed for the $g_d=1$ and 2 cases in a strictly 2D EL.

126
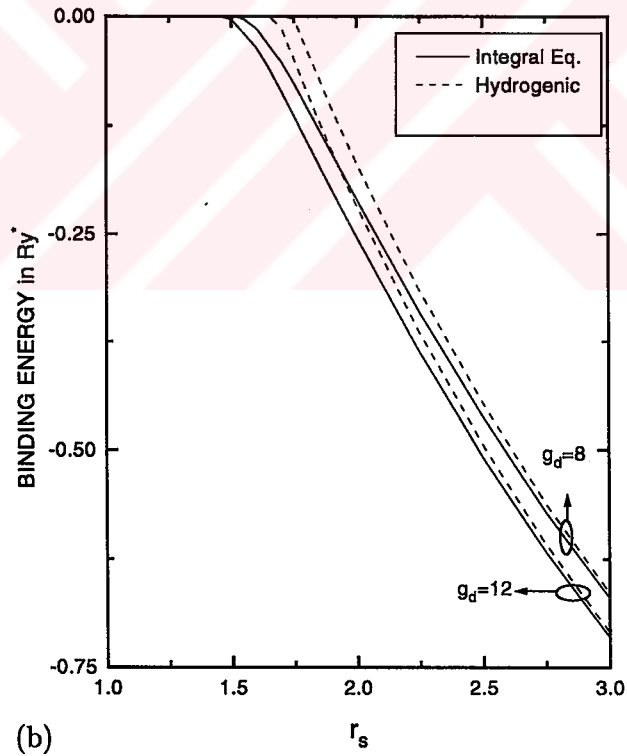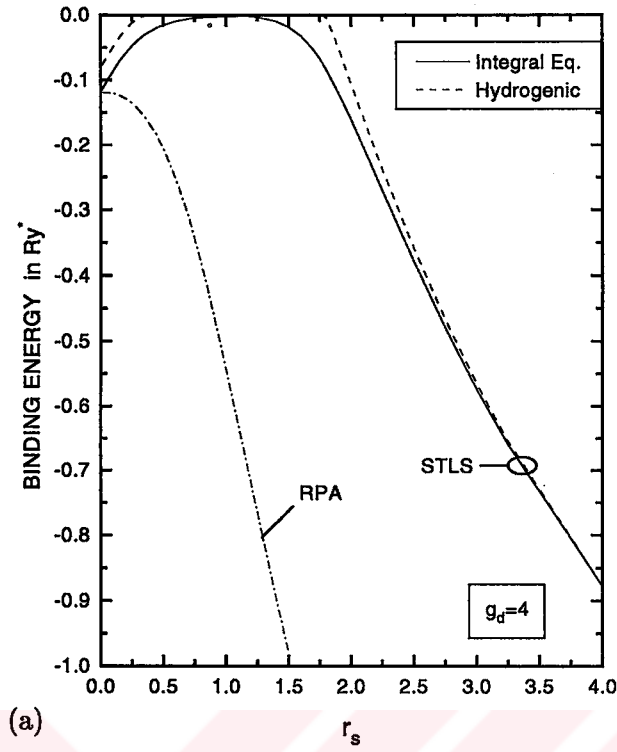
Figure 6.5: Binding energy of a bound electron within a 2D EL versus r_s (a) for $g_d=4$ (i.e., two valley degeneracy), and (b) for $g_d=8$ and 12 (i.e., four and six valley degeneracies). Solid line denotes the integral equation solution and the dashed line denotes 2D hydrogenic variational wave function result, both utilizing the STLS screening. Dash-dot line in (a) refers to RPA screening based on the integral equation solution.

several dielectric functions (RPA, Hubbard, and STLS) on the impurity binding energy. Apart from some sizeable quantitative differences, they all agree about the lack of the Mott transition for $g_d = 2$. It is seen that STLS dielectric function has stronger screening power leading to a weaker binding. Note the agreement of the three for $r_s \to 0$ as expected. Hubbard follows STLS at the high density end where exchange effects are dominant. Finally, from Fig. 1.5 we observe that RPA does not predict a Mott transition for $g_d = 4$ case.
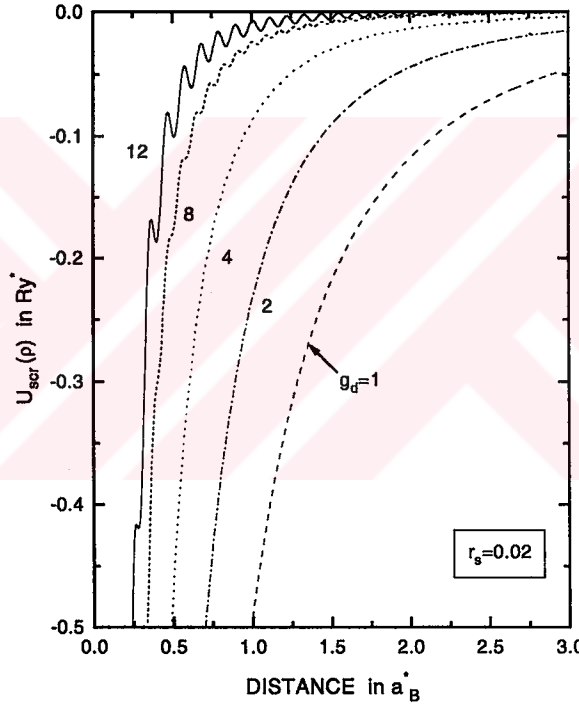
Figure 6.6: Potential energy distribution due to a screened, singly-ionized attractive impurity versus distance. The effect of the degeneracy factor g_d is illustrated from spin-polarized ($g_d = 1$) to six-valley degeneracy ($g_d = 12$); all at a very high density ($r_s = 0.02$) of a 2D EL.

The recent experiments [129, 130, 131, 132] using MOSFET structures detected a possible MNM transition around $r_s \simeq 8 - 9$. As this value is quite large when compared to the 3D counterparts, the MNM transitions in 3D and 2D seem to be

128
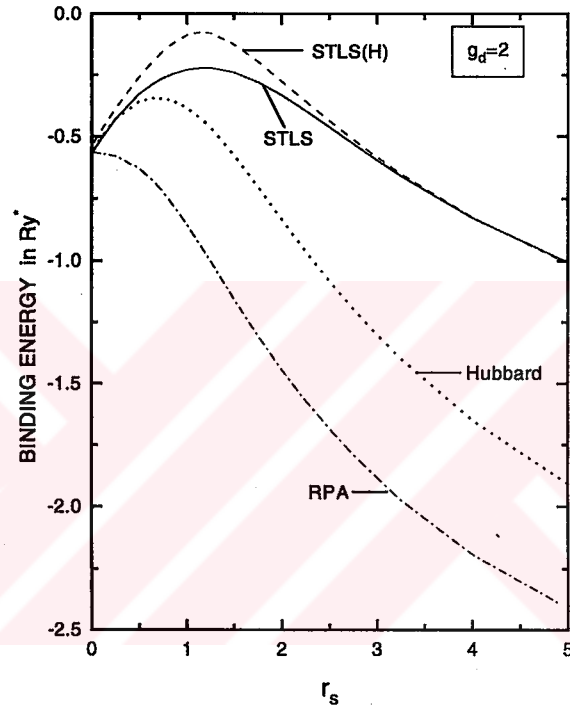
Figure 6.7: The effect of dielectric function on the binding energy for 2D EL using RPA, Hubbard and STLS screenings; all computed by solving the integral equation. Also the STLS screened binding energy is shown based the 2D hydrogenic wave function labeled by STLS(H).

governed by different phenomena. In the light of our work we think that, the experimentally observed critical transition density will not be obtained by the Mott transition mechanism alone even with the Coulomb softening due to finite extension of the charge distribution in real systems included. As a matter of fact, recent theoretical works stressed the role of disorder in the observed 2D MNM transition, and identified the insulator phase as a disorder driven electron solid [153, 154] and a metastable frozen electron solid [155, 156]. It needs to be stressed that the mystery behind these experiments is not yet unraveled.

CHAPTER 7

CONCLUSIONS

7.1 Contributions

The workhorse of the conventional electronic systems is the electron liquid model. We consider three- and two-dimensional ELs and obtain the longitudinal DF using the self-consistent local-field correction scheme of Singwi and co-workers, known as STLS. Our treatment is general, in the sense, we consider arbitrary spin and valley degeneracies. As an interesting remark, if the valley degree of freedom is replaced by the *isospin*[1], then our formulation is directly extended to non-relativistic nuclear matter problem; its isospin-polarized case is the neutron matter which has astrophysical importance in neutron stars [157]. Our preliminary investigation suggests that the dielectric formulation of the 3D nuclear matter with the STLS technique is promising. However, unlike the condensed matter physics, in the nuclear physics bare

---

[1] Actually, we first introduced an additional isospin freedom to tackle with the nuclear matter problem, then used this simple idea in the EL problem to account for the arbitrary valley degeneracy. The nuclear matter problem was suggested by Prof. Ş. Ayık from Tennessee Technological University (USA).

nucleon-nucleon interaction is not known quantitatively. Furthermore, its form is exceedingly complicated, with tensorial, velocity- and spin-isospin-dependent features [158]. A great deal of effort is necessary to fully implement the STLS technique to the nuclear and neutron matter problems.

Turning back to our actual problem, the electron liquid, knowing the wave number- and frequency-dependent DF, variety of many-body related terms such as the self-energy, carrier lifetime, and mobility are routinely accessible. For this reason an accurate dielectric characterization is vital for the equilibrium and electronic transport properties. We pursue a systematic assessment of the STLS DF by comparing it with QMC data and the polarization potential theory of Pines and co-workers both in 3D and 2D. Apart from the violation of the compressibility sum rule, which shows itself with a poor long-wavelength behavior, and the degraded form towards the Wigner solid densities, STLS displays an impressive performance within the practical electron densities. We can summarize our observations on the STLS DF as, a good agreement with the QMC for intermediate and small wavelengths over all realistic r_s values, and almost non-negative pair-correlation function. However, for the low-dimensional, artificial electronic structures, the most important virtue of the STLS technique, is its self-consistent scheme which does not require any fitting to experiment or simulation data (in contrast to the pseudopotential approach), where QMC data is not available. In the 2D normal-state single-valley EL case we offer analytical forms for the DF and the LFC to enable a widespread use of the STLS technique by other researchers. We calculate the correlation energy and the compressibility and compare them with the published results.

We also apply the STLS technique to characterize the dielectric properties of

132

the quasi-two-dimensional EL, in particular GaAs/AlGaAs heterojunction within the EQL. We pay special attention to an accurate treatment and consider the penetration of the Q2D EL to the barrier-acting material; the corresponding Coulomb form factor is also handled rigorously. The DF and the plasmon dispersion of the Q2D EL are presented for a wide range of electron and ionized acceptor densities, including the analytically fitted expressions to these results. We also investigate the effect of the first- excited subband population on the Coulomb form factor.

We finally apply the STLS dielectric screening to the Mott transition in 3D and 2D ELs. In the last three decades many theoretical works have claimed to have reproduced the experimentally observed MNM transition densities in 3D electronic systems. Each successive work then declared the previous agreement to be accidental due to some simplification in the treatment. Admittedly, Mott transition model alone cannot account for the observed MNM transition in real systems, however, it serves to the solution of the problem by revealing the role of electron-electron interactions. Not to sacrifice accuracy, we avoid variational techniques and choose to formulate the problem that lead to an integral equation for the bound electron wave function. We propose a rapidly converging Newton's method in the operator form. The exchange effects are investigated from spin-polarized single-valley EL to six-valley EL. In the 3D case, it is seen that the exchange effects are dominant for the spin-polarized and normal-state single-valley EL, and gradually Mott constant begins to be less sensitive for larger valley degeneracies. Based on our isotropic effective mass model, the closest agreement with the observed MNM transition is for the n-doped $Al_xGa_{1-x}As$ system, having a small mass anisotropy. The difference may be attributed to the disorder effects. In 2D, electron-electron correlations and

particularly, the Friedel oscillations are enhanced and lead to interesting physics. We observe that an attractive singly-ionized impurity can bind an electron in the presence of screening, and hence, no Mott transition exists for spin-polarized and normal-state single-valley EL, at zero temperature. The binding energies for these two cases are seen to be increased as $r_s \rightarrow 0$ due to exchange effects. The wave function based on the integral equation solution indicates that the bound electron favors the well regions of the Freidel oscillations as compared to the variational approach. We believe that the same behaviour will be operative in the 2D excitons under screening, and there, the hydrogenic variational form needs to be improved, especially for the high degeneracy cases. Similarly, the particular form of the dielectric screening employed has a first-order effect on the Mott constant and binding energies. Finally, we think that disorder effects and the finite extensions of the electronic distribution along the third dimension play a determining role in reproducing the experimentally observed [129, 130, 131, 132] 2D MNM transition.

7.2 Improvements

Having mentioned what has been accomplished by this thesis, we now would like to discuss possible improvements and future directions, to aid potential researchers. For the electrial engineers, a formulation at zero temperature is of limited use. The screening needs to be extended to room temperature [159, 160]. The EL model in our work assumes mass isotropy, but most semiconductors having a multi-valley conduction band (such as Si and Ge) possess highly anisotropic dispersion characteristics (i.e., $E - \vec{k}$ relation) near the conduction band minima. Borges *et al.* [142] have very recently taken this step to incorporate the mass anisotropy to STLS screening. In

our treatment the positive background which represents the ionic lattice, is taken to be rigid without any polarizability. The lattice screening, or in technical terminology, electron-LO phonon (Fröhlich) coupling can be taken into account easily within the dielectric formulation [42]. Similarly, the weak disorder effects are phenomenologically accounted for easily based on the relaxation-time approximation, again within the dielectric formulation, as proposed by Mermin [161, 162]. The improvements that we mentioned up to this point are well within the reach, and as a matter of fact, have been implemented by several groups. A more challenging improvement is to incorporate a dynamic LFC, that is to say, to account for the inertia of the Pauli-Coulomb hole around each electron. Even though several recent attempts have been made towards this direction [159, 163], this field has not become mature yet [55]. A secondary improvement to STLS-type treatments is the inclusion of the multi-pair excitations. This point has been particularly stressed in Ref. [73].

7.3 New Directions

We would like to mention currently promising directions in the mesoscopic and low-dimensional electronic systems; inevitably this section is rather speculative and superficial. A well-defined problem that seems to be easily accessible using our present formulation is the valley phase transition [61]. The driving mechanism is the competition between the kinetic and the exchange-correlation energies for a multi-valley EL. As mentioned by Bloss, Sham and Vinter in analysing the Si(100) surface, an equal population of all valleys minimizes the kinetic energy, whereas the exchange-correlation energy is lowered when all electrons populate a single valley [164]. This is a many-body driven phase transition just like the Mott transition; as the electronic

135

density decreases, the kinetic energy becomes less dominant and electrons after a critical density occupy fewer valleys.

Another direction is to explore the *transverse* dielectric function of the EL, which is related to the current-current correlation function [47]. Its importance is that the transverse DF characterizes the response to an electromagnetic field. Along the same lines, the photon-assisted transport [165, 166] is a promising field that has technological implications, for the least, offering novel millimeter-wave detector possibilities.

For electrical engineers, the subject of quantum transport has gained importance [4] as the size reduction of field-effect transistors reached the limits of the Boltzmann transport regime. Quantum transport of interacting electrons is quite an involved topic with very many alternatives. A conservative approach is the Kubo formalism based on the retarded current-current correlation tensor which falls into the linear response framework. The gate lengths in the future transistors is expected to be less than 0.1 μm, so that very high field transport will be operative. For such applications, the Kubo formalism does not seem to be applicable, where the transport is far from equilibrium [167]. As a remedy, the Keldysh formalism which is essentially a nonequilibrium Green's function approach has recently regained momentum [168, 25]. These techniques are quite advanced and the controversy in this field still persists, but this should not distract potential researchers.

7.4 Final Remarks

We would like to reserve our final but important remarks on the fundamental aspects of our work. As we mentioned in Chapter 3, the dynamo of the (interacting) EL is

the non-interacting polarization insertion, $\pi^0(q, \omega)$. This is simply because the interacting electron liquid is actually based on the *soluble* model, the non-interacting Fermi gas (both in 3D and 2D). The EL model that we employ in this work belongs to the wider class of Fermi liquids [36]. Landau's Fermi liquid theory is based on the idea that the interacting system (at least for the low-energy phenomena, at low temperatures, close to the Fermi surface) is governed by the quasiparticles which are still fermions and carry the same quantum labels as those electrons in the non-interacting system, but with "renormalized" masses and finite lifetimes. Furthermore, the interactions can also develop new collective modes like plasmons in the EL case [169, 3]. In the past years there have been growing concerns on the applicability of the Fermi liquid model to several electronic systems. The leading advocate of the non-Fermi liquid picture is an influential scientist, P. W. Anderson. His main standing point is that cuprate high-temperature superconductors, above the superconducting temperature T_c, that is to say, in their normal non-superconducting states do *not* obey the Fermi liquid model. The primary difference of non-Fermi liquids is that there is no quasiparticle type elementary excitations that can be identified with the original Fermi surface [70]. For instance, in 1D electronic structures it has been shown that there are *bosonic* collective fluctuations named as spinons, carrying spin excitations and holons, carrying the charge excitations[3]. Recall that in Fermi liquids the *quasi*electrons carry both the charge and spin simultaneously, however, in 1D systems an incoming electron (due to electron-electron inetractions and the 1D nature) decays into such charge and spin excitations, and these excitations propagate with different velocities, they segregate. Other well-known non-Fermi liquid behviour systems are 2D heterostructures under a high magnetic field that drives the system to integer and

137

fractional quantum Hall regimes[98, 99], and the superconducting states of the bulk

and low-dimensional superconductors. These so-called strongly correlated systems,

namely, superconductors, quantum Hall systems, 1D electronic structures, as well as

the disordered systems are not dealt with the jellium EL model, but with the Hubbard

model [42] which was originally introduced to deal with the Mott transition (which we

named as the Mott-Hubbard transition in Chapter 6). The Hubbard model defined

on a discretized space (lattice) [170], is currently a very popular theoretical object

among the condensed matter physicists. In response, the mainstream of research in

the field is the strongly correlated systems analyzed by the Hubbard Hamiltonian.

It seems that intense efforts in this field will lead to a unification of the underlying

mechanism in these diverse systems. No wonder, technological impacts will be revo-

lutionary. Among these new directions, the 3D, 2D and Q2D ELs within the Fermi

liquid framework, to a very good extend, represent the doped semiconductors and

normal metals in zero magnetic field and with weak disorder. Before embarking on

the controversial and subtle research topics on strongly correlated systems, the core

of the theory had to be mastered, which constitutes the goal of this work.

APPENDIX A

VARIATIONAL TOTAL SYSTEM ENERGY OF A

HETEROJUNCTION WITH TWO OCCUPIED

SUBBANDS

In this appendix, we include for completeness purposes, the expression for the *total* system energy of a heterojunction, allowing for penetration of the charge density to the barrier-acting region. We assume only the lowest two subbands to be occupied, with the 2D densities $n_{2D,1}$ and $n_{2D,2}$. Throughout this section, all physical quantities are in atomic units, that is to say, all energies are in Rydbergs ($1Ry = m_0 e^4/2\hbar^2$) and lengths in Bohr radius ($a_B = \hbar^2/m_0 e^2$). We also denote normalized effective masses in both regions as $m_{rA}^* = m_A^*/m_0$ and $m_{rB}^* = m_B^*/m_0$.

The variational wave functions for the lowest two subbands as proposed by Bastard are [101]

$$
\varsigma_1(z) = \begin{cases} M_1 \, e^{\kappa_{b1} \, z/2}, & \text{for } z \leq 0 \\[2em] N_1(z + z_0) \, e^{-bz/2}, & \text{for } z \geq 0 \end{cases} \quad , \qquad \text{(A.1)}
$$

139

$$
\varsigma_2(z) \;=\; \begin{cases} M_2\,e^{\kappa_{b2}\,z/2}, & \text{for } z \le 0 \\[2em] N_2(z+z_1)\,(z+z_2)\,e^{-cz/2}, & \text{for } z \ge 0 \end{cases} \qquad (A.2)
$$

We define the occupation ratio of the lowest subband as

$$
\text{occ} = \frac{n_{2D,1}}{n_{2D,1} + n_{2D,2}}. \qquad (A.3)
$$

The form of the variational total system energy per electron is given as

$$
\langle \tilde{E}_{TOT}(b, c, \kappa_{b1}, \kappa_{b2}) \rangle =
$$

$$
\text{occ}\left[\langle T_z \rangle_1 + \frac{1}{2}\left(\langle U_{e-e,1} \rangle_1 + \langle U_{e-e,2} \rangle_1 \right) + \langle U_A \rangle_1 + \langle U_{barrier} \rangle_1 \right]
$$

$$
+ (1 - \text{occ})\left[\langle T_z \rangle_2 + \frac{1}{2}\left(\langle U_{e-e,1} \rangle_2 + \langle U_{e-e,2} \rangle_2 \right) + \langle U_A \rangle_2 + \langle U_{barrier} \rangle_2 \right]. \quad (A.4)
$$

The terms used in this equation represent the following: $\langle T_z \rangle_i$ is the kinetic energy (of the i'th subband electrons) due to motion along the $z-$direction (the confinement direction)[1], $\langle U_A \rangle_i$ is the potential energy due to ionized acceptors, $\langle U_{barrier} \rangle_i$ is the barrier potential due to conduction band offset, and $\langle U_{e-e,j} \rangle_i$ is the Hartree potential produced by the j'th subband electrons on an i'th subband electron. The total energy expression has to be minimized with respect to the variational parameters $b, c, \kappa_{b1}, \kappa_{b2}$. Now we display each term that goes into the energy expression.

The lowest subband expressions are

$$
\langle T_z \rangle_1 = -\frac{M_1^2 \kappa_{b1}}{4\, m_{rB}^*} + \frac{N_1^2}{2\, m_{rA}^*\, b}\,(1 + bz_0 - b^2 z_0^2/2), \qquad (A.5)
$$

$$
\langle U_A \rangle_1 = \frac{8\pi}{\bar{\epsilon}} N_{depl} \left[\frac{6N_1^2}{b^4}\left(1 + \frac{2}{3}bz_0 + \frac{b^2 z_0^2}{6} \right) - \frac{M_1^2}{\kappa_{b1}^2} \right], \qquad (A.6)
$$

---

[1] The $x-y$ plane kinetic energy term does not depend on the variational parameters, and for this reason, not included in the total energy expression.

$$\langle U_{barrier} \rangle_1 = \frac{U_b M_1^2}{\kappa_{b1}}, \qquad (A.7)$$

and

$$\langle U_{e-e,1} \rangle_1 = \frac{8\pi}{\bar{\epsilon}} n_{2D,1} \left[\frac{N_1^4}{b^7} \left(\frac{33}{4} + \frac{25bz_0}{2} + \frac{17b^2z_0^2}{2} + 3b^3z_0^3 + \frac{b^4z_0^4}{2} \right) \right.$$
$$\left. - \frac{N_1^2 M_1^2}{\kappa_{b1}^2 b^3} (z_0^2 b^2 + 2bz_0 + 2) \right]. \qquad (A.8)$$

For the remaining expressions we define some auxiliary quantities as

$$t_1 = \frac{\kappa_{b2} \, m_{rA}}{2 \, m_{rB}} + \frac{c}{2}, \qquad (A.9)$$

$$d = \frac{b+c}{2}, \qquad (A.10)$$

$$t_2 = \frac{1}{6 + 2 d z_0} \left[\frac{2 d^4 z_0}{\kappa_{b1} + \kappa_{b2}} + 2 d t_1 + d^2 (1 + z_0 t_1) + z_0 d^3 \right], \qquad (A.11)$$

$$z_1 = \frac{-\frac{t_1}{t_2} - \sqrt{\left(\frac{t_1}{t_2}\right)^2 + \frac{4}{t_2}}}{2}, \qquad (A.12)$$

$$z_2 = \frac{-\frac{t_1}{t_2} + \sqrt{\left(\frac{t_1}{t_2}\right)^2 + \frac{4}{t_2}}}{2}, \qquad (A.13)$$

$$t_3 = \frac{1}{c^5} \left[24 + 12 z_1 c + 12 z_2 c + 2 z_1^2 c^2 + 8 z_1 z_2 c^2 + 2 z_2^2 c^2 \right.$$
$$\left. + 2 z_1^2 z_2 c^3 + 2 z_2^2 z_1 c^3 + z_1^2 z_2^2 c^4 \right], \qquad (A.14)$$

$$N_2 = \left(\frac{z_1^2 z_2^2}{\kappa_{b2}} + t_3 \right)^{-1/2}, \qquad (A.15)$$

$$M_2 = N_2 z_1 z_2, \qquad (A.16)$$

$$w_1 = z_1 + z_2, \qquad (A.17)$$

$$w_2 = z_1^2 + z_2^2 + 4 z_1 z_2, \qquad (A.18)$$

$$w_3 = z_1 z_2 (z_1 + z_2), \qquad (A.19)$$

$$w_4 = (z_1 z_2)^2, \qquad (A.20)$$

141

$$h_1 = c\,w_1, \tag{A.21}$$

$$h_2 = c^2\,w_2, \tag{A.22}$$

$$h_3 = c^3\,w_3, \tag{A.23}$$

$$h_4 = c^4\,w_4, \tag{A.24}$$

$$P_0 = \frac{h_4 + 4\,h_3 + 6\,h_2 + 48\,h_1 + 120}{c^6}, \tag{A.25}$$

$$P_1 = \frac{2\,(h_3 + 2\,h_2 + 18\,h_1 + 48)}{c^5}, \tag{A.26}$$

$$P_2 = \frac{h_2 + 12\,h_1 + 36}{c^4}, \tag{A.27}$$

$$P_3 = \frac{2\,h_1 + 8}{c^3}, \tag{A.28}$$

$$P_4 = \frac{1}{c^2}, \tag{A.29}$$

$$\alpha = \frac{1}{b^2}, \tag{A.30}$$

$$\beta = \frac{4}{b^3} + \frac{2\,z_0}{b^2}, \tag{A.31}$$

$$\gamma = \frac{6}{b^4} + \frac{4\,z_0}{b^3} + \frac{z_0^2}{b^2}. \tag{A.32}$$

Then, other terms in the energy expresion become

$$\langle T_z \rangle_2 = -\frac{M_2^2\,\kappa_{b2}}{4\,m_{rB}} + \frac{N_2^2}{4\,m_{rA}\,c^3}\left[-h_4 + 2\,h_3 + 2\,c^2\,(z_1^2 + z_2^2)\right.$$
$$\left. + 4\,h_1 + 8\right], \tag{A.33}$$

$$\langle U_A \rangle_2 = \frac{8\,\pi}{\bar{\epsilon}}\,N_{depl}\left(N_2^2\,P_0 - \frac{M_2^2}{\kappa_{b2}^2}\right), \tag{A.34}$$

$$\langle U_{barrier} \rangle_2 = \frac{U_b\,M_2^2}{\kappa_{b2}}, \tag{A.35}$$

$$\tag{A.36}$$

142

$$\langle U_{e-e,1}\rangle_2 \;=\; -\frac{8\,\pi}{\bar{\epsilon}}\,n_{2D,1}\,N_1^2\,N_2^2\,\Bigg[-\gamma\,t_3 + \frac{720\,\alpha}{(b+c)^7}$$

$$+\,\frac{240\,\alpha\,w_1 + 120\,\beta}{(b+c)^6} + \frac{24\,\alpha\,w_2 + 48\,\beta\,w_1 + 24\,\gamma}{(b+c)^5}$$

$$+\,\frac{12\,\alpha\,w_3 + 6\,\beta\,w_2 + 12\,\gamma\,w_1}{(b+c)^4} + \frac{2\,\alpha\,w_4 + 4\,\beta\,w_3 + 2\,\gamma\,w_2}{(b+c)^3}$$

$$+\,\frac{\beta\,w_4 + 2\,\gamma\,w_3}{(b+c)^2} + \frac{\gamma\,w_4}{b+c} + \frac{M_2^2}{N_2^2\,\kappa_{b2}^2}\left(\frac{z_0^2}{b} + \frac{2\,z_0}{b^2} + \frac{2}{b^3}\right)\Bigg]\,, \quad \text{(A.37)}$$

$$\langle U_{e-e,2}\rangle_1 \;=\; -\frac{8\,\pi}{\bar{\epsilon}}\,n_{2D,2}\,N_1^2\,N_2^2\,\Bigg[\frac{720\,P_4}{(b+c)^7} + \frac{120\,(P_3 + 2\,P_4\,z_0)}{(b+c)^6}$$

$$+\,\frac{24\,(P_2 + 2\,P_3\,z_0 + P_4\,z_0^2)}{(b+c)^5} + \frac{6\,(P_1 + 2\,P_2\,z_0 + P_3\,z_0^2)}{(b+c)^4}$$

$$+\,\frac{2\,(P_0 + 2\,P_1\,z_0 + P_2\,z_0^2)}{(b+c)^3}$$

$$-\,\frac{2\,P_0}{b^3}\left(1 + b\,z_0 + \frac{(b\,z_0)^2}{2}\right) + \frac{z_0^2\,t_3}{\kappa_{b1}^2}\Bigg]\,, \quad \text{(A.38)}$$

$$\langle U_{e-e,2}\rangle_2 \;=\; -\frac{8\,\pi}{\bar{\epsilon}}\,n_{2D,2}\,N_2^4\,\Bigg[\frac{3\,P_4}{8\,c^9}\,(2\,h_4 + 10\,h_3 + 15\,h_2 + 105\,h_1 + 210)$$

$$+\,\frac{3\,P_3}{16\,c^8}\,(2\,h_4 + 8\,h_3 + 10\,h_2 + 60\,h_1 + 105)$$

$$+\,\frac{P_2}{8\,c^7}\,(2\,h_4 + 6\,h_3 + 6\,h_2 + 30\,h_1 + 45)$$

$$+\,\frac{P_1}{8\,c^6}\,(2\,h_4 + 4\,h_3 + 3\,h_2 + 12\,h1 + 15)$$

$$-\,\frac{P_0}{4\,c^5}\,(2\,h_4 + 6\,h_3 + 7\,h_2 + 45\,h_1 + 93) + \frac{M_2^2\,t_3}{N_2^2\,\kappa_{b2}^2}\Bigg]\,. \quad \text{(A.39)}$$

REFERENCES

[1] A. B. Fowler, "A Semicentury of Semiconductors", Physics Today, 59 (October 1993).

[2] M. J. Kelly, *Low-Dimensional Semiconductors: Materials, Physics, Technology, Devices*, (Oxford University Press, Oxford, 1995).

[3] P. Coleman, "Condensed Matter: Strongly Correlated Electrons", Physics World, 29 (December 1995).

[4] D. K. Ferry, H. L. Grubin, C. Jacoboni, A. P. Jauho (editors), *Quantum Transport in Ultrasmall Devices*, NATO ASI Series B:342, (Plenum, New York, 1995).

[5] C. W. J. Beenakker and H. van Houten, "Quantum Transport in Semiconductor Nanostructures", in *Solid State Physics*, edited by H. Ehrenreich, and D. Turnbull (Academic, New York, 1991), Vol. 44, p. 1.

[6] N. G. van Kampen, *Stochastic Processes in Physics and Chemistry*, (North-Holland, Amsterdam, 1981).

[7] S. Datta and M. J. McLennan, "Quantum Transport in Ultrasmall Electronic Devices", Reports of Progress in Physics **53**, 1003 (1990).

[8] A. Weisshaar, J. Lary, S. M. Goodnick, and V. K. Tripathi, "Application of Microwave Techniques in the Analysis of Quantum Waveguide Structures and Devices", Procceedings of the IEEE Microwave Theory and Techniques Symposium, 481 (1991).

[9] C. Bulutay, N. Günalp, and M. Tomak, "Electron Biprism Operation of Split-Gate Heterostructures Having a Single Impurity within the Channel", Journal of Applied Physics **76**, 5309 (1994).

[10] G. Möllenstedt and H. Düker, "Beobachtungen und Messungen an Biprisma-Interferenzen mit Electronenwellen", Zeitschrift für Physik, **145**, 377 (1956) (in German).

[11] A. Tonomura, "Applications of Electron Holography", Reviews of Modern Physics **59**, 639 (1987).

[12] T. Leuthner, H. Litche, and K. H. Herrmann, "STEM- Holography Using the Electron Biprism", Physica Status Solidi A **116**, 113 (1989).

144

[13] H.Z. Zheng, H.P. Wei, D.C. Tsui, and G. Weimann, "Gate Controlled Transport in Narrow GaAs/Al$_x$Ga$_{1-x}$As Heterostructures", Physical Review B **34**, 5635 (1986).

[14] C.C. Eugster, J.A. del Alamo, M.R. Melloch and M.J. Rooks, "Effects of Single Scatterers on Transport and Tunnelling in a Dual Electron-Waveguide Device", Physical Review B **46**, 10146 (1992).

[15] G. Timp, in Semiconductors and Semimetals, edited by M.A. Reed (Academic, New York, 1992), Vol. 35, p. 113.

[16] C.S. Chu and R.S. Sorbello, "Effect of Impurities on the Quantized Conductance of Narrow Channels", Physical Review B **40**, 5941 (1989).

[17] P.F. Bagwell, "Evanescent Modes and Scattering in Quasi-One-Dimensional Wires", Physical Review B **41**, 10354 (1990).

[18] E. Tekman and S. Ciraci, "Ballistic Transport Through a Quantum Point Contact: Elastic Scattering by Impurities", Physical Review B **42**, 9098 (1990).

[19] Y.B. Levinson, M.I. Lubin, and E.V. Sukhorukov, "Short-Range Impurity in a Saddle Point Potential: Conductance of a Microjunction", Physical Review B **45**, 11936 (1992).

[20] S.A. Gurvitz and Y.B. Levinson, "Resonant Reflection and Transmission in a Conducting Channel with a Single Impurity", Physical Review B **47**, 10578 (1993).

[21] M. Okada, M. Saito, M. Takatsu, P.E. Schmidt, K. Kosemura and N. Yokoyama, "Electron Waves through Quantum Point Contacts", Semiconductor Science and Technology **7**, B223 (1992).

[22] L.W. Lyo and P. Avouris, "Field-Induced Nanometer to Atomic- Scale Manipulation of Atomic Surfaces with the STM", Science **253**,173 (1991).

[23] D. M. Eigler and E. K. Schwizer, "Positioning Single Atoms with a Scanning Tunneling Microscope", Nature **344**, 524 (1990).

[24] R.G. García, "Atomic-Scale Manipulation in Air with the Scanning Tunneling Microscope", Applied Physics Letters **60**, 1960, (1992).

[25] A. E. Tekman, *Ballistic Transport and Tunnelling in Small Systems*, Ph. D. Thesis, Bilkent University (October 1990).

[26] R. Frohne and S. Datta, "Electron Transfer Between Regions with Different Confining Potentials", Journal of Applied Physics **64**, 4086 (1988).

[27] S. Datta, "Quantum Devices", Superlattices and Microstructures **6**, 83 (1989).

[28] F. Sols, M. Macucci, U. Ravaioli, and K. Hess, "On the Possibility of Transistor Action Based on Quantum Interference Phenomena", Applied Physics Letters **54** 350 (1989).

[29] T. J. Thornton, "Mesoscopic Devices - What are They ?", in *Quantum Transport in Ultrasmall Devices*, edited by D. K. Ferry, H. L. Grubin, C. Jacoboni, A. P. Jauho, NATO ASI Series B:342, (Plenum, New York, 1995), p. 141.

[30] T. Ikoma, T. Odagiri, and K. Hirakawa, in *Quantum Effect Physics, Electronics and Applications*, edited by K. Ismail, T. Ikoma, and H. I. Smith (IOP Publ., New York, 1992).

[31] A. Jacoby, U. Sivan, C. P. Umbach, and J. M. Hong, "Interference and Dephasing by Electron-Electron Interaction on Length Scales Shorter than the Elastic Mean Free Path", Physical Review Letters **66**, 1938 (1991).

[32] F. Müller, B. Lengeler, Th. Schäpers, J. Appenzeller, A. Förster, Th. Klocke, and H. Lüth, "Electron-Electron Interaction in Ballistic Beams", Physical Review B **51**, 5099 (1995).

[33] S. Das Sarma, "Screening and Many-Body Effects in Low-Dimensional Electron Systems", in *Quantum Transport in Ultrasmall Devices*, edited by D. K. Ferry, H. L. Grubin, C. Jacoboni, A. P. Jauho, NATO ASI Series B:342, (Plenum, New York, 1995), p. 339.

[34] S. W. Koch, T. Meier, J. Hader, K.-C. Je, F. Rossi, and P. Thomas, "Equilibrium and Nonequilibrium Optical Effects in Semiconductor Heterostructures", in *Frontiers in Nanoscale Science of Micron/Submicron Devices*, edited by A.-P. Jauho and E. V. Buzaneva, NATO ASI Series E:328, (Kluwer, Dordrecht, 1996), p. 459.

[35] S. Datta, *Quantum Phenomena*, (Addisson-Wesley, Reading, 1989), p. 8.

[36] D. Pines and P. Nozières, *The Theory of Quantum Liquids* (Benjamin, New York, 1966), Vol. I.

[37] A. A. Abrikosov, L. P. Gorkov, I. E. Dzyaloshinski, *Methods of Quantum Field Theory in Statistical Physics*, (Dover, New York, 1963).

[38] R. D. Mattuck, *A Guide to Feynman Diagrams in the Many-Body Problem*, 2nd ed. (McGraw-Hill, New York, 1976), republished in 1992 by Dover Publications.

[39] S. Doniach and E. H. Sondheimer, *Green's Functions for the Solid-State Physicists*, (Addisson-Wesley, Reading, 1974).

[40] J. W. Negele and H. Orland, *Quantum Many-Particle Systems*, (Addisson-Wesley, Reading, 1988).

[41] C. P. Enz, *A Short Course on Many-Body Theory Applied to Solid-State Physics*, (World Scientific, Singapore, 1992).

[42] G. Mahan, *Many-Particle Physics*, 2nd ed. (Plenum, New York, 1990).

[43] E. Fradkin, *Field Theories of Condensed Matter Systems*, (Addisson-Wesley, Reading, 1991).

[44] L. V. Keldysh, D. A. Kirzhnitz, and A. A. Maradudin (editors), *The Dielectric Function of Condensed Systems*, (Elsevier, Amsterdam, 1989).

[45] C. Bowen, G. Sugiyama, and B. J. Alder, "Static Response of the Electron Gas", Physical Review B **50**, 14838 (1994).

[46] C. Balanis, *Advanced Engineering Electromagnetics*, (Wiley, New York, 1989).

[47] H. Haug and S. Schmitt-Rink, "Electron Theory of the Optical Properties of Laser-Excited Semiconductors", Progress in Quantum Electronics **9**, 3 (1984).

[48] J. D. Jackson, *Classical Electrodynamics* (Wiley, New York, 1975).

[49] F. Mandl and G. Shaw, *Quantum Field Theory*, (Wiley, New York, 1984).

[50] D. A. Dahl and L. J. Sham, "Electrodynamics of Quasi-Two-Dimensional Electrons", Physical Review B **16**, 651 (1977).

[51] A. L. Fetter and J. D. Walecka, *Quantum Theory of Many-Particle Systems* (McGraw-Hill, New York, 1971).

[52] J. Lindhard, Kgl. Danske Videnskab. Selskab, Mat. Fys. Medd. **28**, No. 8 (1954).

[53] D. Pines, *Elementary Excitations in Solids* (Benjamin, New York, 1963).

[54] G. Senatore, "Local-Field Correction of the Electron Gas", Seminar Notes, (given in METU Physics Department, unpublished) (1995).

[55] V. D. Gorobchenko, V. N. Kohn, E. G. Maksimov, "The Dielectric Function of the Homogeneous Electron Gas" in *The Dielectric Function of Condensed Systems* edited by L. V. Keldysh, D. A. Kirzhnitz, and A. A. Maradudin (Elsevier, Amsterdam, 1989).

[56] P. V. Panat and V. V. Paranjape, "Screening Effects in Two-Dimensional Electron Gas", Solid State Communications **62**, 829 (1987).

[57] N. Iwamoto, "Static Local-Field Corrections of Two-Dimensional Electron Liquids", Physical Review B **43**, 2174 (1991).

[58] G. Barton, *Elements of Green's Functions and Propagation: potentials, diffusion and waves* (Clarendon, New York, 1989).

[59] J. S. Thakur and K. N. Pathak, "Some Properties of Quantum Two-Dimensional Electron Gas with $\ln(r)$ Interaction", Journal of Physics C: Solid State Physics **16**, 6551 (1983).

[60] D. Olego, A. Pinczuk, A. C. Gossard, and W. Wiegmann, "Plasma Dispersion in a Layer Electron Gas: a Determination in GaAs-(AlGa)As Heterostructures", Physical Review B **26**, 7867 (1982).

[61] A. Isihara, "Electron Correlations in Two-Dimensions", in *Solid State Physics*, edited by H. Ehrenreich, and D. Turnbull (Academic, New York, 1989), Vol. 42, p. 271.

[62] F. Stern, "Polarizability of a Two-Dimensional Electron Gas", Physical Review Letters **18**, 546 (1967).

[63] C. Bulutay and M. Tomak, "Dielectric Function of the Two-Dimensional Electron Liquid: an Analytical Fitting", Physical Review B **53**, 7317 (1996).

[64] G. D. Mahan, "Correlation Energy of the Two-Dimensional Electron Gas", Physica Scripta **32**, 423 (1985).

[65] U. de Freitas and N. Studart, "Electron Correlations in Semiconductor Heterostructures", Physical Review B **36**, 6677 (1987).

[66] L. C. Ioriatti and A. Isihara, "On the Ground-State Energy of a Two-Dimensional Fluid", Zeitschrift für Physik B **44**, 1 (1981).

[67] K. S. Singwi, M. P. Tosi, R. H. Land, A. Sjölander, "Electron Correlations at Metallic Densities", Physical Review **176**, 589 (1968).

[68] J. Hubbard, "The Description of Collective Motions in Terms of Many-Body Perturbation Theory: II. The Correlation Energy of a Free-Electron Gas", Proceedings of the Royal Society (London) **A243**, 336 (1957).

[69] H. Haug and S. W. Koch, *Quantum Theory of the Optical and Electronic Properties of Semiconductors*, 3rd ed. (World Scientific, Singapore, 1994).

[70] P. W. Anderson, "Condensed Matter: the Continuous Revolution", Physics World, 37 (December 1995).

[71] S. Moroni, D. M. Ceperley, and G. Senatore, "Static Response and Local-Field Factor of the Electron Gas", Physical Review Letters **75**, 689 (1995).

[72] D. Pines, "Excitations and Transport in Quantum Liquids", in *Highlights of the Condensed-Matter Theory*, Proceedings of the International School of Physics "Enrico Fermi", edited by F. Bassani, F. Fumi, and M. P. Tosi (North-Holland, Amsterdam 1985), p. 580.

[73] N. Iwamoto and D. Pines, "Theory of Electron Liquids. I. Electron-Hole Pseudopotentials", Physical Review B **29**, 3924 (1984).

[74] N. Iwamoto, E. Krotscheck, and D. Pines, "Theory of Electron Liquids. II. Static and Dynamic Form Factors, Correlation Energy, and Plasmon Dispersion", Physical Review B **29**, 3936 (1984).

[75] B. Tanatar, and D. M. Ceperley, "Ground State of the Two-Dimensional Electron Gas", Physical Review B **39**, 5005 (1989).

[76] S. Moroni, D. M. Ceperley, and G. Senatore, "Static Response from Quantum Monte Carlo Calculations", Physical Review Letters **69**, 1837 (1992).

[77] N. H. March and M. Parrinello, *Collective Effects in Solids and Liquids*, (Adam Hilger, Bristol, 1982), p. 9.

[78] C. H. Aldrich III and D. Pines, Journal of Low Temperature Physics **32**, 689 (1978).

148

[79] D. M. Ceperley and B. J. Alder, Physical Review Letters **45**, 566 (1980).

[80] D. J. W. Geldart and S. H. Vosko, "The Screening Function of an Interacting Electron Gas", Canadian Journal of Physics **44**, 2137 (1966).

[81] G. Senatore, private communication.

[82] N. Iwamoto, "Sum Rules and Static Local-Field Corrections of Electron Liquids in Two and Three Dimensions", Physical Review B **30**, 3289 (1984).

[83] K. S. Singwi, A. Sjölander, M. P. Tosi, R. H. Land, "Electron Correlations at Metallic Densities. IV", Physical Review B **1**, 1044 (1970).

[84] P. Vashishta, K. S. Singwi, "Electron Correlations at Metallic Densities. V", Physical Review B **6**, 875 (1972).

[85] C. Bulutay, N. Günalp, and M. Tomak, "Screening in Two-Dimensional Electron Liquid", in *Frontiers in Nanoscale Science of Micron/Submicron Devices*, edited by A.-P. Jauho and E. V. Buzaneva, NATO ASI Series E:328, (Kluwer, Dordrecht, 1996), p. 533.

[86] M. Jonson, "Electron Correlations in Inversion Layers", Journal of Physics C: Solid State Physics **9**, 3055 (1976).

[87] D. L. Freeman, "Coupled-Cluster Summation of the Particle-Particle Ladder Diagrams for the Two-Dimensional Electron Gas", Journal of Physics C: Solid State Physics **16**, 711 (1983).

[88] D. L. Freeman, "Application of the Coupled-Cluster Expansion to the Correlation Energy of Electrons in Two-Dimensional and Quasi-Two-Dimensional Sytems", Solid State Communications **26**, 289 (1978).

[89] J. P. Eisenstein, L. N. Pfeiffer, and K. W. West, "Compressibility of the Two-Dimensional Electron Gas: Measurements of the Zero-Field Exchange Energy and the Fractional Quantum Hall Gap", Physical Review B **50**, 1760 (1994).

[90] N. K. Patel, I. S. Millard, C. Foden, E. H. Linfield, M. Y. Simmons, D. A. Ritchie, and M. Pepper, "Compressibility Studies of Two-Dimensional Electron Gases", Superlattices and Microstructures **21**, 125 (1997).

[91] A. Gold and L. Calmels, "Many-Body Effects in Quantum Wells: Finite Width Effects", Solid State Communications **88**, 659 (1993).

[92] O. V. Dolgov, D. A. Kirzhnits, and E. G. Maksimov, "On an Admissible Sign of the Static Dielectric Function of Matter", Reviews of Modern Physics **53**, 81 (1981).

[93] K. Takayanagi, and E. Lipparini, "Dynamic Response of a Two-Dimensional Electron Gas: Exact Treatment of Coulomb Exchange in the Random-Phase Approximation", Physical Review B **52**, 1738 (1995).

[94] G. Sugiyama, C. Bowen, and B. J. Alder, "Static Dielectric Response of Charged Bosons", Physical Review B **46**, 13042 (1992).

[95] S. Ichimaru, "Strongly Coupled Plasmas: High-Density Classical Plasmas and Degenerate Electron Liquids", Reviews of Modern Physics, **54**, 1017 (1982).

[96] S. Wang, *Fundamentals of Semiconductor Theory and Device Physics*, (Prentice-Hall, London, 1989).

[97] C. P. Poole, T. Datta, H. A. Farach, *Copper Oxide Superconductors*, (Wiley, New York, 1988).

[98] M. Stone, (editor), *Quantum Hall Effect*, (World Scientific, Singapore, 1992).

[99] T. Chakraborty and P. Pietilanien, in *The Fractional Quantum Hall Effect*, Springer Series in Solid-state Sciences Vol. 85 (Springer-Verlag, Berlin, 1988).

[100] G. Bastard, "Self-Consistent Variational Calculation and Alloy Scattering in Semiconductor Heterojunctions", Surface Science **142**, 284 (1984).

[101] G. Bastard, *Wave Mechanics Applied to Semiconductor Heterostructures* (Les Editions de Physique, Cedex, 1988), p. 155.

[102] M. Ayman Magdy, R. A. Al-Khader, and M. Tomak, "Electronic Structure of Modulation-Doped $In_{0.53}Ga_{0.47}As/n - In_{0.52}Al_{0.48}As$ Heterostructure", Nuovo Cimento D**17**, 357 (1995) and references therein.

[103] F. J. Fernández-Velicia, F. García-Moliner, and V. R. Velasco, "Dielectric Response of an Inhomogeneous Quasi-Two-Dimensional Electron Gas", Physical Review B **53**, 2034 (1996).

[104] P. Y. Yu and M. Cardona, *Fundamentals of Semiconductors*, (Springer, Berlin, 1996), p. 314.

[105] T. Ando, A. B. Fowler, and F. Stern, "Electronic Properties of Two-Dimensional Systems", Reviews of Modern Physics **54**, 437 (1982).

[106] S. Das Sarma, "Polaron Effective Mass in GaAs Heterostructure", Physical Review B **27**, 2590 (1983).

[107] S. Das Sarma and B. A. Mason, "Screening of the Polar Interaction in Quasi-Two-Dimensional Semiconductor Microstructures", Physical Review B **31**, 5536 (1985).

[108] W. Xiaoguang, F. M. Peeters, and J. T. Devreese, "Screening of the Electron-Phonon Interaction in GaAs Heterostructures", Physica Status Solidi (b) **133**, 229 (1986).

[109] A. Gold and L. Calmels, "Correlation in Fermi Liquids: Analytical Results for the Local-Field Correction in Two and Three Dimensions", Physical Review B **48**, 11622 (1993).

[110] C. Bulutay and M. Tomak, "Dielectric Properties of the Quasi-Two-Dimensional Electron Liquid in Heterojunctions", Physical Review B **54**, 14643 (1996).

[111] F. Stern and S. Das Sarma, "Electron Energy Levels in GaAs/Al$_x$Ga$_{1-x}$As Heterojunctions", Physical Review B **30**, 840 (1984).

[112] T. W. Hickmott, P. M. Solomon, R. Fischer, and H. Morkoç, "Negative Charge, Barrier Heights, and the Conduction-Band Discontinuity in Al$_x$Ga$_{1-x}$As Capacitors", Journal of Applied Physics **57**, 2844 (1985).

[113] D. Arnold, A. Kettersen, T. Henderson, J. Klem, and H. Morkoç, "Electrical Characterization of GaAs/AlGaAs Semiconductor-Insulator-Semiconductor Capacitors and Application to the Measurement of the GaAs/AlGaAs Band-Gap Discontinuity", Journal of Applied Physics **57**, 2880 (1985).

[114] M. O. Watanabe, J. Yoshida, M. Mashita, T. Nakanisi, and A. Hojo, "Band Discontinuity for GaAs/AlGaAs Heterojunctions Determined by $C-V$ Profiling Technique", Journal of Applied Physics **57**, 5340 (1985).

[115] K. S. Singwi and M. P. Tosi, in *Solid State Physics*, edited by F. Seitz, H. Ehrenreich, and D. Turnbull (Academic, New York, 1981), Vol. 36, p. 177.

[116] D. Heitmann, "Surface- and Two-Dimensional Plasmon Excitations in Microstructured Metal Films and Semiconductor Heterostructures", Physica Scripta **T25**, 294 (1989) and references therein.

[117] J. J. Baumberg, and D. A. Williams, "Coherent Phonon-Plasmon Modes in GaAs:Al$_x$Ga$_{1-x}$As Heterostructures", Physical Review B **53**, R16140 (1996).

[118] S. Hiyamizu, Semiconductors and Semimetals **30**, 53 (1990).

[119] H. Kamimura and H. Aoki, *The Physics of Interacting Electrons in Disordered Systems* (Clarendon, Oxford, 1989).

[120] N. F. Mott, *Metal-Insulator Transitions* 2nd ed. (Taylor & Francis, London, 1990).

[121] N. F. Mott, Proceedings of the Physical Society (London) **62**, 416 (1949).

[122] D. Belitz and T. R. Kirkpatrick, "The Anderson-Mott Transition", Reviews of Modern Physics **66**, 261 (1994).

[123] S. L. Sondhi, S. M. Girvin, J. P. Carini, and D. Shahar, "Continuous Quantum Phase Transitions", Reviews of Modern Physics **69**, 315 (1997).

[124] J. Hubbard, Proceedings of the Royal Society (London) **A281**, 401 (1964).

[125] P. W. Anderson, "Absence of Diffusion in Certain Random Lattices", Physical Review **109**, 1492 (1958).

[126] P. Lee and T. V. Ramakrishnan, "Disordered Electronic Sytems", Reviews of Modern Physics **57**, 287 (1985).

[127] E. Abrahams, P. W. Anderson, D. C. Licciardello, and T. V. Ramakrishnan, "Scaling Theory of Localization: Absence of Quantum Diffusion in Two-Dimensions", Physical Review Letters **42**, 673 (1979).

[128] M. Ya. Azbel', "Quantum Particle in Random Potential: Exact Solution and its Implications", Physical Review B **45**, 4208 (1992).

[129] S. V. Kravchenko, D. Simonian, M. P. Sarachik, W. Mason, and J. E. Furneaux, "Electric Field Scaling at a $B = 0$ Metal-Insulator Transition in Two Dimensions", Physical Review Letters **77**, 4938 (1996).

[130] J. E. Furneaux, S. V. Kravchenko, W. Mason, V. M. Pudalov, and M. D'Iorio, "Scaling of a Metal/Insulator Transition in a 2D System at $B = 0$", Surface Science **361/362**, 949 (1996).

[131] S. V. Kravchenko, W. Mason, G. E. Bowker, J. E. Furneaux, V. M. Pudalov, and M. D'Iorio, "Scaling of an Anomalous Metal-Insulator Transition in a Two-Dimensional System in Silicon at $B = 0$", Physical Review B **51**, 7038 (1995).

[132] S. V. Kravchenko, G. V. Kravchenko, J. E. Furneaux, V. M. Pudalov, and M. D'Iorio, "Possible Metal-Insulator Transition at $B = 0$ in Two Dimensions", Physical Review B **50**, 8039 (1994).

[133] C. Bulutay, I. Al-Hayek, and M. Tomak, "Mott Transition and Impurity Binding Energies in Three- and Two-Dimensional Electron Liquids", submitted for publication.

[134] J. B. Krieger and M. Nightingale, "Dielectric Screening and the Mott Transition in Many-Valley Semiconductors", Physical Review B **4**, 1266 (1971).

[135] R. L. Greene, C. Aldrich, and K. K. Bajaj, "Mott Transition in Many-Valley Semiconductors", Physical Review B **15**, 2217 (1977).

[136] C. Aldrich, "Screened Donor Impurities in Many-Valley Semiconductors with Anisotropic Masses", Physical Review B **16**, 2723 (1977).

[137] A. Neethiulagarajan and S. Balasubramanian, "Effect of Electron-Mass Anisotropy and Effective Dielectric Function on Donor Binding Energies in Silicon", Physical Review B **28**, 3601 (1983).

[138] F. Martio, G. Lindell, and K. F. Berggren, "Metal-to-Nonmetal Transition in $n-$Type Many-Valley Semiconductors", Physical Review B **8**, 6030 (1973).

[139] A. Neethiulagarajan and S. Balasubramanian, "Concentration-Dependent Donor Energies and Mott Constant in Heavily Doped $n-$Type Silicon", Physical Review B **32**, 2604 (1985).

[140] A. Gold and A. Ghazali, "Bound States in the Three-Dimensional Electron Gas with Repulsive or Attractive Test Charges: Many-Body Effects", Journal of Physics Condensed Matter, **8**, 7393 (1996).

[141] L. Hulthén, Ark. Mat. Astron. Fys. **28** A, No. 5 (1942).

[142] A. N. Borges, O. Hipólito, and V. B. Campos, "Electron Correlation Effects in Screened Hydrogenic Impurity States in Many-Valley Semiconductors", Physical Review B **52**, 1724 (1995).

[143] J. Serre, A. Ghazali, and A. Gold, "Impurity Levels, Impurity Bands, Excited Impurity Bands, and Band Tails: the Electronic Density of States in Quantum Wells and Heterostructures", Physical Review B **39**, 8499 (1989).

[144] A. Gold, "Local-Field Correction for the Electron Gas: Effects of the Valley Degeneracy", Physical Review B **50**, 4297 (1994).

[145] W. H. Press, B. P. Flannery, S. A. Teukolsky, and W. T. Vetterling, *Numerical Recipes The Art of Scientific Computing* (Cambridge University Press, Cambridge, 1989).

[146] E. Zeidler, *Applied Functional Analysis: Applications to Mathematical Physics* (Springer-Verlag, New York, 1995).

[147] L. B. Rall, *Computational Solution of Nonlinear Operator Equations* (Wiley, New York, 1969).

[148] P. P. Edwards and M. J. Sienko, "Universality Aspects of the Metal-Nonmetal Transition in Condensed Media", Physical Review B **17**, 2575 (1978).

[149] S. Katsumoto, F. Komori, N. Sano, and S. Kobayashi, "Fine Tuning of Metal-Insulator Transition in $Al_{0.3}Ga_{0.7}As$ Using Persistent Photoconductivity", Journal of the Physical Society of Japan **56**, 2259 (1987).

[150] J. A. Brum, G. Bastard, and C. Guillemot, "Screened Coulombic Bound States in Semiconductor Quantum Wells", Physical Review B **30**, 905 (1984).

[151] M. H. Degani, O. Hipólito, "Bound Polaron in GaAs-GaAlAs Quantum-Well Structures", Physical Review B **33**, 4090 (1986).

[152] E. A. de Andrada e Silva and I. C. da Cunha Lima, "Impurity Bands in $n-$Type Si/SiO_2 Semiconductors", Physical Review Letters **58**, 925 (1987).

[153] S. T. Chui and B. Tanatar, "Impurity Effect on the Two-Dimensional-Electron Fluid-Solid Transition in Zero Field", Physical Review Letters **74**, 458, (1995).

[154] B. Tanatar and S. T. Chui, "Quantum Monte Carlo Simulation Study of Two-Dimensional Electrons with Impurities", Turkish Journal of Physics **19**, 51 (1995).

[155] J. S. Thakur and D. Neilson, "Frozen Electron Solid in the Presence of Small Concentrations of Defects", Physical Review B **54**, 7674, (1996).

[156] Private communication with J. S. Thakur.

[157] R. B. Wiringa, "From Deuterons to Neutron Stars: Variations in Nuclear Many-Body Theory", Reviews of Modern Physics **65**, 231 (1993).

[158] B. L. Cohen, *Concepts of Nuclear Physics*, (McGraw-Hill, New York, 1971).

[159] H. K. Schweng and H. M. Böhm, "Finite-Temperature Electron Correlations in the Framework of a Dynamic Local-Field Correction", Physical Review B **48**, 2037 (1993).

153

[160] H. K. Schweng and H. M. Böhm, "Finite-Temperature investigations of a Two-Dimensional Electron Liquid", Zeitschrift für Physik B **95**, 481 (1994).

[161] N. D. Mermin, "Lindhard Dielectric Function in the Relaxation-Time Approximation", Physical Review B **1**, 2362 (1970).

[162] A. K. Das, "The Relaxation-Time Approximation in the RPA Dielectric Formulation", Journal of Physics F: Metal Physics bf 5, 2035 (1975).

[163] R. K. Moudgil, P. K. Ahluwalia, and K. N. Pathak, "Static and Dynamic Correlation Functions of a Two-Dimensional Quantum Electron Fluid", Physical Review B **52**, 11945 (1995).

[164] W. L. Bloss, L. J. Sham, and V. Vinter, "Interaction Induced Transition in Silicon Inversion Layer", Physical Review Letters **43**, 1529 (1979).

[165] S. Feng and Q. Hu, "Far-Infrared Photon-Assisted Transport Through Quantum Point Contact Devices", Physical Review B **48**, 5354 (1993).

[166] L. Y. Gorelik, M. Jonson, R. I. Shekhter, and O. Tageman, "Non-Equilibrium Mesoscopic Physics: Microwave-Induced Coherent Transport in Two-Dimensional Semicoductor Microstructures", in *Frontiers in Nanoscale Science of Micron/Submicron Devices*, edited by A.-P. Jauho and E. V. Buzaneva, NATO ASI Series E:328, (Kluwer, Dordrecht, 1996), p. 225.

[167] A. -P. Jauho, "Interacting and Coherent Time-Dependent Transport in Semiconductor Heterostructures", in *Quantum Transport in Ultrasmall Devices*, edited by D. K. Ferry, H. L. Grubin, C. Jacoboni, A. P. Jauho, NATO ASI Series B:342, (Plenum, New York, 1995), p. 301.

[168] L. V. Keldysh, Soviet Physics JETP **20**, 1018 (1964).

[169] J. Voit, "One-Dimensional Fermi Liquids", Reports on Progress in Physics, 979 (1996).

[170] A. Montorsi, (editor), *The Hubbard Model*, (World Scientific, Singapore, 1992).

154

VITA

Ceyhun Bulutay was born in Ankara on October 13, 1967. He received his B.S. degree with high honors from the Department of Electrical and Electronics Engineering (EEE) of the Middle East Technical University (METU) in Ankara, in 1989. He was awarded the M.S. degree in June 1991, in the area of fields, waves and optics from the Electrical and Computer Engineering Department of the Northeastern University in Boston, USA. For his Ph.D. study he returned back to the EEE Department of METU. While with the Northeastern University, he was a research assistant working under the supervision of Prof. S. Prasad on the microwave characterization of the heterojunction bipolar transistors and the three-dimensional computational electromagnetics. Between 1991-94 he was an assistant in METU and since September 1994 he has been an instructor in the same institution. His research in METU concentrated on mesoscopic devices and many-body formulation of bulk and low-dimensional electronic systems under the guidance of Prof. M. Tomak from the Physics Department of METU. He was also a member of the research group on active phased-array antennas led by Prof. T. Birand. His research has been published in the journals IEEE transactions on Electron Devices, Microwave Theory and Techniques, Journal of Applied Physics and the Physical Review B, as well as in international conference proceedings.